Mechanically Processed Alumina Reinforced Ultra-high Molecular Weight Polyethylene (UHMWPE) Matrix Composites

Hesham Moh A Elmkharram

Thesis submitted to the faculty of
Virginia Polytechnic Institute and State University
in partial fulfillment of the requirements for the degree of

Master of Science

in

Materials Science and Engineering

Alexander O Aning, Chair
William T Reynolds
Carlos T A Suchicital
Abby Rebecca Whittington

March 8, 2013

Blacksburg, VA

Keywords: Mechanical Alloying, Polymer Matrix Composites, Particles Reinforcement

Mechanically Processed Alumina Reinforced Ultra-high Molecular Weight Polyethylene (UHMWPE) Matrix Composites

By

Hesham Elmkharram

ABSTRACT

Alumina particles filled Ultra-high Molecular Weight Polyethylene (UHMWPE), with Al_2O_3 contents 0, 1, and 2.5 wt% were milled for up to 10 hours by the mechanical alloying (MA) process performed at room temperature to produce composite powders. Compression molding was utilized to produce sheets out of the milled powders. A partial phase transformation from orthorhombic and amorphous phases to monoclinic phase was observed to occur for both the un-reinforced and reinforced UHMWPE in the solid state, which disappeared after using compression molding to produce composite sheets. The volume fraction of the monoclinic phase increased with milling time, mostly at the expense of the amorphous phase. The melting temperature decreased as a function of milling time as a result of modifications in the UHMWPE molecular structure caused by the milling. At the same time, for a given alumina composition the activation energy of melting increased with milling time. Generally, the crystallinity of the molded sheets increased with milling time, and this caused the yield strength and elastic modulus to increase with milling time for a given alumina composition. However, the tensile strength and ductility remained about the same.

This work is dedicated to:

- The strong woman who has wise foresight, my Grandmother **Gamairaa Allenbas**

- The great man and woman who gave me the love and affection, also who taught me the optimum ways of life and looking into the future as beckons bright and promising, my father **Mohamed Elmkharram** and my mother **Hawaa Besher**

- Those who shared with them happyness and sadness days of my childhood and they gave me love, my brother **Hithem**, my sisters **Kharia** and **Hamida Elmkharram**

- The little boy who his presence gives me the hope and life for the future of honorable, my son **Mohamed Elmkharram**

- The beautiful woman who believed in me and gave me love and I love her forever, my wife **Safa Elkhal**

- The new **Libya**

Acknowledgements

First and foremost I would like to thank ALLAH who gave me this grace to accomplish this work. I have realized how much ALLAH helped me during this time and all the time of my life, and I could never have done this work without ALLAH's willing.

I would like to thank my academic advisor, mentor, and friend during my studies at Virginia Tech, Dr. Alex Aning. His constant enthusiasm, encouragement, patience and optimism have always motivated me; his extraordinary ability to guide students in the right direction has always benefited me. Whenever I had trouble with my research or personal issues, he was always there helping me. I cannot thank him enough.

Also, I would like to thank my committee members: Dr. William Reynolds, Dr. Carlos Suchicital, and Dr. Abby Whittington, for the guidance and support that they so generously gave me to complete this document.

Acknowledgements are given to Dr. Donald G. Baird and his former PhD student Dr. Gregorio Velez at Virginia Tech Chemical Engineering Department, for using his Polymer Processing Laboratory.

I would like to extend my gratitude to Virginia Tech Materials Science and Engineering Department for providing a partial financial support, and equipment to achieve this work. Also I would specifically like to thank the Department Head of Virginia Tech Materials Science and Engineering, Dr. David Clark for giving me the opportunity of a graduate assistantship position during my financial hardship.

Special thanks to David Berry for his kind assistance and teaching how to use the various equipment in the MSE Department during the journey of this work.

I am grateful to Ms. Christine Bala Burgoyne for her and advice and the editing of this document.

I would also like to thank former PhD students at Dr. Aning's research group, Dr. Niven Monsegue and Dr. Andrew Zeagler, for their assistance and advice when I joined to Dr. Aning's research group.

Special thanks go to current members of Dr. Aning's research group: Josh Anderson, Ibrahim Khalfallah, Mohamed Mohamedali, and Gabriella Mirabelli, for their great company throughout the years.

I would like to say thanks to the Libyan Ministry of Higher Education and Scientific Research for providing most of the financial aid in support of my master's degree program.

I also would like to say thanks to the Canadian Bureau for International Education for managing my Libyan North American Scholarship Program.

I would like to thank my fellow graduate students and friends Jebreel Mohamed Muftah Salem, Michel Vargas, Jonathan Huang, and William Cary Hill, for making my stay in Blacksburg that much more pleasant. I am very grateful to all of you.

I wish to express my sincere gratitude to all my uncles of the Besher family, and their presence surely made a positive impact in my life and was a constant source of moral support. It was also all of you who originally triggered my passion for science and research with your constant discussions on scientific issues. Dear Uncles Abdul Salam, Dr. Almirghani, Solomon, Bashir, Lamin, and Abu Bakr, to all of you I would like to say thank you.

From the bottom of my heart, I would like to thank my brother Hithem, my sisters Kharia and Hamida Elmkharram for their love, support, and constant encouragement I have gotten from them over the years; and their belief in me that has helped to give me the strength and resolve that I needed to produce this work.

The biggest thanks of all go to my father Mohamed Elmkharram and my mother Hawaa Besher and without their constant support, unconditional love, and providing a wonderful family environment, obtaining this degree would not have been possible. My dear father, it has been years since you passed away, your lessons about hardworking, responsibility, and aiming high are still vivid in my mind. Now, you must be very proud of me for this achievement. My dear mother never stopped praying, spiritually supporting, and loving me from thousands of miles away, even in the course of experiencing major health problems. I would like to say thank you again my mother, and I ask ALLAH to bless you with good health. I am indebted to you and my father for my successes in this regard.

My deep thanks go to my son Mohamed Elmkharram who missed out on a lot of Daddy time, while I pursued my research these three past years. Thank you my son for your patience and I love you more than you will ever know.

I would like to extend my deepest thanks to my loving wife, Safa Elkhal for support, love, advice, and inspiration throughout the past three years of pursuing my master's degree. Safa gave me her full support even during the time of her mother's severe illness and her eventual passing away. She preferred to be by my side thousands of miles away from her mother's home. I feel sad that she could neither go home to see her mother when she was battling her disease nor attend her funeral when she passed away. I am really proud and grateful for her understanding and patience during those times when there seemed to be no light at the end of the tunnel. Thank you Safa, your love and prayers have been the main source of my successes in life and particularly in obtaining my master's degree.

Finally, I would like to thank several people who were instrumental in making my dream of graduate education a reality: Dr. Nuri Bhieh, Dr. Abdulhamid M. Dajan, and Dr. Anwar Hasshkel. Their advice and encouragement were very key to my journey to do my graduate work in the USA.

Table of Contents

List of Figures

List of Tables

Chapter 1

1. Introduction

In last three decades polymer-matrix composites (PMCs) have been of interest to industry and researchers, particularly in the areas of automotive, aerospace, electronic systems, medical products, civil construction, chemical industries, and consumer appliances [1, 2]. This interest is driven by properties and qualities such as high strength to weight ratio, good electrical insulation, non-corrosive, ability to transfer load, easy and inexpensive processing, etc. [3, 7]. PMCs generally consist of fibers (carbon, nylon, rayon or glass) or particles (SiO_2, Al_2O_3, TiO_2, and $CaCO_3$) reinforcing a polymer matrix to produce material has superior and unique mechanical and physical properties [4].

Fiber reinforcement represents physical rather than a chemical means of changing a material to suit various engineering applications [8-15]. While, particle fillers are employed to improve high temperature performance, reduce friction, increase wear resistance and to reduce shrinkage [16, 17]. The particles also share the load with the matrix, but to a lesser extent than a fiber [3]. Particle reinforcements are therefore used to improve stiffness but not generally to strengthen [18]. From the mechanical point of view it cannot be said that the incorporation of fillers in polymer matrix always positive effects. For example, elastic modulus, hardness and wear resistance can lead to deterioration of tensile strength and ductility deteriorated.

Some properties can be evaluated a priori with sufficient accuracy (elastic modulus); however the processing technique that is used has a lot to do with the actual property values obtained. The strain to failure, for example, is very sensitive to defects that can easily be introduced into the material during processing. The aggregates are also an element of discontinuity in the material, which determines the deterioration of some important mechanical properties, such as impact resistance; the formation of aggregates must be prevented from forming during processing. In this field experience has shown that the physical and mechanical characteristics of the composite depend, in addition to the properties of the individual components, the size, the shape and degree of dispersion of the particles, as well as the degree of accession between the latter, and the polymer matrix [8-15].

With the growing demand of particles reinforcement polymer matrix composites, economic competition and ecological pressure, there is an increasing need to synthesis particles reinforcement polymer matrix composites from a cost effective source and by a cheap method. The incorporation of particle fillers in a polymer matrix can bring about dramatic changes in the properties of polymer matrix. To produce a PMC which has good properties by using particle reinforcement, a narrow particle size distribution, high surface area and homogenous dispersion should be achieved. Without a good proper dispersion of the nano or micro particles in the composite, filler aggregates would act as defective sites; these defective sites (agglomerates and segregation) limit the mechanical performance [8, 19-21]. In order to acquire a good dispersed composite with separated particles, the manner of combining polymers and particles should be considered as the most important key to gain the desired material properties. For dispersing the particles in polymer, mechanical alloying has been established as a good processing tool which breaks up agglomerates and distribute filler particles homogeneously in the polymer [21-23]. This unique capability of mechanical alloying is a reason for choosing mechanical alloying as a processing technique for this work.

In this study, Ultra-high Molecular Weight Polyethylene (UHMWPE) and alumina powders were milled to achieve intimate blends in the solid state. The mechanical-alloyed powders were then molded by compression to produce polymer composite sheets of UHMWPE/ Al_2O_3 and then characterized using X-ray diffraction (XRD), differential scanning calorimetry (DSC), and tensile testing of sheets samples. Likewise, powder samples from milling were characterized by XRD and DSC.

Chapter 2

2. Background

2.1 Polymer Matrix Composites

Polymer-matrix composites (PMCs) have been widely used in engineering applications in the last four decades, but humans have known composite materials since ancient times. The first use of composites date back to the 1500s B.C. when early Egyptians used a mixture of mud and straw to create strong and durable buildings [24]. In general, composites are materials that are combinations of two or more organic or inorganic components. One material serves as a "matrix," which is the material that holds everything together, while the other material serves as reinforcement, in the form of fibers or particles embedded in the matrix. The matrix holds the reinforcement to form the desired shape while the reinforcement improves the overall mechanical properties of the matrix. When designed properly, the new combined material exhibits better strength than would each individual material [3- 5]. The concept of composites is not a human invention. For example, wood is a natural composite material consisting of one species of polymer-cellulose fibers with good strength and stiffness in a resinous matrix of another polymer, the polysaccharide lignin [3]. According to a study in 1973, around 80% of the research and development in composite materials has been done since the early 1960s [25]. For 60 years, scientists have focused to understand the concepts of composite materials composed of reinforcement such as fibers, particles, flakes, and/or fillers embedded in matrixes of the polymers, metals, or ceramics and develop it to use in different applications [4]. PMCs had a large share in this research on different application, including the aerospace and automotive industries, electronic systems, medical products, civil construction, chemical industries, and consumer appliances [1, 2].

The first modern polymer used in composites was thermosetting phenol formaldehyde resin, discovered by Belgian chemist Leo Baekeland in 1909; it was called Bakelite resin [24, 26]. The following years, especially in 1930s, saw much developments in the synthesize of new polymers by Carleton Ellis, Carothers, Kienle and many others. These works later became the backbone of the matrices of composites that have been most prominent in the decades after. When fiberglass

became more commercially available in the early 1940s, the aircraft radomes in the United State began to be built by fiberglass reinforced polymers (FRP) [27]. In 1950s, application of fiber-reinforced plastics expanded to include industry of boat hulls, car bodies, and truck cabs [4]. FRP showed many uses at that time since it is easy to make them into complex shapes.

There are three major types of composite matrices namely metals, ceramics and polymers. These are used to produce metal matrix composites (MMC), ceramic matrix composites (CMC), and polymer matrix composites (PMC). Typical reinforcements used in PMC are fiber (glass, carbon and boron) or minerals particles such as SiO_2, Al_2O_3, TiO_2, and $CaCO_3$. In general reinforcement used to improve strength, stiffness, impact resistance, and wear resistance to the relatively weak matrix. For example in fiberglass reinforced polymers, the fiber reinforcement carries the load applied to the material and the polymer matrix transfers stresses between adjoining fibers through adhesion. The reinforcement also offers resistance to weathering and corrosion [3-7]. PMCs have grown so rapidly during the past several decades because they are easy to process; they also melt at low temperatures compared with metals and ceramics and this low melting point keeps the fibers safe from the effect of the high temperature.

One classification scheme of polymers is based on their response to rising temperatures. The two subdivisions are thermoplastic and thermoset (Figure 1).

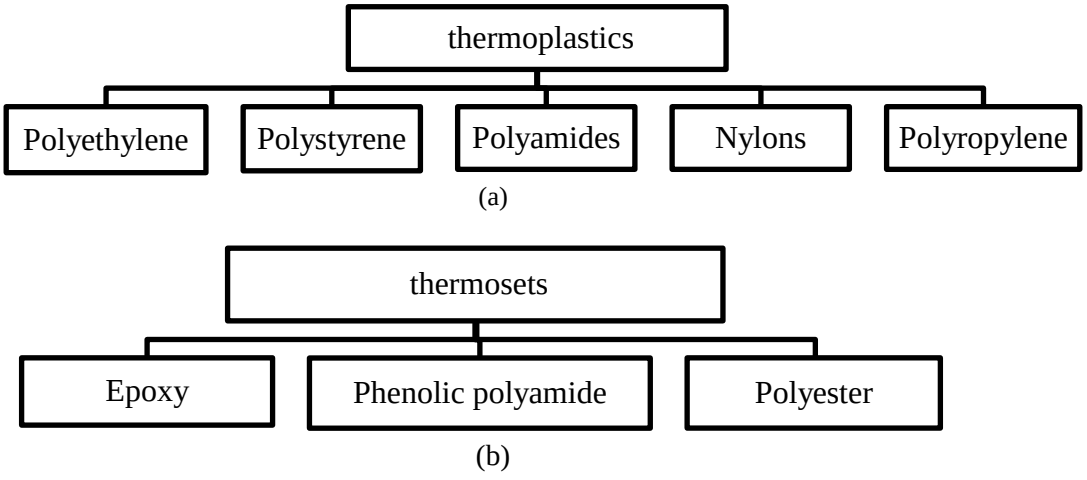

Figure 1: (a) Thermoplastics polymer. (b) Thermosets polymer.

2.1.1 Thermosetting polymer matrix

Thermoset or Thermosetting polymers have cross-linked or network structures that consist of long hydrocarbon molecules with primary bonds holding the atoms in the molecule together [3-5, 24, 28, 29]. Since the intermolecular covalent bonds cannot be broken easily without breaking the intramolecular covalent bonds, thermosets cannot be melted or soften by heating, but decompose on heating. The particularity of primary bonds and three dimensional cross-linked structures for thermosetting polymers makes them tend to have high dimensional stability, high temperature resistance, good resistance to solvents, and good bonding to reinforcement; furthermore, thermoset polymers have low cost, low viscosity and ease of processing [3-5, 24, 29]. The most common thermoset polymers used as composite matrices are unsaturated polyesters, epoxies, vinylesters, and high-performance thermosets.

2.1.2 Thermoplastic polymer matrix

Thermoplastic polymers have linear or branched structures consisting of long hydrocarbon molecules that are held together by secondary (van der Waals) bonds and mechanical entanglements [3-5, 24, 28, 29]. Thermoplastic polymers melt to a viscous liquid at the processing temperature, when the thermal energy is sufficient to overcome secondary bonds. The main advantages of thermoplastics are toughness, easy processing, recyclability and low volatile emissions, but their high viscosity and poor adhesion with reinforcement reduces the chances as composite matrices [30]. Thermoplastic polymers are divided into two parts: amorphous glassy thermoplastics and semicrystalline thermoplastics. Amorphous glassy thermoplastics like poly(ether sulfone) (PES) or poly(etherimide) (PEI) are of some interest for use as advanced FRP matrix materials, but there remain concerns over their solvent resistance [29]. If the thermoplastic solidified from the melt state and its molecules arranged itself in a regular pattern, it is called a semicrystalline thermoplastic [3-5, 24, 28, 29]. The degree of crystallinity depends on the cooling rate which means that the higher degree of crystallinity has slower cooling rates, and the degree of crystallinity has significant effect on the final matrix properties [3-5, 24, 28, 29]. Semicrystalline thermoplastics polymer are tough and stronger than amorphous thermoplastics. They are also have more resistant to dissolution and temperature environmental compared with amorphous thermoplastics [3-5, 24, 28, 29]. Semicrystalline thermoplastics

polymer with these advantages have ample chances to be used in many advanced applications as composite matrices. For example, poly(phenykene sulfide) (PPS), poly(ether ether ketone) (PEEK), and poly(ether ketone ketone) (PEKK) with carbon fiber are used in aerospace applications [31-33], and polypropylene (PP) [34] Polyamides (PA6, PA66) [35] are widely used in FRP applications in the automotive industry. Whereas, hydroxyapatite/polyethylene (HA/PE), carbon fiber/ultra high molecular weight polyethylene (CF/UHMWPE), carbon fiber/poly(ether ether ketone) (CF/PEEK) [36, 37], carbon fiber/ polyamide12 (CF/PA12), carbon fibre/ polyamide12/ hydroxyapatite (CF/PA12/HA) [38-41], alumina particles/ ultra high molecular weight polyethylene (Al_2O_3/UHMWPE) [16], titanium dioxide particles/ultra high molecular weight polyethylene (TiO_2/UHMWPE) [17] are used in biomedical and biomaterials applications.

2.2 Some issues effects on the properties of the polymer composite

In the preliminary definition of the composites materials, we said that the composites materials consist from two or more components combined together. In other words, two or more phases at macro, micro, or nanoscopic levels, not soluble in each other are combined together in order to enhance the matrix properties. Thus, the properties of the composite material depend on the matrix, the reinforcement and the boundary layer between the matrix and reinforcement, called "interphase zone" [8-10, 42]. Consequently, in order to design a polymer composite material that has good and optimal properties, there are many variables related to the matrix; reinforcement and interface zone should be considered to achieve the desired properties.

First, the type of matrix plays an important role because every matrix has its unique physical properties from other matrices. In general, the physical properties that are most important for processing polymers as a composite matrix are viscosity, temperature, cycle time, and work environment. In this research project, we use semicrystalline thermoplastic UHMWPE matrix and there are other factors that should be considered such as the degree of crystallinity, spherulite size and crystalline orientation have a profound effect on the ultimate properties of the polymer composite [10, 11].

Second, the reinforcements also are not less important than the matrices type in influencing the properties of the composites. Reinforcement types as (fibers or particles), filler content,

aspect ratio, strength, orientation, and the interfacial strength are of prime importance to the final balance of the properties of the composite [8-15]. As we use Al_2O_3 particles, with size of 0.3 μm, as reinforcement in this work, the narrow particle size distribution, high surface area and homogenous should be achieved to get composite has good properties. Without a good proper dispersion of the nano or micro filler particles in the composite, filler aggregates will form which tend to act as defect sites; these defect sites limit the mechanical performance. Agglomerates and segregation also adversely influence physical composite properties such as optical transmissivity [8, 19-21]. In order to acquire a good dispersed composite, the manner of combining polymers and particles should be considered as the most important key to gain the desired material properties. For dispersing the particles in polymer, mechanical alloying has been established which applies high shear forces during a dispersion process in order to break up agglomerates and to distribute the individual fillers homogeneously in the polymer [21, 23]. This mechanism for mechanical alloying to curb the agglomerates occurring is one of the reasons that led to choose mechanical alloying known as “attrition milling” to use it as dispersing technique in this work.

Finally, the performance and success of the polymer reinforcement essentially depend on the bonding or adhesion between matrix and filler. However, the properties of the polymer composites are a result of the combination of the filler and matrix properties and the ability to transfer stresses across the filler-matrix interface “interphase zone” [8, 43-45]. The interphase zone in composites is the part of the matrix surrounding the filler surface, and possessing local properties different from those of the bulk matrix. The size, structure and type of interphase vary strongly and depend on the nature of the filler and its surface as well as on the polymer matrix [46-50]. On the other hand, the size, structure, and type of interphase have critical effect to the mechanical strength of the adhesive bond [43, 44, 51]. High adhesive strength can be expected only when strong polar interactions or chemical bonds exist across it. Otherwise, several modification methods are used to enhance and improve the interfacial adhesion between the filler and matrix such as the filler surface treatment “sizing agents” and increasing the surface contact area of the filler with the polymer matrix [8, 51]. Occurrence of mechanical alloying process offset by a reduction in the particle size leads to increase the surface area, and increase the number of interfaces [52]; and as we use particulate reinforcement in this work, mechanical

alloying has been used as the method to increase the surface area contact to enhance and improve the interfacial adhesion between the Al_2O_3 filler and the UHMWPE matrix.

2.3 Mechanical Alloying

Mechanical alloying (MA) is a solid-state powder processing technique used to produce homogeneous materials by blending and alloying dissimilar elemental powder mixtures. However, MA is a high energy ball milling process technique based on the principle of the deforming, fracturing, welding, and rewelding, which repeatedly occur to the trapped powder particles between two or more colliding balls, to create homogeneous alloyed microstructure or uniformly dispersed particles in a matrix [53]. This technique was developed in the late 1960's by John Benjamin and co-workers at the International Nickel Company (INCO) to produce complex oxide dispersion-strengthened (ODS) alloys [53-56]. In general, MA techniques be based on grinding media (vial and balls) and agitating source (shaking, vibration, attrition and planetary mill) [57]. However, during MA processing, powders are loaded into a vial along with hard wear-resistant charge balls and milling by one of the agitating sources that mentioned above for the desired time and the charge ratio (weight of charge balls divided by weight of powders). The high energy impacts between the balls and the powder that is trapped between them or with the vial walls induces deforming, fracturing, welding, and rewelding when the agitating process begins as seen in Figure 2.

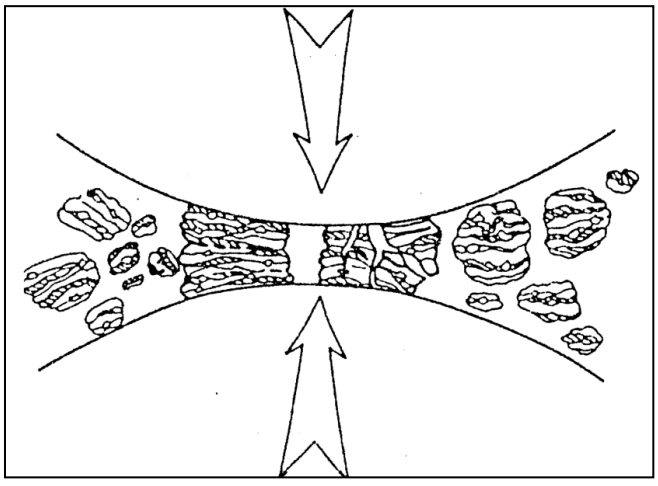

Figure 2: Illustration of a collision between two balls and trapped powder [57]

As agitating or milling begins and continues, the high energy impacts, attrition, shear and compression occur causing deformation to the powder particles, leading to reduction in the particles size and work hardening. At a constant rate, the collisions occur repeatedly by fracture, deformation and interdiffusion thereby cold welding on the powder particles, and forming a lamellar structure [57-58]. Over time, a steady state particle size is achieved, while structure refinement continues as shown in Figure 3.

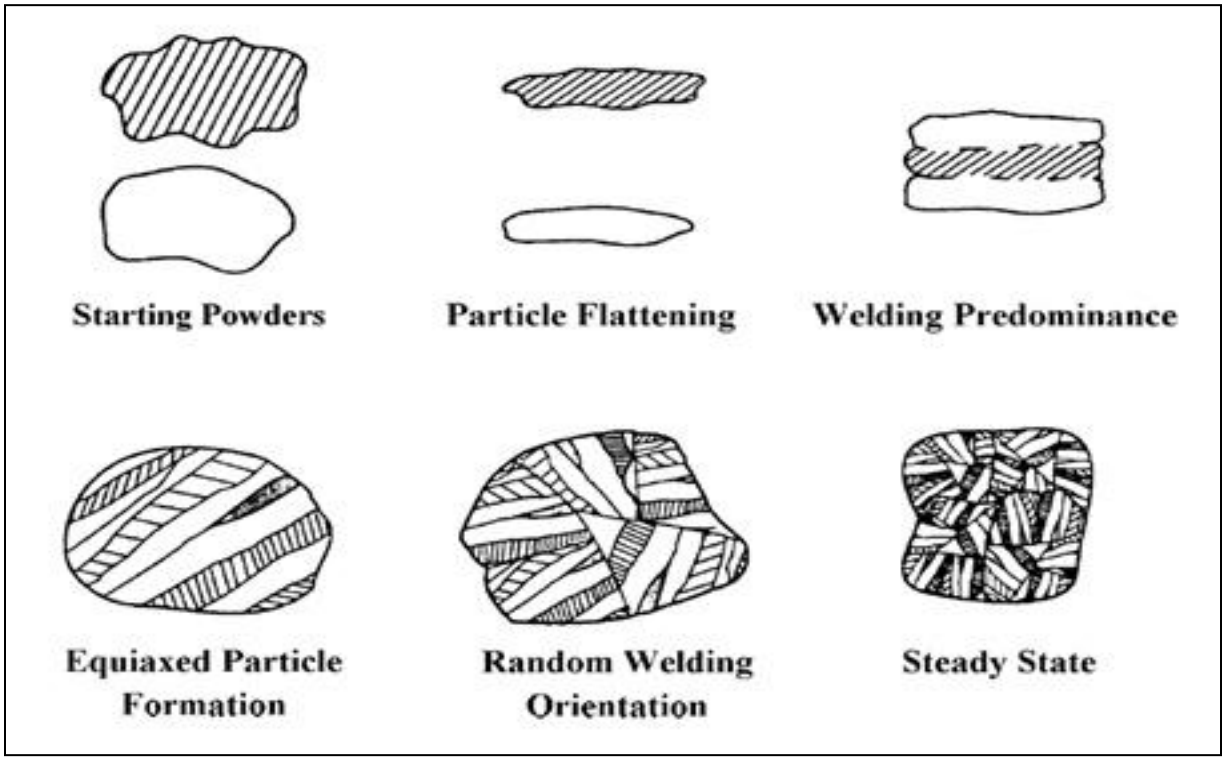

Figure 3: Particle evolution during mechanical alloying. [59]

Different types of milling equipment have been developed for mechanical alloying such as SPEX mill, planetary ball mill and attritor mill. The SPEX mill is functionally described as a shaker mill or high-energy ball mill; this Mixer/Mill shakes a vial loaded with 10-20 g of the powder of known composition that needs to process hard wear-resistant balls by using movable arm to generate different movements back, forth, and lateral at approximately 1200 Hz as shown in Figure 4 [57].

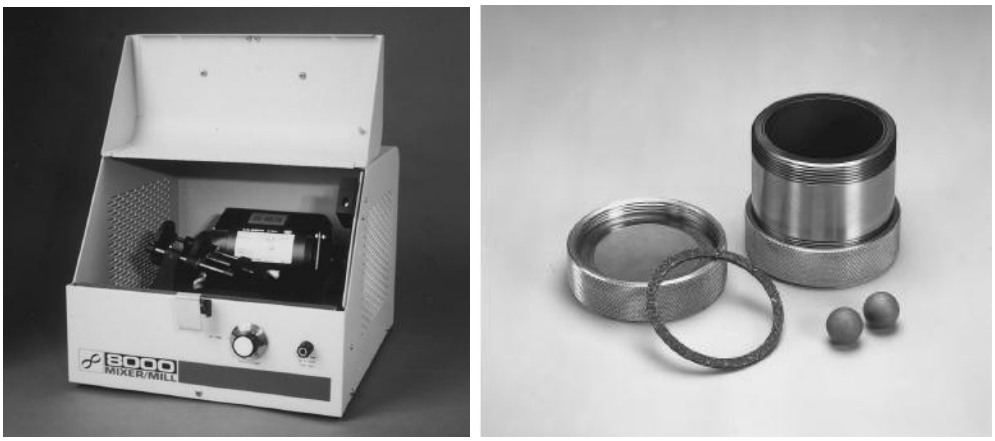

Figure 4: SPEX 800 mill Vial and grinding media

The planetary ball mill, also known as centrifugal or ball mills, simply consists of a set of vials that arranged on a rotating support disk. The vials are rotated on their axis and also on a disk the opposite direction producing planetary motion and centrifugal force. Since the vials and the supporting disk rotate in opposite directions, the centrifugal forces alternately act in like and opposite directions. This motion causes both impact and friction effects as the balls collide with the vial wall and run down the side as seen in Figure 5.

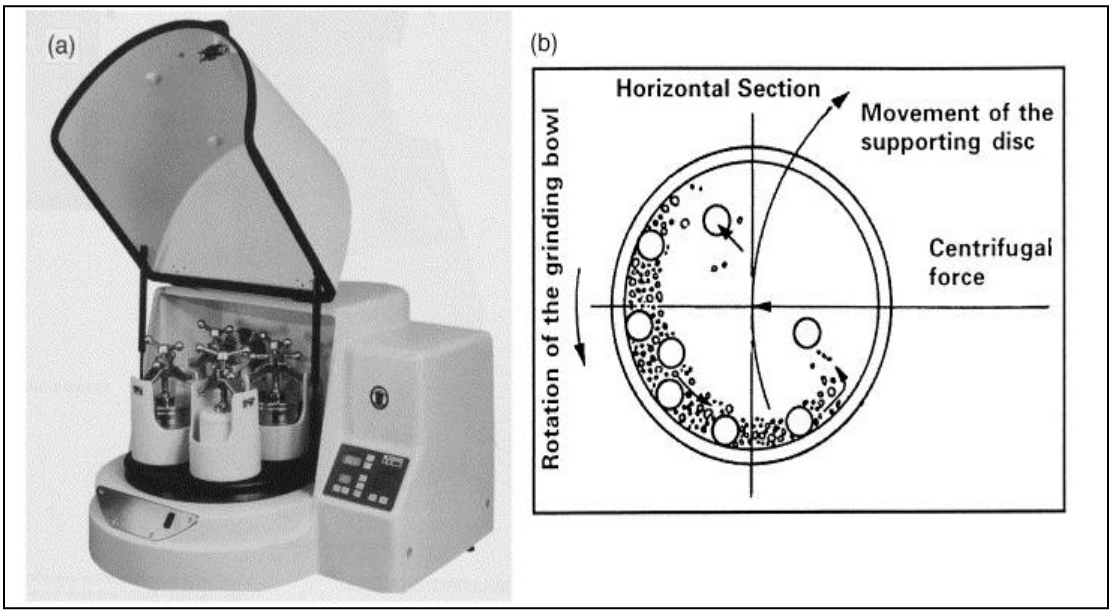

Figure 5: (a) Fritsch Pulverisette P-5 four station ball mill. (b) Schematic depicting the ball motion inside the ball mill [57].

In the Szegvari attritor mill that we used in this study, the powder to be milled is charged into a vertical tank filled with grinding media. Both the powder and grinding media are then agitated by an impeller with arms causing the media to exert shearing and impact forces on the powder particles leading to repeated fracture and welding as seen in Figures 6 and 7. This action produces extremely fine and homogenous dispersions powder particles. Attritors have the advantage of large-scale production with capacities between 0.5 and 40 kg which can be milled at a time. The velocity of the grinding medium in the attritors as linear velocity is much lower (about 0.5 m/s) than in the planetary or SPEX mills, and consequently the energy of milling in the attritors is low [57].

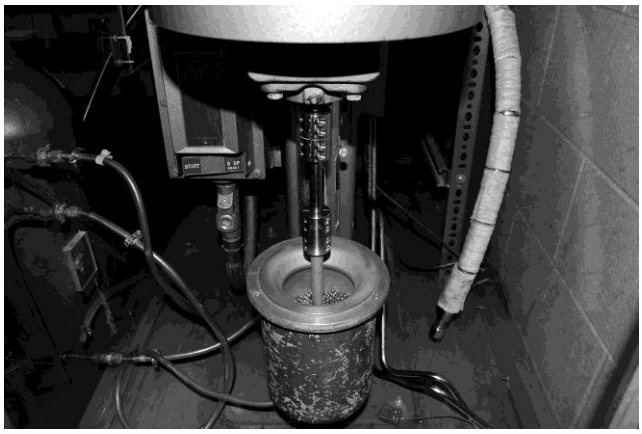

Figure 6: The Szegvari attritor mill. Professor Alex Aning's lab, MSE VT, Blacksburg, VA

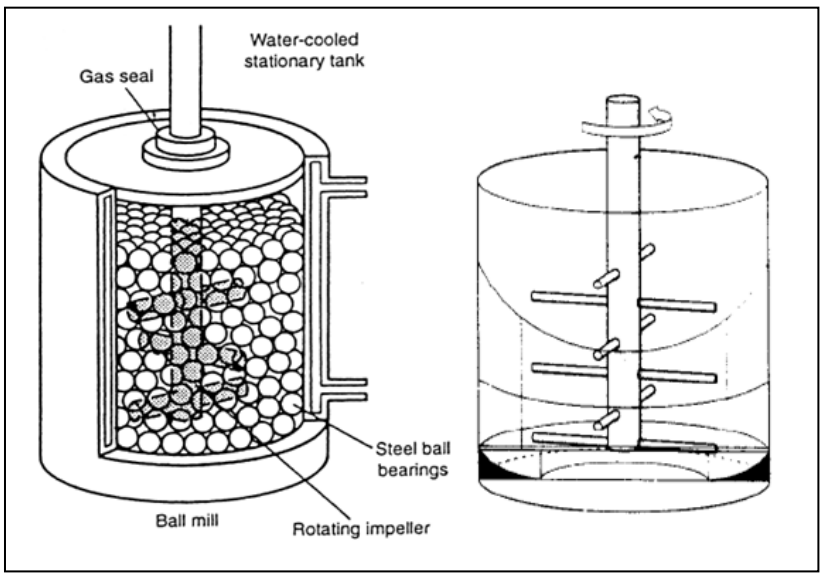

Figure 7: Diagram of the components of the stationary tank of an attritor mill [57].

High-energy ball milling is a complex process, which requires optimization of many parameters to achieve the desired product. The parameters of important a during the mechanical alloying process are grinding or milling media type, atmosphere, process control agent (PCA) and the input energy parameters such as charge ratio, milling time, milling speed, and milling temperature [57].

Grinding media, the contamination arising from the grinding media (vial and balls) is of great importance during the material processing. The degree of contamination depends largely on the mechanical properties of the powder that is being milled, as well as the chemical affinity of the material to some of the elements of the milling media [60]. For example, during the milling of Ni for 24h by SPEX milling, the Fe contamination was 13.6 wt%, while Nb, milled at the same parameters developed only 4.03 wt% Fe contamination [61]. Also, high energy mills systems such as the SPEX mills with longer milling times have big effects on the milled material due to the increased amount of contamination [57]. Occasionally, the level of contamination could be significantly high. For example, over the synthesis of Ni-AL alloys by using stainless steel vials and balls, the Fe contamination gets values of up to 18% [62]; Fe contamination has also been as high as 33% in some Tungsten milling experiments [63]. The suggestions to control and reduce this issue are: use low energetic mills whenever possible, inert milling media, and tungsten carbide vials and balls are also preferred. Sometimes, the milling media are built up from the same material as the powders, although this can often become technologically difficult and expensive [57].

The control of the milling atmosphere is also an important issue during the milling process and involves prevention of any undesired reactions of mechano-chemical nature or contamination that could happen in the product materials. When using milling process in air atmosphere, the product will contain a significant amount of contamination from oxygen and nitrogen [57]. Usually these effects are not desirable, and the best way to overcome this issue is by carrying out the milling process under the vacuum or in an inert gas, such as argon or helium [57].

Mechanical alloying may not be a successful and feasible process if the balance between the cold welding and fracturing of the powder particles is not achieved [57]. Without adding a process control agent (PCA) into the powder matrix during milling, cold welding will dominate

and the particles will agglomerate [57]. A PCA acts as a lubricant or surfactant, absorbs on the surface of the powder particles, and limits cold welding; and a typical PCA used in high-energy ball mills is stearic acid, with a concentration of 1-5 wt% of the total powder charge [57].

The other important parameters, which should be considered, are called input energy parameters (milling time, charge ratio, milling speed, and milling temperature). The time that is spent on the milling is the most important parameter. However, milling time used to achieve a steady state between the fracturing, cold welding and diffusion of the powder particles which they have influence on the powder microstructure and phase evolution when changing milling time and milling system type [64-66]. In fact, the milling time required for a mechanical alloying process varies depending on the type of milling system used, the type of material, the ball-to-powder ratio and the temperature of milling [57].

Charge ratio is the ratio of the weight of the balls to the powder and it has a significant effect on the milling time. However, the milling process with higher charge ratio has shorter processing time because of the increasing of the number of impacts events which means more energy transferred to the powder particles which is explained by increasing the kinetic energy per unit mass of ball mill powder, and consequently milling process takes place faster [57]. For example, the Ti-Al powder mixture was milled by SPEX to produce amorphous phase took 7 hours with charge ratio of 10:1, and it took 2 hours by using charge ratio of 50:1, and only 1 hour by using charge of 100:1 [57]. Lisboa et al. showed that when milled $Al_{50}Si_{30}Fe_{15}Ni_{15}$ by SPEX 8000 for 40 hours with charge ratio of 15:1 and 95 hours with charge ratio of 10:1, both the milled gave almost similar patterns considering phases, position of crystalline peaks and relative intensities [67].

Milling speed is one of the important parameters that affects mechanical alloying products. The mechanical alloying processes with the higher milling speed have higher input energies compared with the lower milling speed because of the increasing the number ball collisions with the charge powder and therefore increasing mechanical alloying process [57]. Therefore, it is easy to form a homogeneous alloyed microstructure or uniformly dispersed particles in the matrix, and amorphous due to the increase of the strain and defects concentration as the milling speed increased [68]. Sadrnezhaad et al. reported that the amounts of amorphization and diffusion for Ni-Ti powder mixture that was milled by a vertical attritor, are functions of the

milling speed and other input parameters [69]. In contrast, very low rotational speeds lead to very long periods of milling and a large inhomogeneity in the alloy because of inadequate energy input [70]. On the other side, very high milling speed leads in a reduction of milling time and thus effectiveness of alloying decreases because of the decrease in time available for diffusion of the solute. Also, very high milling speeds originate greater contamination due to the excessive heat and wear between the balls by themselves or with the vial walls [70].

Milling temperature is also an important parameter, and must be considered during the mechanical alloying process because of its influence on the final structure of the milled powder. However, during mechanical alloying, some of the mechanical energy converts to heat through plastic deformation. Also, the nature of the exothermic chemical reactions that happen during the milling process is another cause to the increase of the temperature. The increasing of the temperature, higher concentration on the lattice defects, and larger grain boundary surface accelerate the diffusion processes [57]. Since diffusion processes are involved in the formation of alloy phases irrespective of whether the final product phase is a solid solution, intermetallic, nanostructure, or an amorphous phase, it is expected that the milling temperature will have a significant effect in any alloy system [57]. For example, "during planetary ball milling of a Cu-37at%Ag powder mixture, it was noted that a mixture of an amorphous and crystalline (supersaturated solid solution) phases was obtained on milling at room temperature; instead, only a Cu-8at%Ag solid solution was obtained on milling the powder at 200°C. Similar results were also reported by others in the Cu-Ag, Zr-Al, and Ni-Ag alloy systems and were explained on the basis of the increased diffusivity and equilibration effects at higher temperatures of milling [57]." Milling at lower temperatures, such as cryomilling, has been shown to reduce the time required to produce nanocrystalline materials. For example, Al powder was milled for 20 hours by a high-energy ball mill at room temperature produced a grain size of approximately 25 nm, while it took 8 hours of milling in a Szegvari cryomill to achieve the same result [71].

Mechanical alloying has achieved great success as a processing technique for preparation of alloyed powders or composites in powder form [57-58]. In the early 1980s, the era of the 'Solid State Amorphization' (SSA) was started by using a mechanical alloying technique [72] which did not confine on the SSA materials only, but also it drove up and spreaded to include many different synthesized materials, such as nanocrystalline materials [73], stable and metastable

materials [57], composites and nanocomposites materials [74-75], and intermetallic compounds [76]. MA widely applied to metallic systems, but in the late of 1980s, and early of 1990s Shaw and coworkers studied the possibility to use mechanical attrition to the polymeric materials for blending and alloying and its effects on the structure and properties of the processed material [77-80]. Subsequently, others have studied milling-induced changes in the structure of several semicrystalline and amorphous homo-polymers [18, 81-93]. Recently, MA was used for preparing binary polymer/polymer mixtures and to disperse nano-fillers into polymer matrices [93-95]. We used the mechanical alloying attritor technique in this work to obtain composite powders with improved reinforcement distribution and also to study this process by means of some process parameters and their influence on some of the material properties.

2.3.1 Mechanically alloying polymer

Mechanical alloying of polymeric materials career is a relatively new technique; however, the ideas and concepts to use mechanical alloying for processing polymeric materials appeared for the first time by Shaw in 1988 [96], where he and his team presented through their preliminary experiments in early of 1990s the possibility of using mechanical alloying technique for processing polymeric materials and the extent of its implementation and promising on the future [97-98]. Shaw's team has studied and characterized cryomilling for several types of thermoplastic polymers, including polyamide (PA), and polyethylene (PE) as singly processing and equal mixture [96], also Pan and Shaw studied polypropylene (PP), polystyrene (PS), acrylonitrile-butadiene-styrene (ABS), ultra high molecular weight polyethylene (UHMWPE), PA- UHMWPE and PA-ABS blends [77-80, 97-100]. After initial efforts and success to Shaw's team, many studies have been conducted in order to use MA for polymer processing. For example, Ishida reported a study about MA for PTFE and PE as milled separately and as 50/50 blends [81]. In this study, the MA was carried out in a high-energy vibration ball-mill under an argon atmosphere and charge ratio of 70:1, using stainless steel balls. Also, Farrel et al. studied MA and MM blends of PP and Vectra B950 by using a SPEX 8000 mixer/mill with charge ratio of 4:1 [18]. Castricum et al. also had work on milling pure polymer and structure phase transformation, including PS and polyethylene glycol (PEG) by using a vibratory mill and PE by using planetary mill [82]. In contrast, Font et al. have studied several works on polymeric materials, using centrifugal ball mill to amorphize the organic compounds sucrose and PET [83],

and PBT as well as alloying of PET/PBT [93]. Also, Font's group studied prepared binary mixtures of poly(etherimide) (PEI) with poly(ethylene terephthalate) (PET), poly(butylene terephthalate) (PBT), and poly(ether ether ketone) (PEEK) by centrifugal ball mill [92]. More studies on MA of polymeric materials were by Archie P. Smith et al. at North Carolina State University (NCSU) [85-91, 101-105]. The NCSU group has studied Vectra and PET with different degrees of crystallization, relied to use MA to get a refined microstructure on a smaller scale than is achievable by conventional melt processing [85, 91, 105]. On other works, NCSU group have studied poly(methyl methacrylate) (PMMA), poly (ethylene-alt-propylene) (PEP), and polyisoprene (synthetic rubber, SR) [86, 88-103]. Thereafter, NCSU group started studying phase morphology to the polymeric materials included PMMA/SR and PMMA/PEP, processed by MA, using scanning electron microscopy, transmission electron microscopy, scanning transmission X-ray microscopy (STXM) and near-edge X-ray absorption fine structure (NEXAFS) microscopy, which takes advantage of the differences in relative X-ray absorption of the two polymer components in the mechanically alloyed blend [85-91, 101-105].

Later, many studies with different ideas and concepts have been done [94, 95, 106-114]. For example, using MA for coating a ceramic ($BaTiO_3$) with a polymer (LaRC-TPI) for composite grain boundary capacitor applications [106], and study the miscibility of low density polyethylene (LDPE) and isotactic polypropylene (ìPP) by (CO_2 assisted mechanical alloying) [107]. Other studies like cryogenically mechanically alloyed polymer–polymer system polycarbonate (PC) and poly(aryl ether ether ketone) (PEEK) [108], cryogenically milled post-consumer mixed plastic waste stream consisting primarily of PP and PE [109], and morphology changes on Ultra-high molecular weight polyethylene (UHMWPE) milled by MA [110].

Recently, Nanoscale Polymer Blends via Mechanical Milling takes place in the MA application [94, 95, 111-114]. For example, a study of Acrylic/nano-silica composite latexes prepared by blending via high shear stirring and ball milling [94], effects of ball milling dispersion of Nano-SiO_x particles on impact strength and crystallization behavior of Nano-SiO_x–Poly(phenylene sulfide) Nanocomposites [95]. Azhdar et al. studied the efficacy of preparing composite powder of nickel-ferrite ($NiFe_2O_4$) nanopowders and ultrafine PMMA, by comilling the mixture of PMMA and $NiFe_2O_4$ in the solid state by low-temperature mechanical alloying, and producing polymer nanocomposite PMMA/$NiFe_2O_4$ using high-velocity cold compaction

[111]. In contrast, Zhang et al. have studied mechanical properties of PEEK/nano-SiO_2 composites compounded using a ball milling technique [112]; also, Jose´ et al. reported that the high energy milling can be used as processing technique for polymer matrix nanocomposites and as an effective approach to disperse ceramic SiO_2 nanoparticles in a polymer matrix of epoxy[113]. Whilst, Vertuccio et al. worked on nano clay reinforced poly(ε-caprolactone) (PCL)/starch blends obtained by high energy ball milling [114].

2.3.1.1 Particle Size

Through the studies mentioned above, we concluded that the mechanical milling gives rise to the reduction of the particle size of the milled powders with increased milled time [77, 81, 90, 91, 97, 99, 105]. For example, Pan and Show [97] reported that the PA particle size is a function of time, when they used cryogenic MM. However, the reduction of particle size happens rapidly and considerably in the first 6 hours, after that it keeps continuing on, but with a much slower rate as seen in Figure 8.

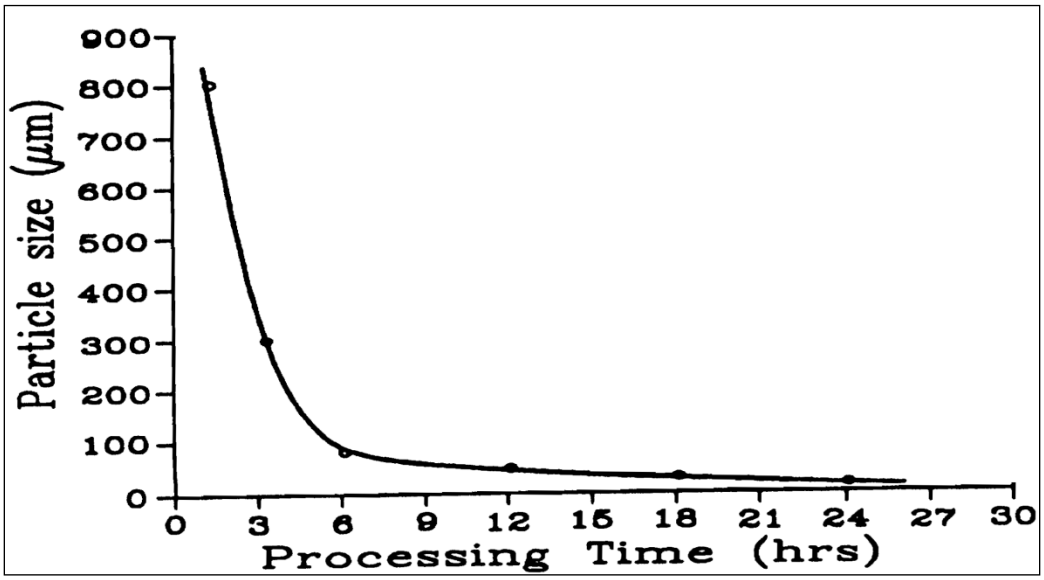

Figure 8: PA particle size vs. milling time for PA powder milled by cryogenic mill at -150°C [97].

Also, Ishida [81] observed the reduction of particle size and the effect of milling time on particle size for the PTFE/PE mixture powders, when using the high-energy vibration ball-mill for mechanical alloying of PTFE and PE. After 1h of milling, agglomerated flattening has been

obtained, and after 5h of milling, rapid reduction in powder size occurs, and after 25h of milling the degree of decrease in the powder size becomes small as seen in Figure 9.

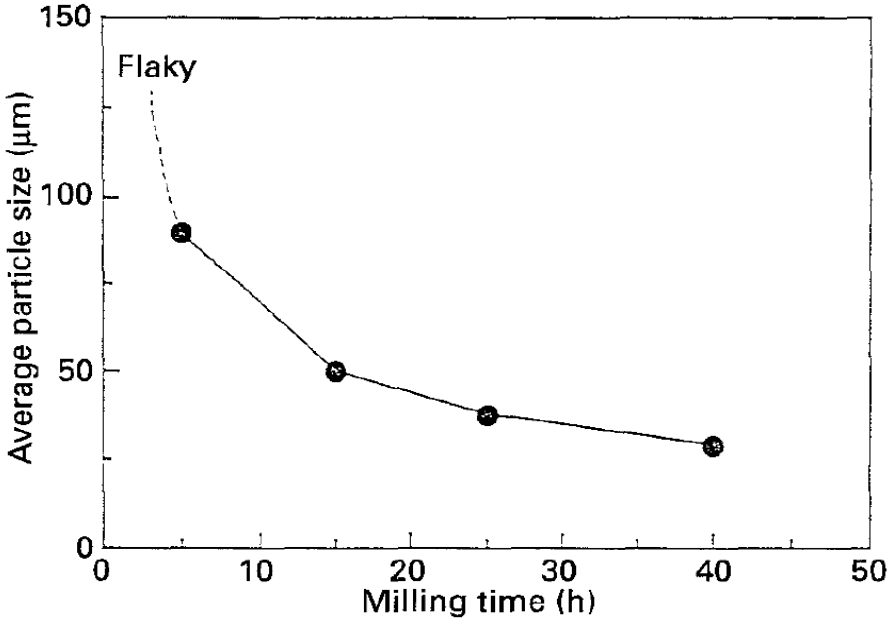

Figure 9: Average of particle size as a function of milling time for PTFE/PE mixture powders [81].

Other work done by Smith et al. [90] using cryogenic MA to blend the PMMA and either PEP or PI resulted in particle size reduction being effected over time in the high-energy ball mill, as was a reduction in crystallite grain size, both of which reached minimum values at extended milling times. In contrast, when using MM on polymeric materials at room temperature, it will note an initial increase in average particle size as flake-like agglomerates form, and a reduction in size at longer milling times occurs as a complex deformation field in which shear, multi-axial extension, fracture, and cold welding proceed concurrently [91].

2.3.1.2 Crystallization and Crystal Structure

Through mechanical milling and alloying polymeric materials has also been shown that a crystal structure transformation amorphization or happens, which is in a way similar to metals [93, 105, 115]. However, the transformation could occur by changing in the degree of the polymer crystallinity by reduction in crystallinity or complete amorphization and depend largely on the nature of each polymer [80, 81, 83, 99].

Shaw et al. in studies of MM and MA for PA and PE [78, 79, 97, 99, 100] reported that when characterized the solidified PA and PE milled and regular thermal PA and PE by using X-ray diffraction, the mechanically processed PA and PE showed a decrease in the amount of crystallinity compared to the regular thermal materials. Also, the crystal structures had been altered somewhat due to special interactions between the molecules such as chemical reaction and physical interpenetration.

Font et al. [83] have reported that there is a complete amorphization for the sucrose and PET with increasing the milling time and differences between the amorphization and crystallization that produced by MA and melt quenching as shown in Figure 10.

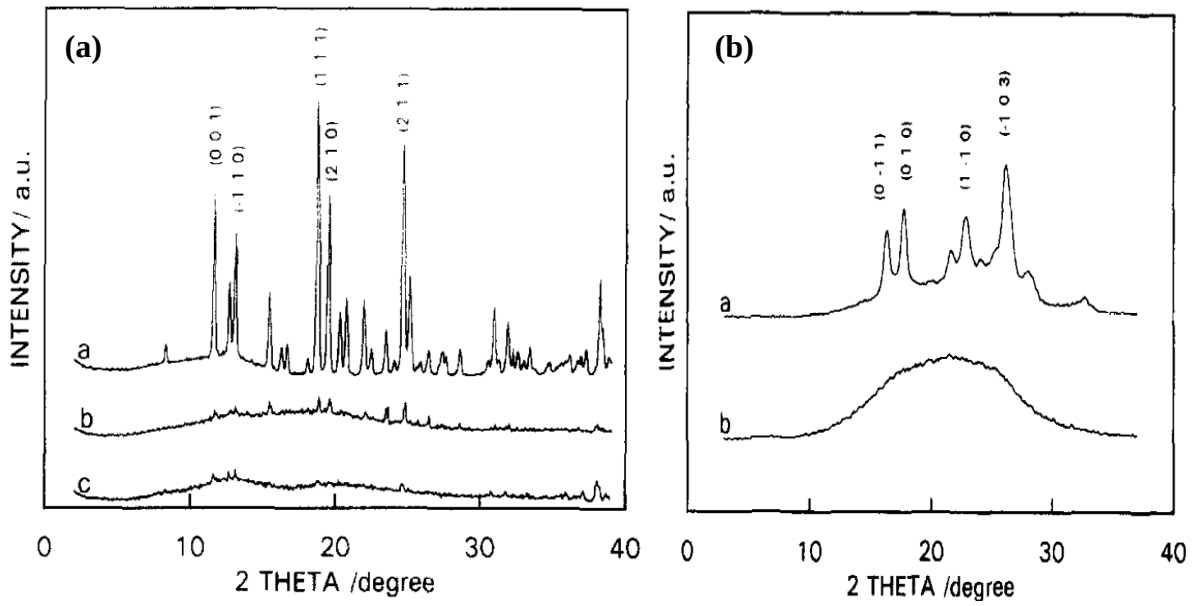

Figure 10: (a) XRD patterns of Sucrose: a: crystalline, b: amorphous produced by quenching, and c: amorphous produced by ball milling for 60h. (b) XRD patterns of PET: a: produced by slow cooling from the melt, and b: amorphous produced by ball milling for 20h [83].

In contrast, PBT milled for 8 days in work done by Font et al. [93], showed no noticeable effects by ball milling and only a little smoothing of the diffraction peaks as seen in Figure 11, also in this study they worked on blends of PET and PBT and they found the amorphization of PET within the blend and that the differences in recrystallization depend on the concentration of PBT present as shown in Figure 12.

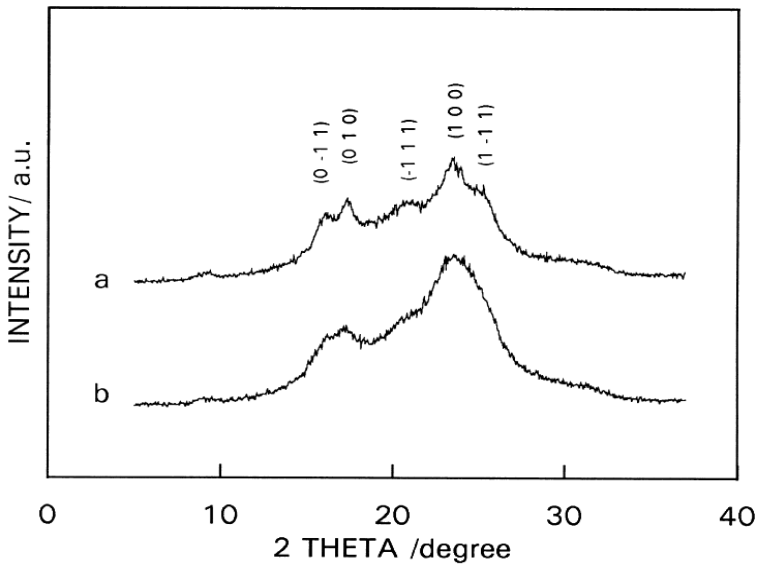

Figure 11: XRD patterns of PBT: a: as received, and b: as milled for 8 days [93].

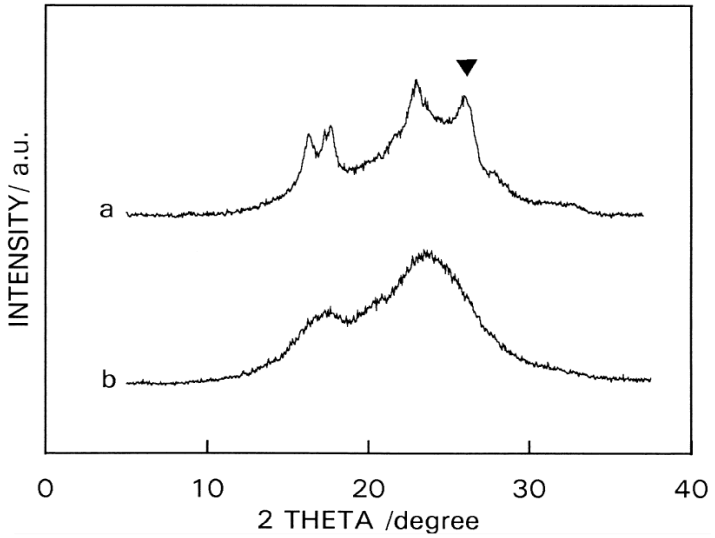

Figure 12: XRD patterns of 50% PBT/PET mixtures: a: unmilled mixing and b: prepared by milled for 15h. (-103) reflection peak of PET is indicated in curve a by ▼ [93].

Also, Font et al. in another work on semicrystalline PEEK reported that partial amorphization has been created by using ball milling [115], and Figure 13 shows that the diffraction pattern of milled material being smoother than that of unmilled PEEK. Therefore, X-ray diffraction results confirm the recrystallization of the fraction of material amorphized by ball milling.

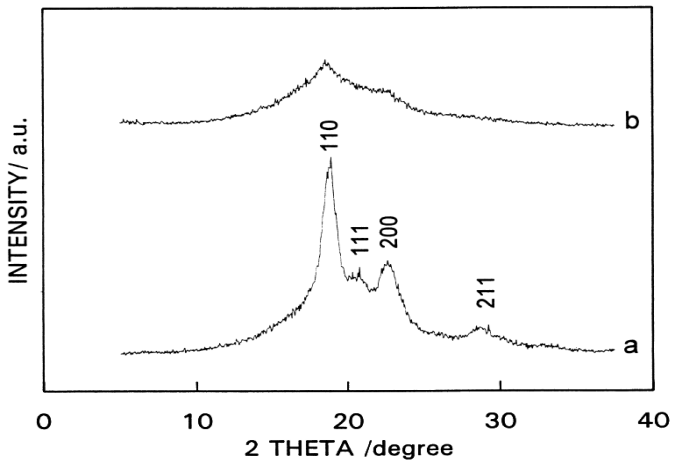

Figure 13: Room temperature XRD patterns for PEEK samples: (a) unmilled, and (b) milled for 24h [115].

Also, Martin and Kander [108] reported a complete amorphous material occurring in PC/PEEK system, prepared by cryogenic MA for 10 hrs as seen in Figure 14.

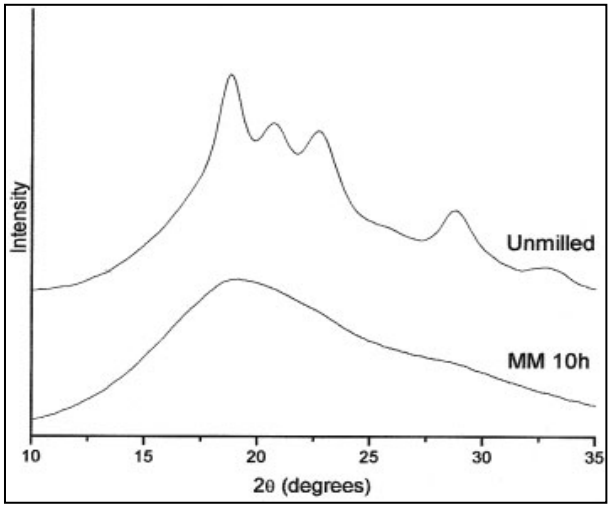

Figure 14: WAXD spectra of semicrystalline, unmilled PEEK and amorphous PEEK MM 10h [108].

Ishida characterized PE, PTFE and PE/PTFE before and after 26h of ball milling by using X-ray diffraction [81]. The results showed that the XRD lines of the PTFE and PE processed

individually became broadened and with less intensity after ball milling as shown in Figures 15 and 16, respectively.

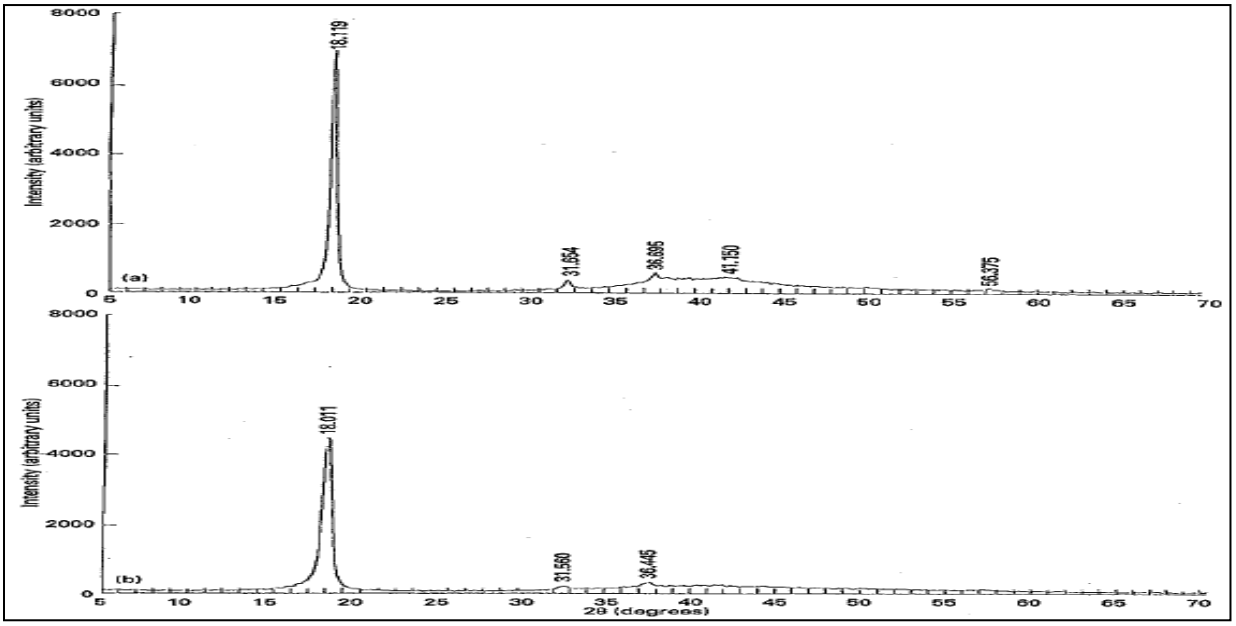

Figure 15: XRD patterns for PTFE (a) before and (b) after 26h of ball milling [81].

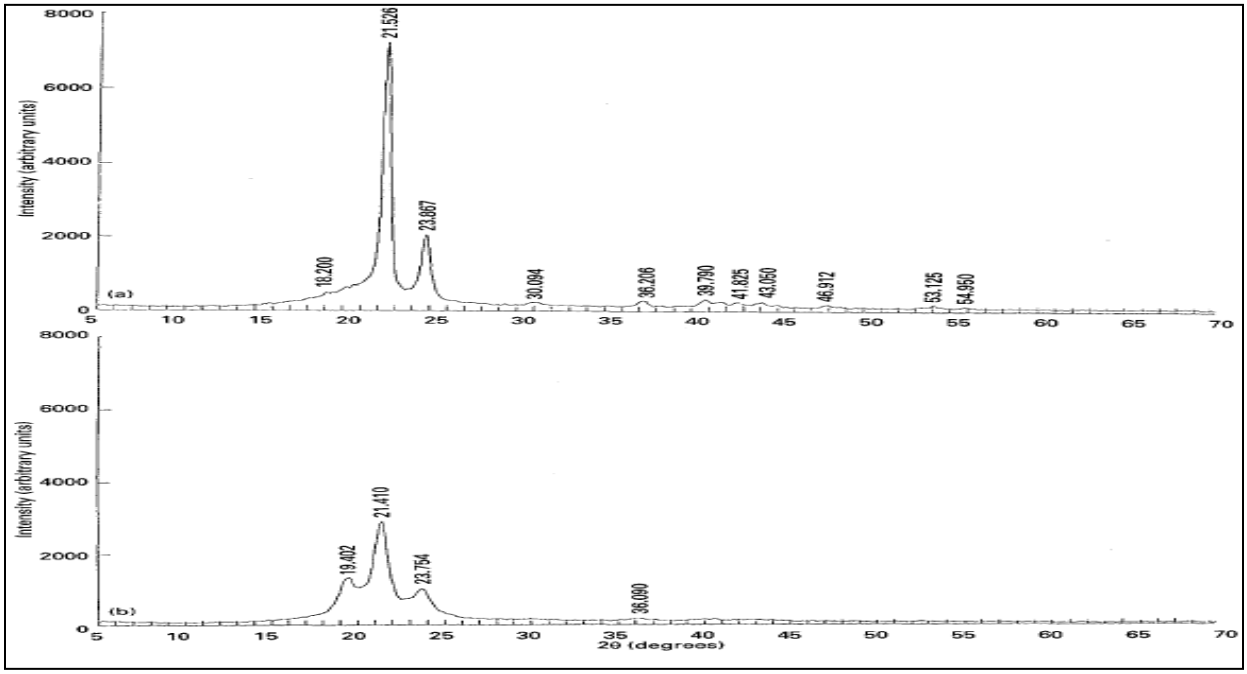

Figure 16: XRD patterns for PE (a) before and (b) after 26h of ball milling [81].

The PE displayed more affected than the PTFE because the amorphization of PE is affected faster than that of PTFE; also PE after MM shows a change in the crystal structure by transformation from monoclinic to orthorhombic. In case of PTFE/PE the XRD patterns in Figure 17 showed that the peaks become broadened due to the strains that develop and because of reduction in the particle size and peaks of PE are lowered as amorphization is approached, while there is considerable residual crystalline peak of PTFE. Therefore, mechanical alloying of polymer systems has the possibility of the producing amorphous powders.

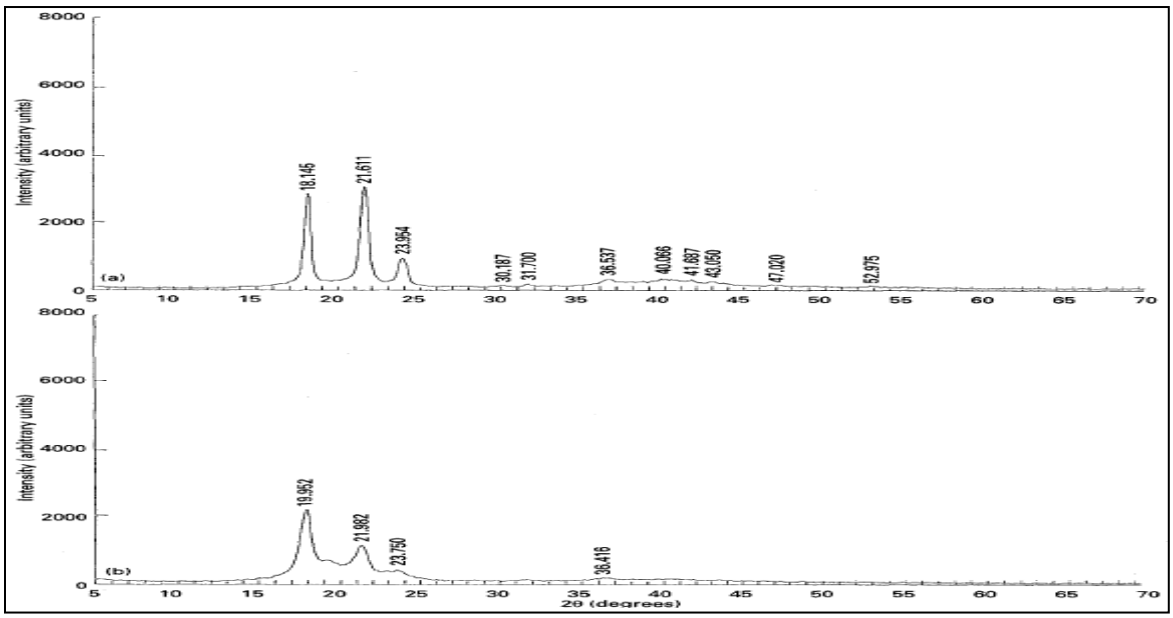

Figure 17: XRD patterns for PTFE/PE (a) before and (b) after 26h of ball milling [81].

Castricum et al. also reported that an almost complete phase transformation from the orthorhombic to the monoclinic structure happened to the HDPE milled by planetary milling technique [82]. The XRD patterns in Figure 18 showed the phase transformation from the orthorhombic to the monoclinic structure and the effect of the milling time on the degree of transformation. Also, Castricum reported that HDPE with flakes shape was used, the transformation was most complete. Castricum concluded that the degree of transformation depending on the milling time, molecular mass, particle size and shape of the polymer.

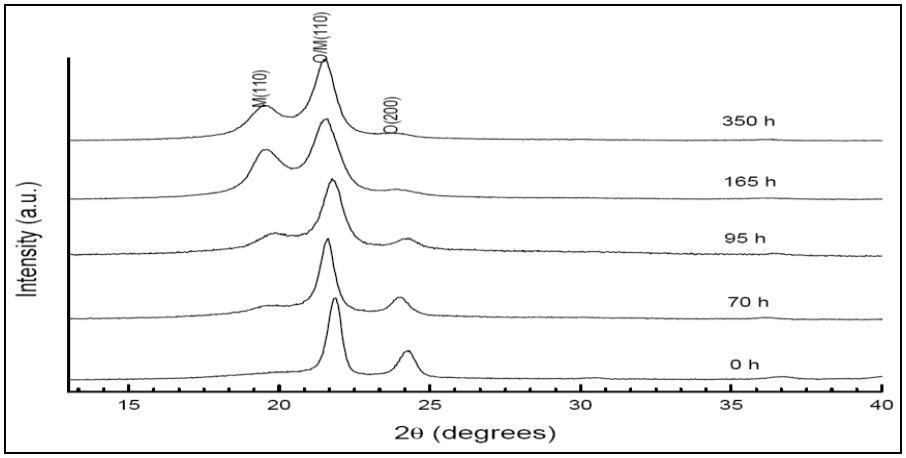

Figure 18: XRD patterns for HDPE after various periods of milling [82].

Gabriel et al. [110] also noted that phase transformation took place in UHMWPE, using different techniques of High-energy mechanical milling. The XRD patterns in Figure 19 showed the phase transformation from the orthorhombic to the monoclinic. This work proved that larger phase transformation occurred for the UHMWPE milled in attritor mill; and Gabriel thought that happening due to the high intense shear forces between the polymer and the milling balls and/or to the smaller temperature achieved into attritor drum.

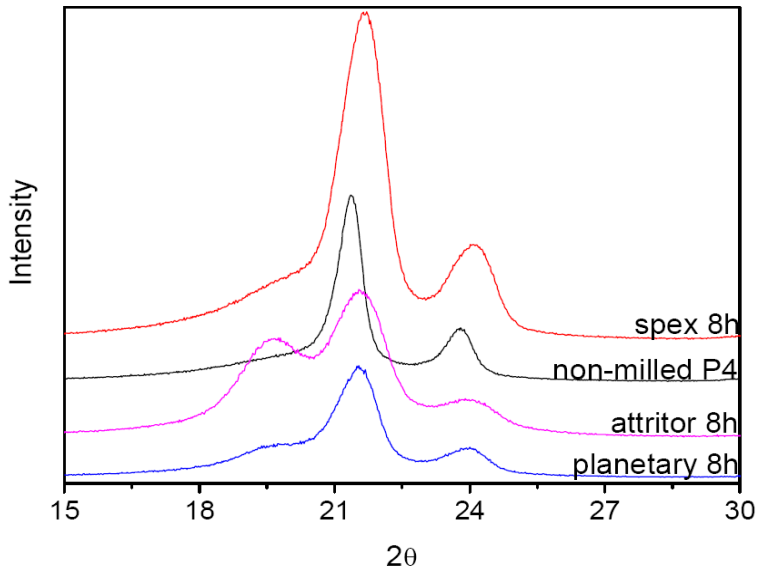

Figure 19: XRD patterns for UHMWPE: non-milled P4 and polymer milled in planetary, SPEX and attritor mills for 8h [110].

Balik et al. [91] at NCSU reported that amorphous occurs to PET during mechanical milled at room temperature and at cryomilled, whilst a changing in crystallinity occurs very rapid and occurring within the first hour of milling when milled at room temperature. Balik explained that the PET molecules become aligned with their phenyl rings in a stacked parallel arrangement, but such stacking is lost upon further milling and the molecules become rotationally disordered about the chain axis as seen in the Figures 20 and 21 for WAXS. The degree of crystallinity increases for PET samples with an initially low crystallinity, and tends to decrease for samples with an initially high crystallinity. Also, through observation, the effect of milling time on crystallinity for the low crystallinity samples appears very similar to that of annealing the sample at 190°C.

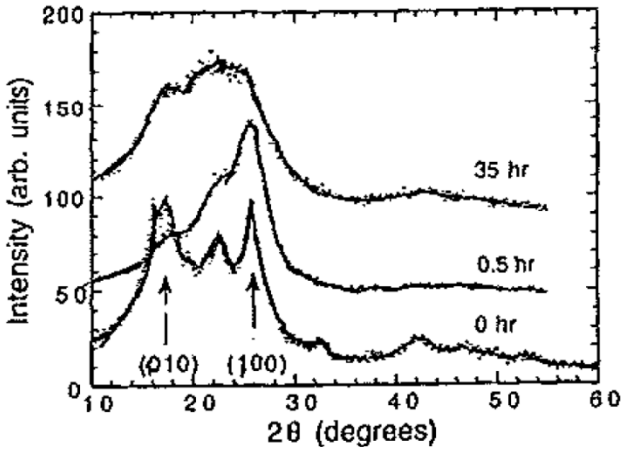

Figure 20: WAXS patterns of high crystallinity PET milled at room temperature [91].

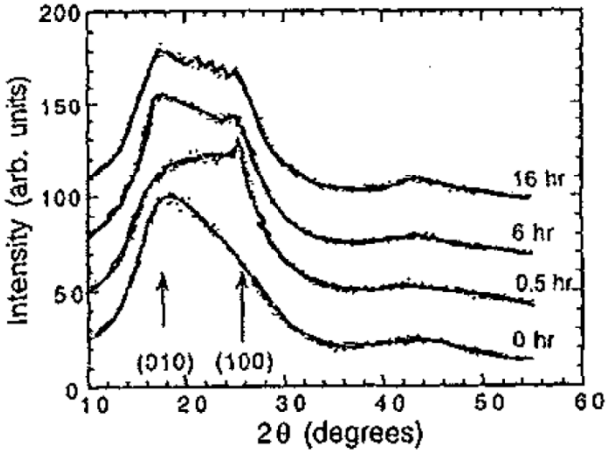

Figure 21: WAXS patterns of low crystallinity PET milled at room temperature [91].

Also, in another work at NCSU simillar to Balik's work, but more complete study to the effects of MM on PET done by Bai et al. [105] have been confirmed Balik's results and observations. WAXS Figures 22, 23, and 24 show same results on Balik's work.

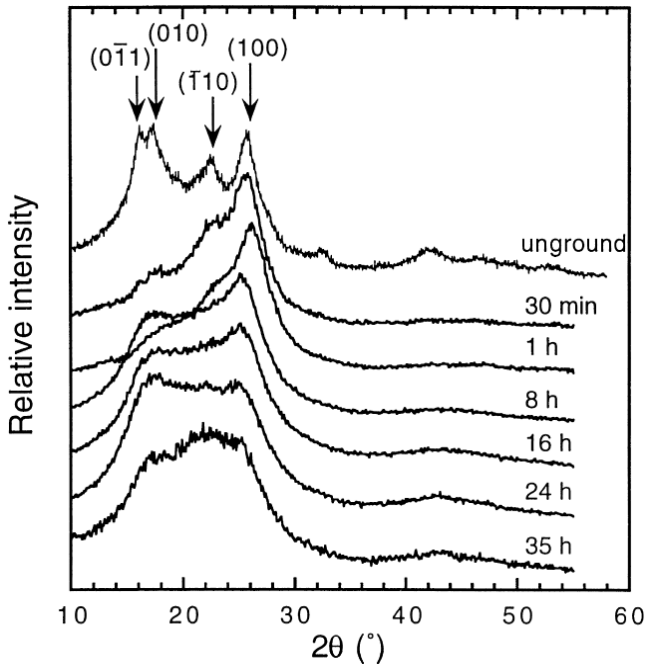

Figure 22: WAXS patterns of high crystallinity PET milled at room temperature [105].

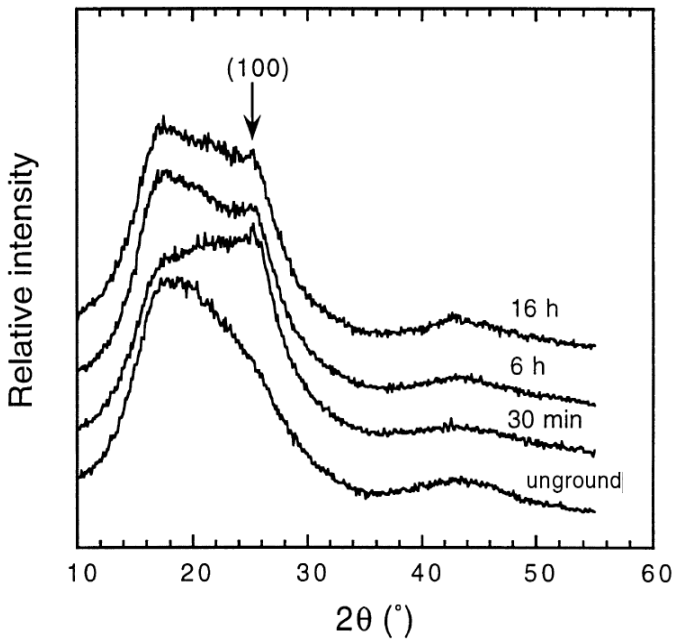

Figure 23: WAXS patterns of low crystallinity PET milled at room temperature [105].

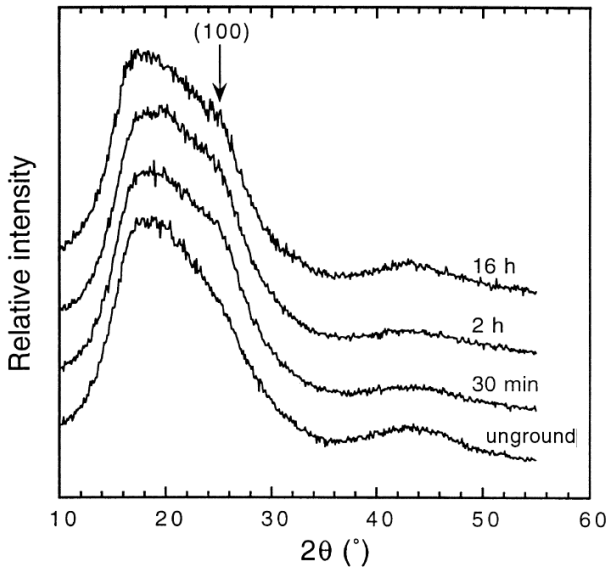

Figure 24: WAXS patterns of low crystallinity PET cryomilled at – 180 °C [105].

In contrast, Farrell et al. [18] in studying for PP MM reported that PP milled for 4h did not show any change in crystalline structure or the degree of crystallinity, and it was evidently clear from XRD pattern as shown in the Figure 25.

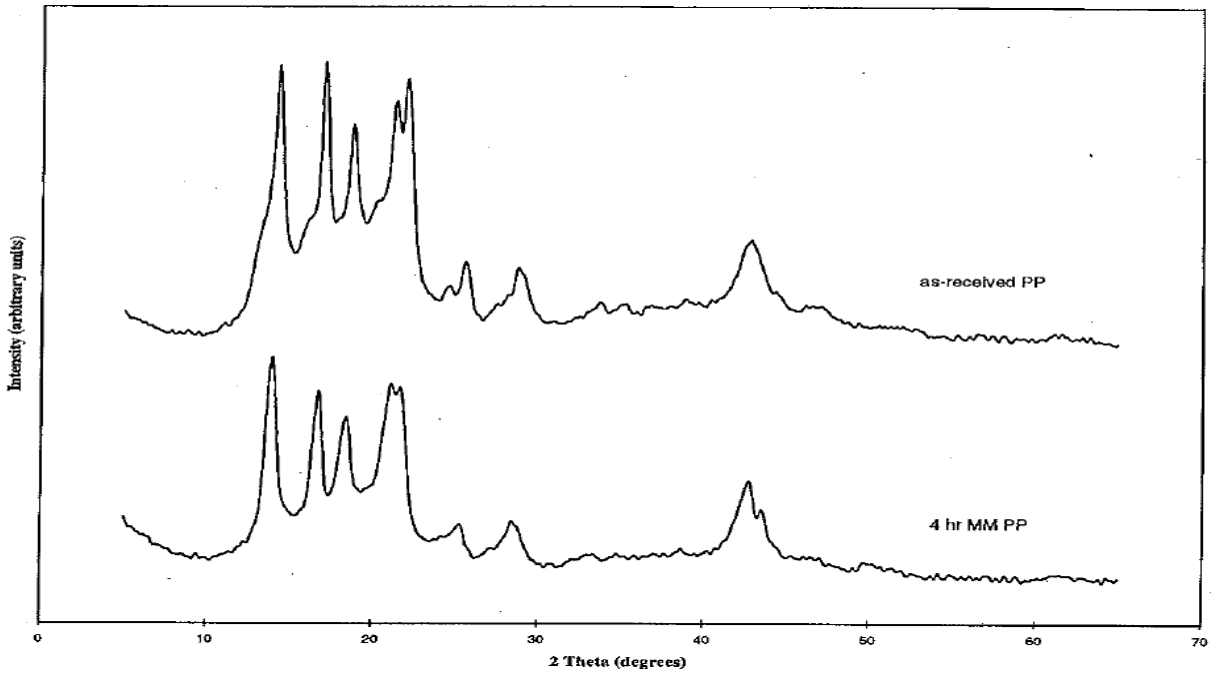

Figure 25: XRD patterns for PP: as- received and milled 4h [18].

2.3.1.3 Thermal Properties

As the MM and MA causes reductions in the particles size of the material by repeating the fracturing, deforming, cold welding, and diffusing together to these particles, with increased milling time. Since we are regarding polymeric materials, a reduction in molecular weight or polymer degradation is expected; and this degradation leads to changes on the polymer properties such as mechanical, and physical. Thus, many studies have looked into the effect of MM and MA on the thermal properties for several different polymers.

Work done by Smith et al. [87] at NCSU using high energy mechanical milling to mill the PMMA, PI, and PEP showed that the milling of PMMA with three different grades in number- and weight average molecular weight showed decreasing in glass transition temperature with increasing the milling time and milling temperature. Figure 26 shows the relation between the change in glass transition temperature (ΔT_g = milled glass transition temperature – unmilled glass transition temperature) and milling time. Also, PEP milled via cryogenic mechanical milling showed decreasing in glass transition temperature; however, the rate of the decreasing glass transition temperature is much slower compared with the PMMA case as shown in Figure 27.

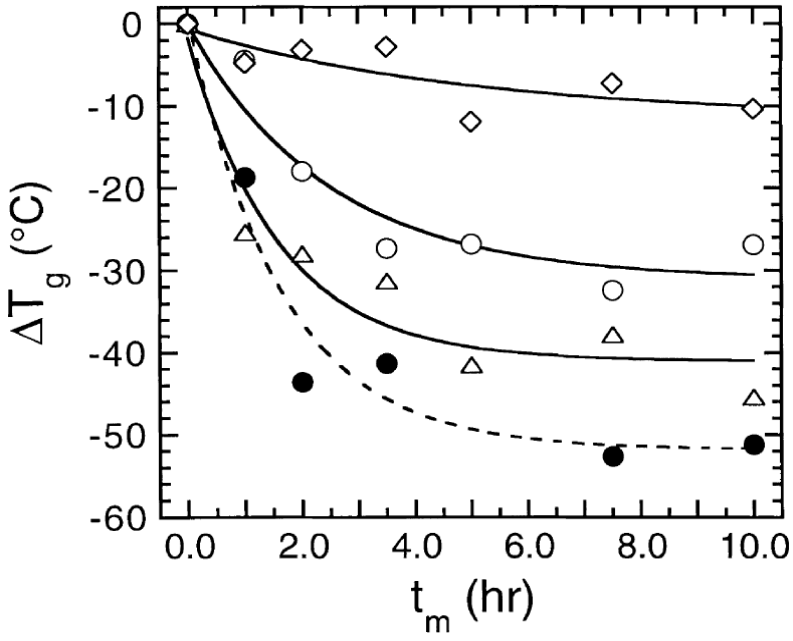

Figure 26: The relationship between the change in glass transition temperature ΔTg and milling time: cryomilled h-PMMA (○), ambimilled h-PMMA (●), m-PMMA (Δ) and l-PMMA (◊).The lines (solid for cryomilled samples and dashed for ambimilled samples) [87].

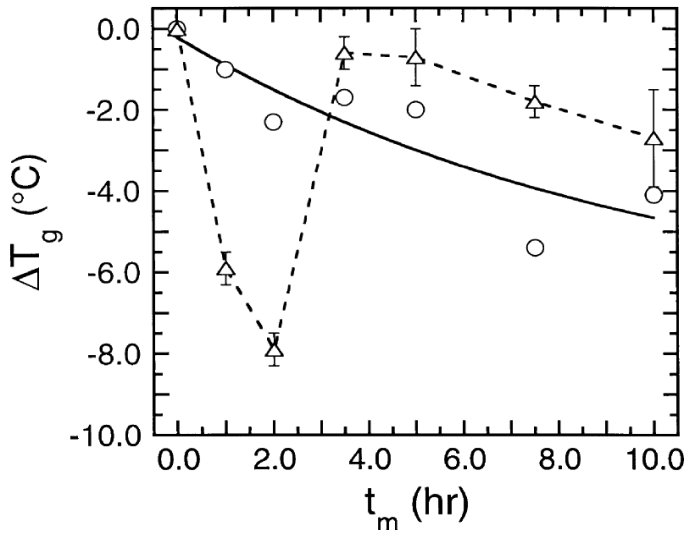

Figure 27: The relationship between the change in glass transition temperature ΔTg and milling time: cryomilled PEP (○) and PI (Δ) [87].

Cryomilled PI also exhibited reduction in glass transition temperature but behaved differently in that the decrease was in the glass transition temperature. Where, the glass transition temperature initially increased and reached a sharp maximum point at a relatively short time about 2h subsequently decreased almost back to zero, increasing slightly from zero by about 2.78°C after 10h, as illustrated in Figure 27 by the relation between the ΔTg and milling time. Smith et al. explained that the PI chains undergo chemical crosslinking during cryomilling. They conceive that with the higher non-equilibrium conditions, two things are happening: (a) a dynamic competition between chains breaking resulting in a decrease in molecular weight, and (b) a crosslinking enhancing an increase in molecular weight.

Also in another work at NCSU, Balik et al. [91] reported that melting temperatures (T_m) of PET increase slightly for milled samples at room temperature, whereas cryomilled samples showed a relatively constant T_m with milling time. In contrast, the crystallization temperature (T_c) of PET showed a decrease from about 130°C to 100°C after 2 hrs of low crystallinity PET in both cases of the milling, room temperature milling and cryomilled. While, T_c for high crystallinity PET decreased to 100°C after 20 min of milling at room temperature and remain constant thereafter. Also in this work, Balik has been covered Vectra and blends of Vectra with a PET via MA, and resulted that the T_m of Vectra milled at room temperature exhibited decreasing

from about 283°C to 274°C after 16h. Whereas, PET/Vectra exhibited essentially the same features as pure PET since the magnitude of the thermal changes occurring in Vectra are relatively insignificant compared with PET.

Font et al. [83] in studying for sucrose and PET to create amorphous by ball milling noted that the temperature of the exothermic crystallization for the amorphous sucrose produced by ball milling can be observed with increasing in the T_c and enthalpy of crystallization as milling time increasing; whereas amorphous sucrose created by melting and quenched does not have it. As for the PET amorphous formed by ball milling for 20h exhibited lower T_g than the amorphous that was created by melting and quenched, while T_c for PET that is mechanically amorphized is higher than in PET quenched, just before T_m.

Ishida [81] have studied PE/PTFE prepared by MA for 40h and he found that there is a slight increase in T_m of the PE and a clear decrease in enthalpy of the PE, while PTFE showed decreasing in T_m from 338.4°C to 326.3°C and decreased a little bit in the enthalpy does not take into account. Also, Ishida noted that there is a reduction in the temperature of the start of decomposition after mechanical alloying of PTFE and PE and he concluded that PTFE and PE begin to become miscible with a mechanical alloying process.

2.3.1.4 Molecular Weight

Reduction in molecular weight for polymeric materials is as a result of expected in the process MM or MA. However, the repetition for the complex shearing, fracturing and deforming with continuing milling may leads to break the polymer chains and decrease molecular weight [116]. Since many polymer properties depend on the molecular weight, the decrease in the molecular weight leads to degradation of these properties. Therefore, measurement and calculation of molecular weight of a polymer milled or alloyed mechanically was taken into account in several studies for polymer MM and MA [82, 87, 90, 91, 97, 101, 105, 108, 116].

At NCSU, many studies led by Smith have been included measurement and calculation of the molecular weight for polymer milled or alloyed mechanically [87, 90, 101]. Smith et al. in these studies about the response of the PMMA, PI, and PEP to solid state processing using high energy mechanical milling, concluded that the molecular weight has decreased with significant chains breaking preferentially for all polymers milled, and it goes down more with milling time

increased as seen in the Figures 28. Other work done at NCSU to study structural changes in PET induced by mechanical milling, but this time led by Bia [105].

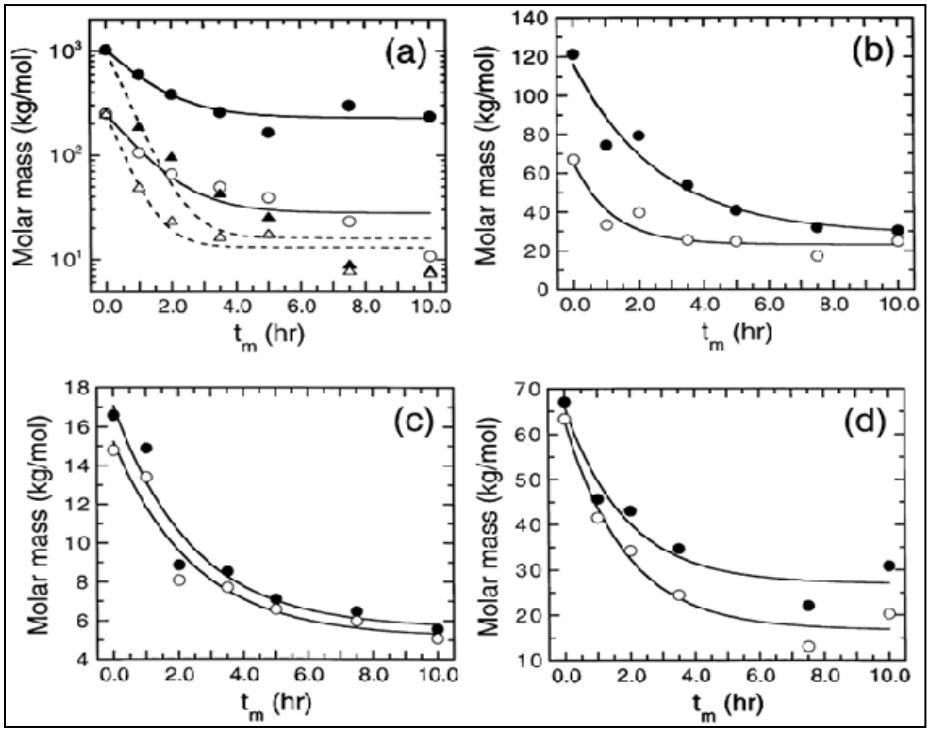

Figure 28: the M_n (open symbols) and M_w (filled symbols) vs. t_m: (a) high molecular weight PMMA subjected to cryomilling (circles, solid lines) and ambimilling (triangles, dashed lines); (b) cryomilled medium molecular weight PMMA; (c) cryomilled low molecular weight PMMA; (d) cryomilled PEP [87].

The decrease in molecular weight of PET upon milling was noted and this reduction in molecular weight of PET is more pronounced for ambimilled compared to cryomilled PET. Also, at NCSU, Balik et al. [91] confirmed Bia's work on the MM of PET that causes a significant reduction in molecular weight, more so for ambimilled than for cryomilled samples.

In the results reported by Martin and Kander [108] about the molecular weight for the PC and PEEK that cryogenically mechanically milled there is an indication of a very small decrease in the molecular weight of the PC milled for 10h. This decrease suggests that some chain degradation might have occurred during cryogenic MM of PC. Whereas, PEEK milled also for

10h showed significant decrease in the molecular weight which decreased from 33,500 g/mol to 20,628 g/mol.

In contrast, Castricum et al. [82] reported that there is no noticeable difference in the Mw, M_n or z-average molecular weights for PS, PE or PEG; this minimal difference means no molecular weight reduction. Castricum suggested that no bond breaking (scission) or chemical changes (crosslinking) took place during milling, and this suggestion exhibits the carbon-carbon bonds strong to break by the energy drove from MM.

At a complete contrast, Shaw et al. [97] noted that there is an increase in the molecular weight of ABS, prepared by MM (18,000 g/mol), compared with that prepared by thermal melt processing (17,000 g/mol); this probably increase in the molecular weight came as a result of crosslinking between the broken chains that produced by chain scission during milling.

2.3.1.5 Mechanical Properties

Pan and Show [78, 80, 96, 97, 99, 100] reported and believed that mechanical processing technique and alloyed polymers can produce a much stronger material than that prepared by traditional processes. They explained the enhancement or improvement shown in the mechanical properties due to the physical interpenetration occurring during MA at the molecular level between amorphous and crystalline regions.

For example, they [99] reported that some mechanical properties for polyamide have shown enhancement when using cryomilled for 24h. However, polyamide prepared by cryomilled for 24h and consolidated showed improvement in hardness, strength, and ductility compared with the traditionally melting process or mechanically cut material.

Also in another work, Pan and Show [80] observed that the hardness of PA and PE cryomilled for 24h have increased much higher compared to those of regular thermal melt material. They reported that the hardness were increased by 12.7% and 31.8% for MM PA and MM PE respectively, compared to those of regular thermal melt materials. Whilst, PA/PE on a 50:50 weight showed a large improvement in hardness around 33% compared to regular thermal melt PA/PE.

NCSU has published several research papers concerning the effects of MM and MA on the mechanical properties of polymeric materials [87, 89-91].

For example, Balik et al. [91] found that significant increase in Knoop hardness for MM of pure PET and Vectra at room temperature compared to the cryomilled. Also, MA of PET/Vectra at room temperature exhibited an increase in Knoop hardness compared to the cryomilled.

Also, Smith et al. [89] reported that there is a significant improvement in impact strength for the MI/PMMA/PI milled cryogenically for 5 hours. Smith's results showed that the impact strength exhibited an improvement with addition MI copolymer, even with low MI concentrations as seen in the Figure 29. Smith et al. explained that the MI copolymer and PI homopolymer can intercrosslink and toughen the PMMA matrix. The impact strength results in Figure 29 showed relatively constant up to 8wt. % copolymer and may reflect the number of molecules that are capable of chemically crosslinking during cryomilling. Also, in Figure 29, the author does not have full understanding of the increase in impact strength that arises when the concentration of MI copolymer reaches 10wt. %. Smith et al thought this increase probably due to the single-phase behavior that affects the impact strength of the blend because the STXM images showed that the sample with 10wt. % copolymer appeared as quasi-homogeneous. Whereas, the relation between the impact strength and milling time showed positive relationship until the continuous PI phase is formed, at which point the impact strength drops precipitously as shown in the Figure 30.

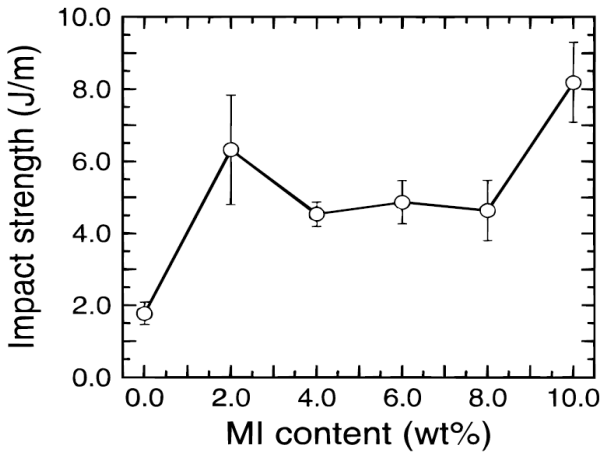

Figure 29: Impact strength Vs. MI copolymer concentration for PI/MI/PMMA blends cryomilled for 5h [89].

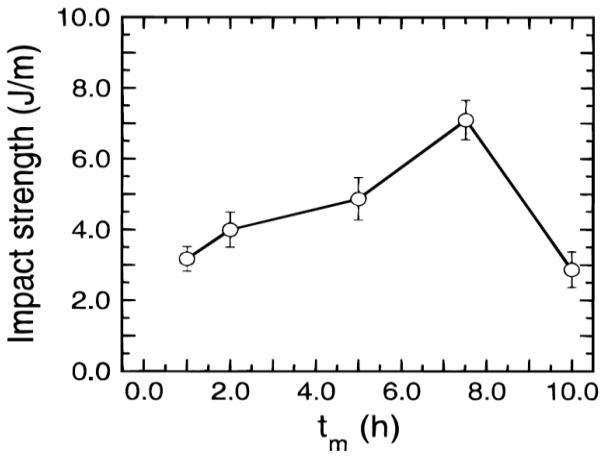

Figure 30: Dependence of impact strength on t_m for 22/6/72 wt % of PI/MI/PMMA blends [89].

In contrast, Smith et al. [87] observed a reduction in the impact strength of PMMA with increasing milling time, and this reduction in the impact strength comes as a result to the molecular weight reduction. However, breaking the chains leads to the reduction in molecular weight which increases substantially with increasing milling time; thus the reduction in the impact strength of the PMMA matrix has occurred to coincide with an increase in milling time.

In other works, Smith et al. [90] reported that the toughness of the PEP/PMMA milled cryogenically for 10h decreased monotonically with the increasing milling time, whereas the impact strength of PI/PMMA also milled cryogenically for 10h is nearly independent of milling time. The impact strength results of PEP/PMMA with concentration below 10wt.% PEP showed relatively constant with no noticeable changed, but an increase of the concentration of PEP more than 10% leads to gradually lower impact strength as seen in the Figure 31. According to Figure 31, the impact strength of PI concentration between 10 and 20wt. % showed some improve. Addition of the all the impact strength results were significantly below that of the as-received PMMA, whereas the PI/PMMA after cryomilling for approximately 8 hrs showed more fracture resistant than the pure PMMA. Also, the difference in impact strength between PEP/PMMA and PI/PMMA returns to the alteration in rubber concentration.

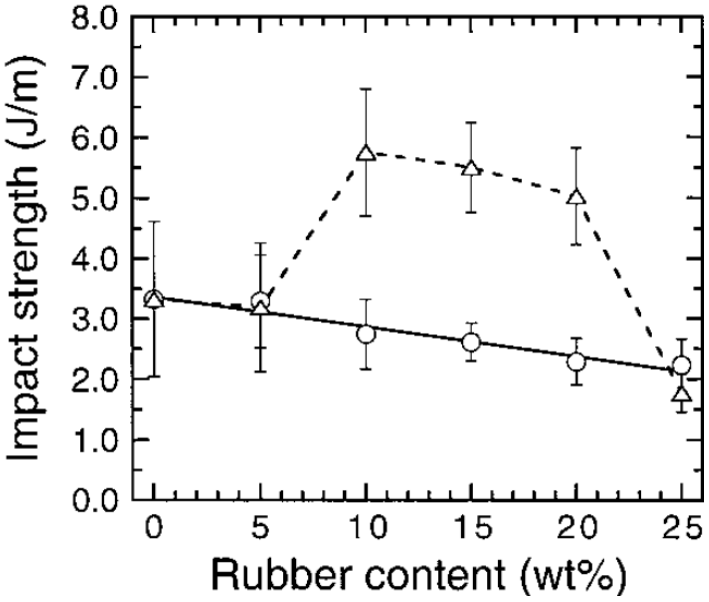

Figure 31: The impact strength vs. rubber concentration for 25/75 PEP/PMMA (○) and 25/75 PI/PMMA (Δ) milled cryogenically for 5h. The solid line denotes a linear regression of the PEP/PMMA data, while the dashed line connects the PI/PMMA data points [90].

Srinivas and Lyons [109] also reported that post-consumer mixed polymer waste, mostly consisting from PE and PP cryogenically milled showed significantly improve in the modulus of the mixed polymer. However, the post-consumer mixed polymer waste milled cryogenically for 15 min an exhibited increase in modulus and reached 45%. Whereas, tensile strength increased to 19% after milled for 5 min, and remained almost the same when milled further.

2.3.2 Mechanically alloying polymer nanocomposites

Polymer nanocomposites materials are classified under particles reinforced polymer matrix. However, the polymer matrix mostly blends with the inorganic particles to enhance the polymer matrix properties, and this issue has been widely investigated in the past decades. It has been found that particle size plays an important role in the improvement of the properties and the composite efficiency. Several studies have reported that the polymer matrix properties such as the mechanical, thermal, dimensional stability, and other properties have gotten significantly improved, by the incorporation of nanoparticles [117-127]. The polymer nanocomposites have

shown great promise for high-performance composite polymer materials with low density and high mechanical strength and stiffness using nanoscale reinforcement. The improvement in properties that occurred goes back to the very large surfaces area of interactions between the polymer matrix and reinforcement, which provide by nanoparticles [124, 125]. In contrast, the nanoparticles susceptibility to agglomerate makes the processing of nanocomposites a rather complex and difficult task, usually when use conventional methods [118-125]. However, the inherent mutual attractive forces for the large surfaces area of the nanoparticles and the high viscosity for some polymer matrices, making nanoparticles dispersing homogeneously difficult. Therefore, it is necessary to find out new methods to achieve this requirement. The "solid state methods," such as mechanical milling (MM) or mechanical alloying (MA) by ball milling might be good alternative not only because of its potential results but also from an economical point of view. Moreover, MM and MA both have two interesting points; first these techniques are useful methods for processing powders materials. Second, they are good methods to reduce and control the particles size distribution, to help the chemical reaction in solid state, to produce phase amorphization and to the synthesis of nanoparticles. Accordingly, several studies have been used high energy ball milling to produce polymer nanocomposites materials and utilizing its advantage in particles size distribution [94, 111-114, 128-133].

Shaw and Gowler were pioneers in using MA to produce polymer composite materials, using PP/SiC mixed cryogenically milled for 19h [128]. Shaw and Gowler found that the crystallinity, compression strength, ductility, hardness for PP/SiC prepared via MA were considerably decreased compared with the melting processing of pure of PP. Whereas, the only positive effect was, increasing in elastic modulus reached to 23% more than that in the melting processing of pure of PP. Shaw and Gowler were optimistic with the results that they obtained, and they concluded that MA technique can induce interactions between the polymer and ceramic leading to a good bonding between them. From this bonding, Shaw and Gowler believed that MA can produce polymer ceramic mechanical alloyed compounds by desired properties, and also has a great promising chance to consider as method to produce polymer ceramic composite materials.

In results presented by Lu and Pan [94], PPS/nano-SiOx powder milled attritorly for 12h. They reported that the systematic interface energy was increased totally by using ball milling, and at the same time the kinetic energy also saw increased, leading to prevent the nano-SiOx

from agglomeration, and by reducing, or prevent attraction between nano-SiOx particles. Also, they observed that ball milling process reduces the surface tension of the interface between nano-SiOx and PPS give rise to high bond density. Furthermore, PPS/nano-SiOx showed an increased in impact strength that reached to 89%. This improvement is due to the good bonding between the polymer matrix and nano-SiOx, helping to transfer the energy between the particles and matrix. Whereas, crystallization temperature, melting temperature, and melting enthalpy showed remarkable reduction, and also crystallinity showed reduction reached to 25%.

The work of Castrillo et al. [130] showed results on MA of PMMA/fumed silica nanoparticles mixtures. It has been observed in the AFM results that homogeneous dispersion of the fumed silica nanoparticles within the PMMA was obtained by using high energy ball milling process. Furthermore, the SEM results exhibited a reduction in the particles size of the PMMA/silica. Also, DSC analysis proved that the chains scission that occurred during the high energy blending process caused reduction in the molecular weight of the PMMA, leading to lower T_g. Through these results, Castrillo concluded that the milling time has a big effect on the properties of the PMMA/fumed silica nanoparticles, and it is possible to produce transparent nanocomposites with excellent moldability by using high energy ball milling process.

In order to produce polymer nanofiller, Azhdar et al. [111] have studied PMMA nanocomposite by using MA, but in this time a metal has been used as nanofiller instead of ceramic. In this work, it has been used a cryogenic MA to alloy PMMA and nickel iron oxide ($NiFe_2O_4$) nanopowders. Azhdar summarized that high energy ball milling process give a good homogeneous dispersions of nanoparticles $NiFe_2O_4$ in the PMMA matrix. However, milling with longer time showed a higher degree of dispersion of the nanopowder on the PMMA particle surfaces.

Zhang et al. [112] incorporated nano-SiO_2 particles into a PEEK matrix by a planetary ball mill for 24h of alloying. The results showed that the incorporation of nano-SiO_2 leads to a significant improvement in material stiffness and a decrease in material ductility, and also wear resistance of PEEK/nano-SiO_2 showed significantly improved. Zhang also reported that the PEEK/nano-SiO_2 mixtures showed an increase in cold crystallization exotherm, and melting temperature. Whereas Zhang noted that nano-SiO_2 content in the composite has effects on the crystallization behavior of PEEK. However, cooling crystallization temperature showed an

increase due to the nucleation sites that provided by the lower content of nano-SiO_2 particles. Whereas, the case of higher contents of nano-SiO_2 particles showed postpone on the cooling crystallization due to prevention the arrangement of the long molecules or impeding the formation of lamellae.

Hedayati et al. [129] followed most of the procedure used in Zhang's [112] work with the exception of added 3-Glycidoxypropyltrimethoxysilane (GPTMS) silane coupling agent to the nano-sized silica particles, and milled for 15h. Hedayati conducted TEM on PEEK/SiO_2 nanoparticles with and without GPTMS milled 15h. Deagglomerated and dispersed homogeneously SiO_2 nanoparticles in PEEK matrix were achieved, and confirmed in this work that the SiO_2 nanoparticles with GPTMS have more uniform dispersion than the ones without GPTMS. According to the XRD results, Hedayati deduced that the degree of crystalline was decreased after milling process due to the hindrance in the PEEK molecular mobility during the cooling crystallization process. Also, crystalline microstructure deteriorated faster during milled and the size of the crystalline lamellae becomes too small. He suggested that the changes in crystalline structure resulted from the strong shear forces induced from the impact of milling media. Whereas, the DSC analysis showed an increase in melting temperature, cold crystallization enthalpy and also a decrease in fusion heat, and crystallization temperature of the milled samples.

Jose´ et al. [113] carried out mechanical alloying of 1–3 wt% SiO_2 nanoparticles blends of SiO_2/epoxy with a SPEX 8000 mill. Jose´ reported that good particle dispersion was achieved and observed in the results of TEM and SEM. He concluded that it is possible to produce polymer nanocomposites with thermoset matrix by using high energy mill processing.

A more recent study about epoxy nanocomposite material produced by mechanical alloying was reported by Lingaraju et al. [132]. Epoxy resin was reinforced with 0.3 up to 3 wt% silica nanoparticle by using planetary ball mill. The results showed a reduction in the particle size occurred rapidly between 4-25h milling, whereas after 25h, there was no significant reduction, but a gradual decrease. Lingaraju conducted SEM photos on epoxy/silica nanocomposites samples. Good and uniform dispersion for the silica particles into epoxy matrix was observed. Also, Lingaraju carried out impact strength, tensile strength, and Barcoll hardness measurements on epoxy/silica nanocomposites samples. The improvement on mechanical properties was

observed, and samples with 1 wt% of silica showed improvement of 6·6% in impact strength, 2·09% in tensile strength, and 2% in Barcoll hardness. Lingaraju also conducted wear test that showed reduction in the wear rate reached to 750%, and he concluded that wear rate is inversely proportional to the hardness of the nanocomposites.

Work was done by Vertuccio et al. [114], using centrifugal ball mill to produce polymer nanocomposite from incorporation of nanoclay into poly(ε-caprolactone) (PCL)/High amylase maize starch. Results showed that PCL crystalline structure as pure or blended with starch and clay did not affect from milling process. Also, the thermal degradation of PCL–starch blend did not affect from milling process, but with addition of 3% of clay seems to influence only the step associated with the PCL degradation. Whilst, XRD patterns for the composite alloyed showed that the clay exhibited a gradual change on its structure by losing its basal plane order with longer milling time. Vertuccio guessed that the clay particles sectioned on the basal plane preferentially during alloyed processing. Whereas, Vertuccio confirmed that the nanometric of clay dispersion into the PCL–starch starts appearing after milled 7h or higher milling times. Also, Vertuccio clearly observed in the SEM results that the bonding and interconnection between the PCL and the starch becomes better when the PCL–starch–clay mixture milled for 10h. Moreover, dynamic mechanical tests confirmed that chains mobility of clay/PCL-starch was decreased due to the increasing intercalation of PCL and starch into the clay sheets. on the other hand, Vertuccio reported that there is an improvement on the elastic modulus, by addition of 3%wt. of clay. From these results on elastic modulus improving, Vertuccio considered that improving in mechanical properties can obtain it, by completing the delamination of the clay structure. Thus, Vertuccio summarized his work that "the milling process is a promising compatibilization method for PCL–starch systems and at the same time it is a useful tool to improve the dispersion of nanoparticles into the polymer blends. A better dispersion of the clay particles, as well as a good compatibilization between PCL and starch can improve both mechanical and barrier properties" [114].

A very recent paper published by Tadayyon et al. [133] has addressed the thermal behavior of medium density polyethylene reinforced with nano-sized alumina after mechanical alloying process, by using planetary ball mill technique. Tadayyon conducted TEM micrographs on medium density polyethylene (MDPE) alloyed mechanically for 5, 10, 20, and 40h, with

different weight percent of Al_2O_3 (0 up to 15wt. %). Increasing the reduction of the Al_2O_3 particles size and dispersal uniformly homogeneously into MDPE matrix with longer milled time was observed. In addition, TEM micrographs showed good adhesion in the MDPE/Al_2O_3 nanocomposite. Also, thermal stability of the MDPE/Al_2O_3 nanocomposite was studied by TGA. The MDPE/Al_2O_3 nanocomposite exhibited higher thermal stability compared with the pure MDPE. Tadayyon interpreted this improvement in the thermal stability that were likely due to two factors: firstly carbon-oxygen bonds that occurred in the MDPE/Al_2O_3 nanocomposite during the milling, makes the degradation of MDPE/Al_2O_3 more difficult. The second thing is interaction between Al_2O_3 particles and MDPE matrix that causes to establish the reinforcements in MDPE matrix. Tadayyon however reported that there was no significant change in crystallization temperature of MDPE as milling time increases. Meanwhile, crystallization temperature of MDPE showed that increased with Al_2O_3, the content increased. Tadayyon explained that it is supposed to be the result of the Al_2O_3 particles being effectively dispersed throughout the MDPE matrix, promoting heterogeneous nucleation. Whereas, the degree of crystallinity of MDPE exhibited decreasing with Al_2O_3 content increased. Tadayyon suggested that as the Al_2O_3 particles were added to the MDPE matrix, the particles were found to obstruct the mobilization of the MDPE macromolecular chain and prevent the macromolecular segment from obtaining ordered alignment of the crystal lattice.

2.4 **Summary of literature research**

In summary, polymer composite materials, and especially thermoplastic polymer composites that are reinforced by using particulate reinforcements have been the subject of recent studies on processing and characterization. As mentioned in the literature review, many published research and studies have shown that particulate reinforcement polymer processing parameters such as blends methods, processing temperature, particles size and distribution, particle and polymer types, and others affect the polymer composites' performance. The most challenging parameter is the uniformed and homogeneous dispersion of the particles in the polymer matrix. However, micro and nanoparticles have a high susceptibility to agglomerate and this agglomeration makes production of polymer particles composites a difficult task. Therefore, it is necessary to find out new methods to achieve this requirement. Thus, several attempts have been done to incorporate the particles uniformly and homogeneously into the polymer matrix, creating polymer particles

composite. One of these methods of incorporating micro and nanoparticles uniformly and homogeneously into the polymer matrix is the mechanical alloying by using high energy ball milling. As introduced, discussed, and mentioned in the literature above, promising results have been observed. This method solves the agglomerate issue, caused by particles aggregation in the polymer matrix. To better understand the behavior of the particle enhanced polymer matrix created using the mechanical alloying method, a study on the composite material UHMWPE/Al_2O_3 processed by MA and characterized will be discussed in this work.

Chapter 3

3. Experimental Procedure

3.1 Material Selection

The materials selected for this research consists of ultra-high molecular weight polyethylene (UHMWPE) powder supplied by Sigma-Aldrich and aluminum oxide (Al_2O_3). The UHMWPE has a melting point of 134°C, a molecular weight M_w of 3,000,000- 6,000,000 and a density of 0.94 g/mL at 25°C; moreover, the UHMWPE was dried at 80°C overnight in a vacuum oven before the milling process. The Al_2O_3 powder specification is deagglomerated Alpha Alumina with particle size of 0.3µ.

These materials were selected because of the interest to enhance the mechanical properties of the polymeric composite material, as mentioned in the introduction and literature. The UHMWPE was especially chosen because of its resistance to wear and impact; UHMWPE continues to find increasing industrial applications, including can and bottle handling machine parts, moving parts on weaving machines, bearings, gears, artificial joints, chutes and slides for directing particulate solids, edge protection on ice rinks, and butchers' chopping boards. Due to these applications, it is of interest to improve UHMWPE mechanical properties. Moreover, the wear of UHMWPE and wear debris generated at the surface is now recognized as the major cause of loosening and failure of the total joint replacement, in the case of artificial joints application. Accordingly, many techniques have been applied to improve the mechanical properties of UHMWPE which is necessary to enhance its matrix and surface properties for biomedical application. For this reason, Al_2O_3 has been used to reinforce UHMWPE by using MA in a move to understand the behavior of the particle reinforced polymer matrix by the MA powder processing technique.

3.2 Powder Processing and Sample Preparation

UHMWPE and 0, 1.0 and 2.5 wt.% Al_2O_3 powders were mechanically alloyed for up 10 hours. The mechanically-alloyed powders were then molded by compression to produce polymer composite sheets of UHMWPE/Al_2O_3 from the melt and characterized. Characterization included X-ray diffraction (XRD), differential scanning calorimetry (DSC), optical microscopy, and

tensile testing of the sheet samples. Likewise, powder samples from milling were characterized by XRD, and DSC.

3.2.1 Mechanical Alloying

Mechanical alloying was conducted using a Union Process Szegvari Attritor as shown in Figure 32. The milling vertical tank and balls in diameter of 6.35 mm used were stainless steel.

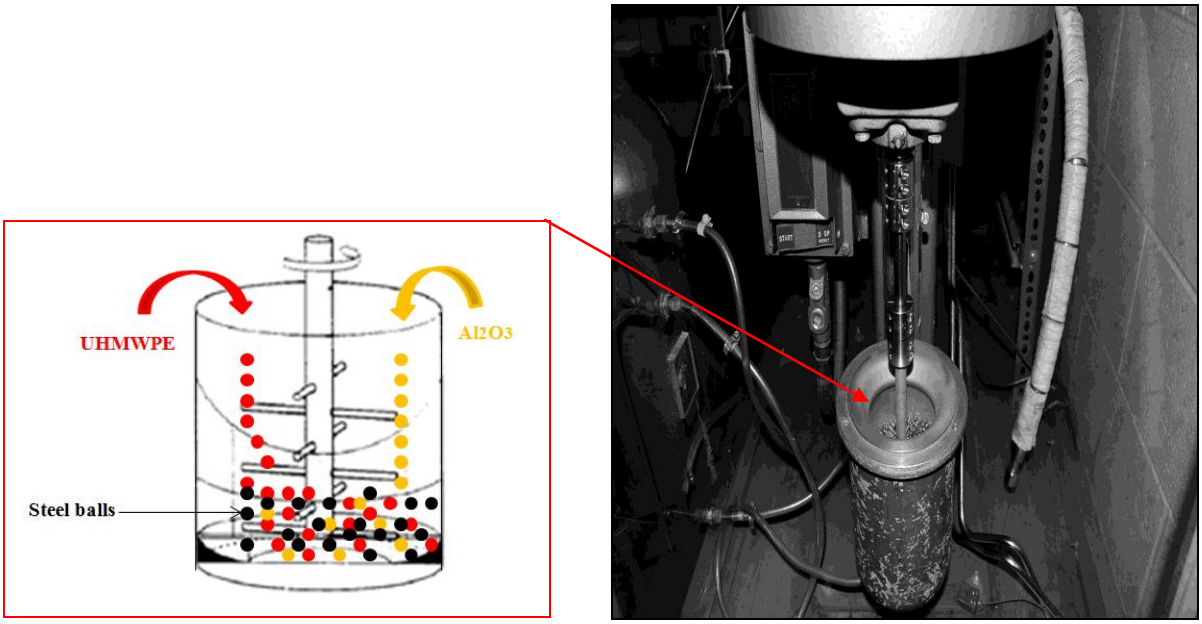

Figure 32: The Szegvari attritor mill that was used in this work. Professor Alex Aning's lab, MSE VT, Blacksburg.

A ratio of milling ball weight to powder weight (charge ratio) of 30:1 was used with balls weighing around 3750-g and powder (UHMWPE + Al_2O_3) weight around 125-g. All the mechanical alloying was conducted at room temperature (20°C) and an air atmosphere with the impeller rotation speed of 300 RPM. The mechanical alloying procedures were carried out to investigate the effect of milling time and Al_2O_3 wt. % content in the milled powder as shown in Table 1.

Table 1: The mechanical alloying experimental design. X signs indicate to the experiments that have been performed.

Milling Time (Hours)	UHMWPE – 0 wt.% Al_2O_3	UHMWPE – 1 wt.% Al_2O_3	UHMWPE – 2.5 wt.% Al_2O_3
0	**X**		
1	**X**	**X**	**X**
2	**X**	**X**	**X**
5	**X**	**X**	**X**
10	**X**	**X**	**X**

3.2.2 Compression Molding

Following the MA mixing, samples were powder-milled and thus were compression-molded into plates with dimensions of 150x50mm under a load of 3 metric tons at 230°C as shown in Figure 33.

(a) (b) (c) (d) (e)

Figure 33: compression molding process steps (a) First, cover the mold base by a kapton film. (b) Second, pour 8 g of the milled powder in the mold. (c) Next, the spread the powder over the mold. (d) Then, cover the powder by a kapton film. (e) Finally, close the mold and press it.

The Carver laboratory press was used in this study as seen in Figure 34. The top and bottom platens of the press are independently controlled and heated with electric resistance heaters. The sample was inserted with a guide between the platens, and a hydraulic pump raised and lowered the bottom platen to apply consistent load to molten polymer.

Figure 34: Carver press used for pressing polymer sheets. Professor Donald G. Baird's lab, Chem E VT, Blacksburg.

First, 8 grams of milled powder have pressed by load of 3 metric tons at room temperature for 3 to 5 min until the load become almost constant. Then, the heaters' temperature was set at 230°C and the sample was left in the hot press for 30 min for isothermal heating. Finally, after 30 mins., the heaters were turned off and the mold was left in the heaters for slow cooling rate until cooled. Subsequently, a polymer sheet with dimensions of 150 x 50 mm and around 1 mm thickness was obtained as seen in Figure 35.

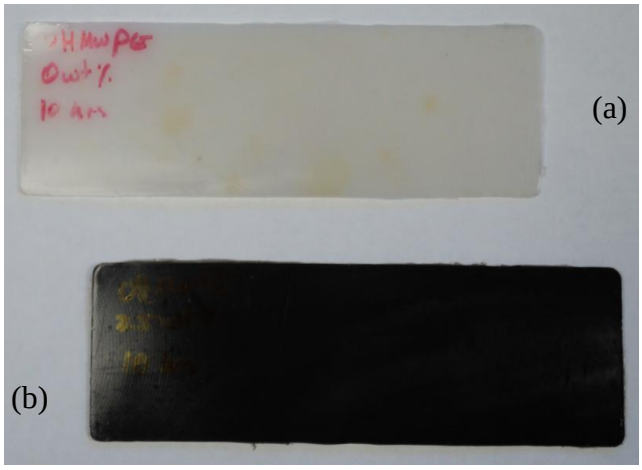

Figure 35: An example shows polymer sheets of (a) UHMWPE milled for 10h. (b) UHMWPE-2.5wt. % Al_2O_3 milled for 10h.

3.3 Characterization

Mechanically alloyed UHMWPE/Al_2O_3 powders and their corresponding compression molding sheets were characterized to investigate the effect of the milling processes and Al_2O_3 content on the structure and properties of the composite.

3.3.1 Differential Scanning Calorimetry (DSC)

Differential scanning calorimetry (DSC) was conducted on the milled pure UHMWPE and UHMWPE/Al_2O_3 powders and their corresponding sheet samples using a Netzsch STA 449 C Jupiter TG-DSC. The samples were placed in an aluminum crucible and then placed on the tray at the DSC chamber. In the next step, the DSC chamber was sealed, two evacuation cycles applied, and then purged with nitrogen gas. The samples were heated in an N_2 atmosphere from 25ºC to 300ºC at rates of 5 ºC/min and 20ºC/min, whereas 25ºC to 400ºC at a heating rate of 40ºC/min. The DSC data showed endothermic peaks which were analyzed using the Proteus software as exemplified in Figure 36. The maximum deviations for the DSC data are in the range of 2% according to the Netzsch's specifications.

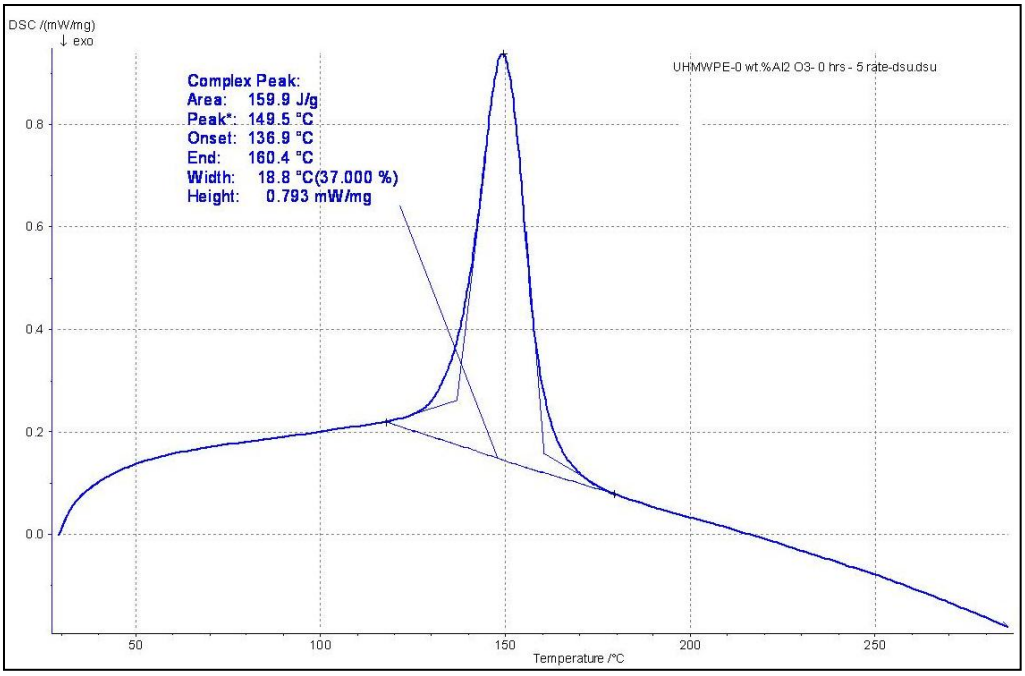

Figure 36: An example of DSC data analyzed for endothermic peak of UHMWPE pure powder as received with heating rate of 5ºC/min using the Proteus software.

3.3.2 X-Ray Diffraction (XRD)

Panalytical X'pert Pro PW 3040 diffractometer generator was used in this work to obtain X-ray diffraction patterns. Panalytical X'pert Pro PW 3040 diffractometer generates the X-rays (k-α) from Cu source using a generator power of 45 kV and 40 mA. for this work, was used the nickel filter, 10 mm mask, 1º anti-scatter slit, and Bragg angle (2θ) range from 0º to 60º. X-ray diffraction spectra were collected for UHMWPE powders and sheets samples before and after mechanical milling processing. Also, X-ray diffraction spectra were collected for UHMWPE/ Al_2O_3 after mechanical alloying processing. These X-rays diffraction spectra were done for all the samples in order to compare crystalline index values as well as crystal structure information. The XRD results were analyzed by using MDI Jade software to separate crystalline from amorphous reflections and calculate the amounts of each phase present in the bulk as seen on the Figure 37.

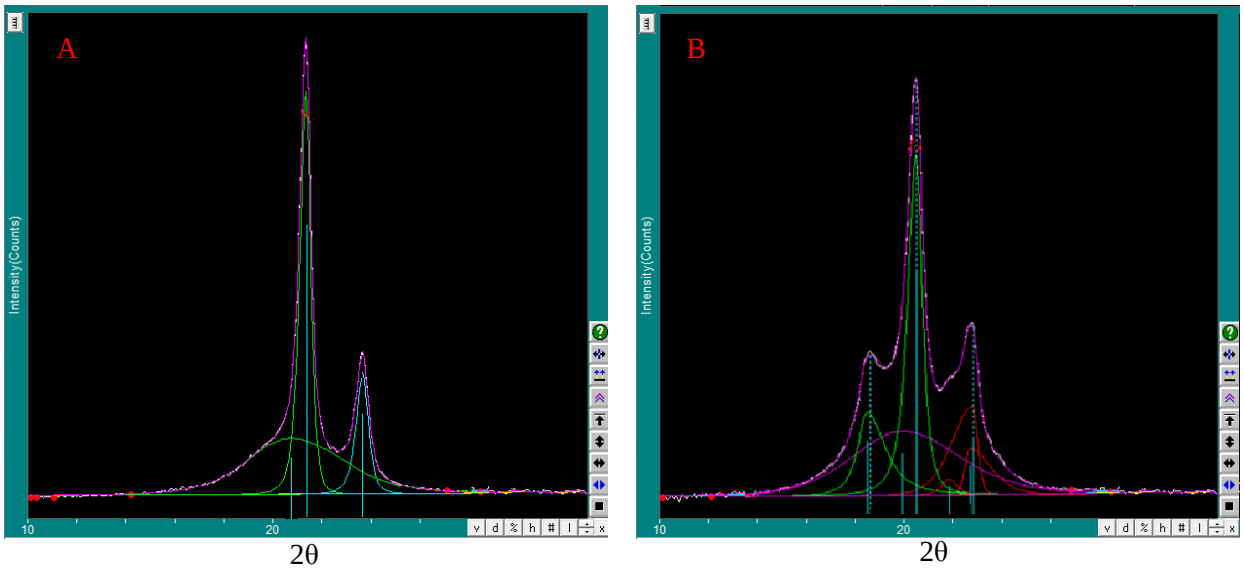

Figure 37: Examples shows the XRD data analyzed for the complex crystalline and amorphous peaks by using MDI Jade software (a) UHMWPE powder unmilled. (b) UHMWPE powder milled for 1 hour.

3.3.3 Microscopy

Microm HM325 Microtom was used to prepare samples for microscopic examination using Carl Zeiss Axiovert 200M microscope.

3.3.4 Tensile test

All the tests were performed at room temperature (20ºC) on a COM-TEN DFM500 universal testing machine at a constant crosshead speed of 1.8 - 2.2 mm/min. The sample dog-bone specifications were according to the ASTM D3039/D3039M-08. The specimens having a 1 mm thickness were machined from the compression molded plates. The length overall of dog-bone specimens is 38 mm. The length and width of narrow section are 14 and 5 mm, respectively as seen on the Figure 38. All presented data corresponds to the average of five measurements.

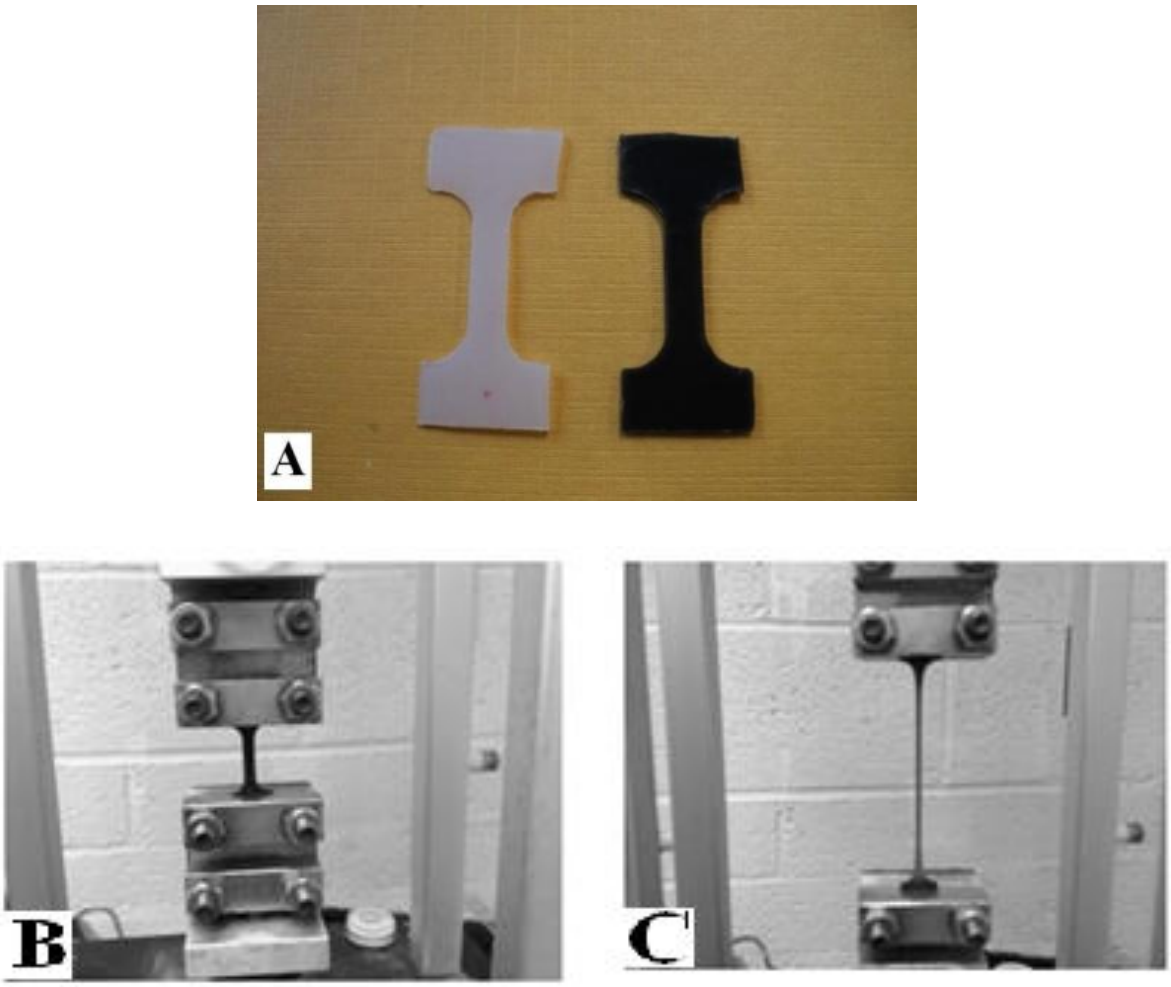

Figure 38: An example of (A) Dog-bone specimens. (B) Set the specimen for tensile test. (C) Tensile test.

Chapter 4

4. Results and Discussion

4.1 Powder Characterization

4.1.1 X-ray Diffraction

X-ray diffraction was performed on the as received and milled UHMWPE powders as well as milled UHMWPE/Al_2O_3 alloy powders. All of the diffraction peaks have been normalized by the largest peak of the scan – the (110) peak of the orthorhombic phase. Figure 39 shows the diffraction patterns representing structural evolution with milling time in pure UHMWPE. Two major changes are observed with milling time. First, a monoclinic crystal structure develops at the expense of the amorphous and orthorhombic structure of the semicrystalline UHMWPE; this stress induced phase transformation phenomenon has been known to occur in UHMWPE for years [134-135]. Generally in this work, the volume of the monoclinic phase increases as those of the amorphous and orthorhombic decrease with milling time. The (001) peak of the monoclinic is evident, but two smaller monoclinic peaks – (002) and (201) – are buried and not evident in these patterns.

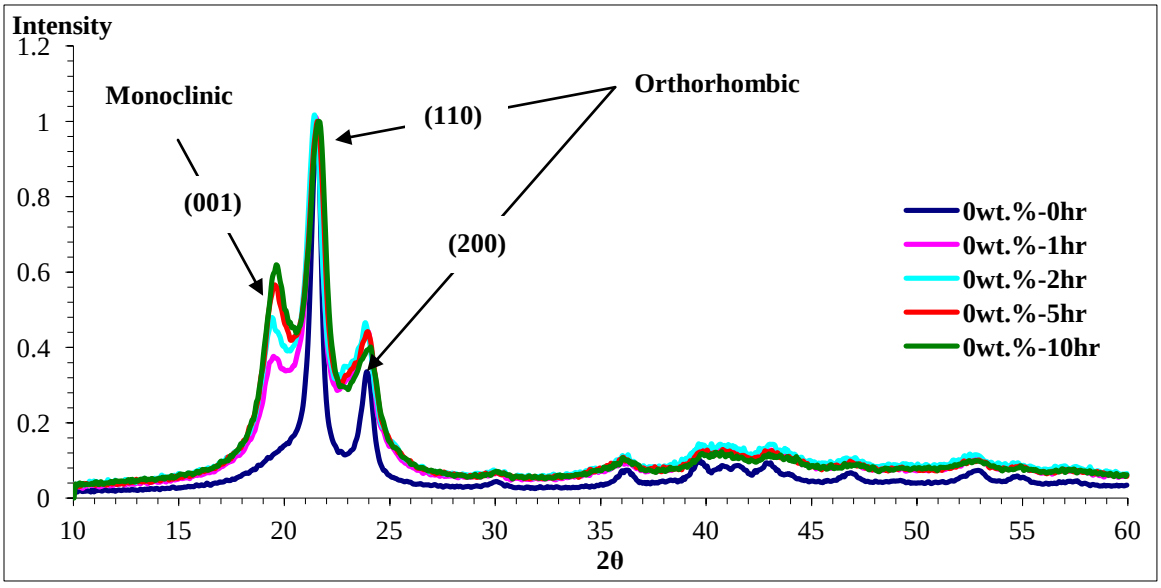

Figure 39: X-ray diffraction patterns for as received UHMWPE milled for up to 10 hours.

These planes are identified when the diffraction patterns are analyzed using MDI Jade software. The monoclinic phase transformation is induced by shear stresses caused by the impacts on the powders trapped between the milling balls. This phenomenon is known to occur in UHMWPE specimens deformed by tension, rolling and mechanical alloying [82, 110, 134-146]. Second, there is broadening in the original orthorhombic peaks with milling time as a result of microstructural refinement and other defects introduced in the power from the milling process [82]. Figure 40 and 41 show the X-ray diffraction patterns for UHMWPE - 1 wt. % Al_2O_3 and UHMWPE - 2.5 wt. % Al_2O_3 blends milled for up to 10 hours. The trends in structural development are similar to that of the milled pure UHMWPE. In general, the total crystallinity increases at the expense of amorphous with milling time for all three cases.

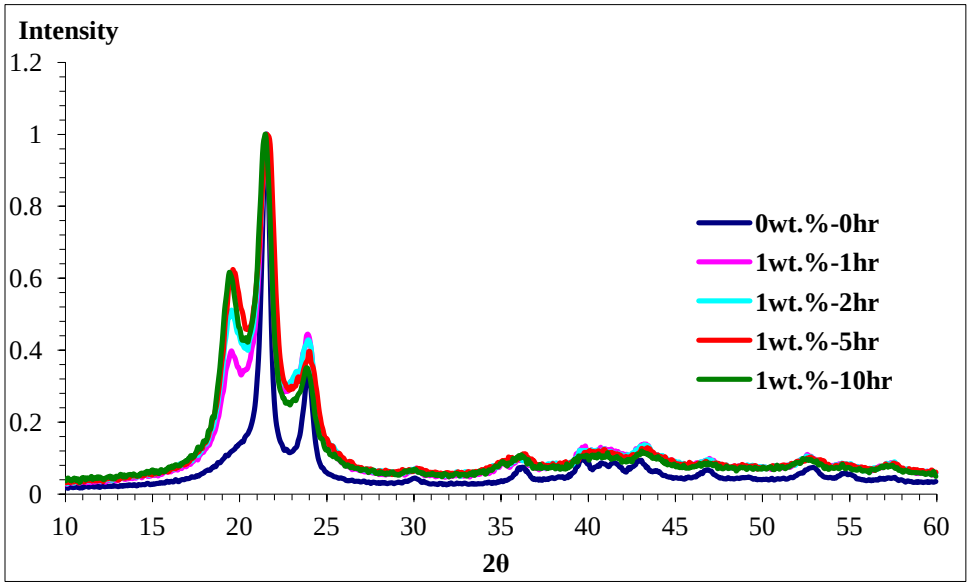

Figure 40: X-ray diffraction patterns for UHMWPE-1wt. % Al_2O_3 milled for up to 10 hours compared with un-milled UHMWPE.

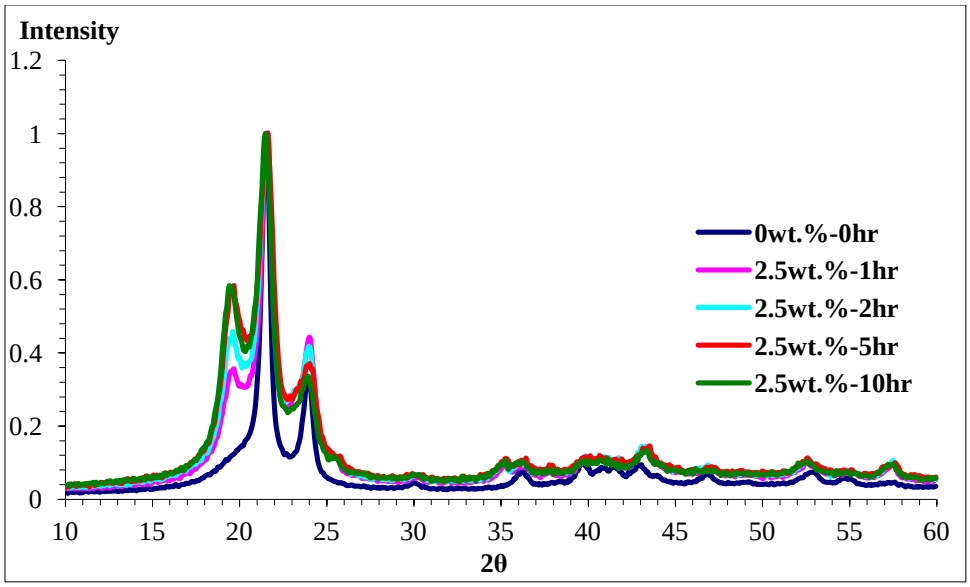

Figure 41: X-ray diffraction patterns for UHMWPE-2.5wt. % Al_2O_3 milled for up to 10 hours compared with un-milled UHMWPE.

Figures 42, 43, 44, and 45 show x-ray diffraction peaks for constant milling times as a function of alumina composition. For a given milling time the monoclinic (001) intensity peaks remain about the same for the zero and 1 wt. % alumina milled powders, however the peaks for the 2.5 wt. % alumina do decrease. In the case of orthorhombic, the intensity of the strongest peak (110) also remains about the same for all compositions and milling times, however the intensities of the (200) peaks decrease with composition for each of the milling times. It must be noted that two of the peaks representing the developing monoclinic structure are buried beneath the orthorhombic (200), and as result the MDI Jade software has been used to deconvolute the spectrum and the results are reported and discussed below.

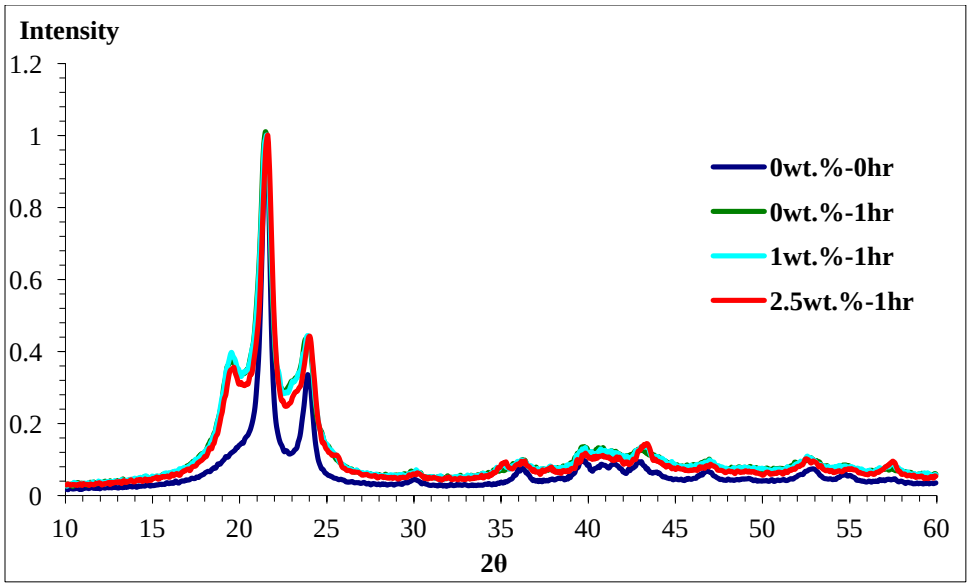

Figure 42: X-ray diffraction patterns for UHMWPE/Al_2O_3 and alloyed for 1 hour.

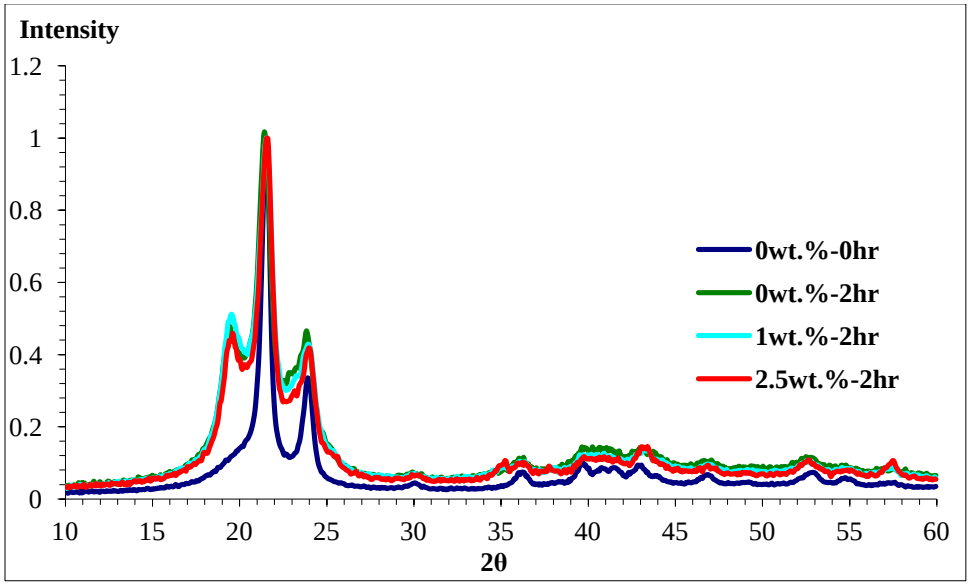

Figure 43: X-ray diffraction patterns for UHMWPE/Al_2O_3 and alloyed for 2 hours.

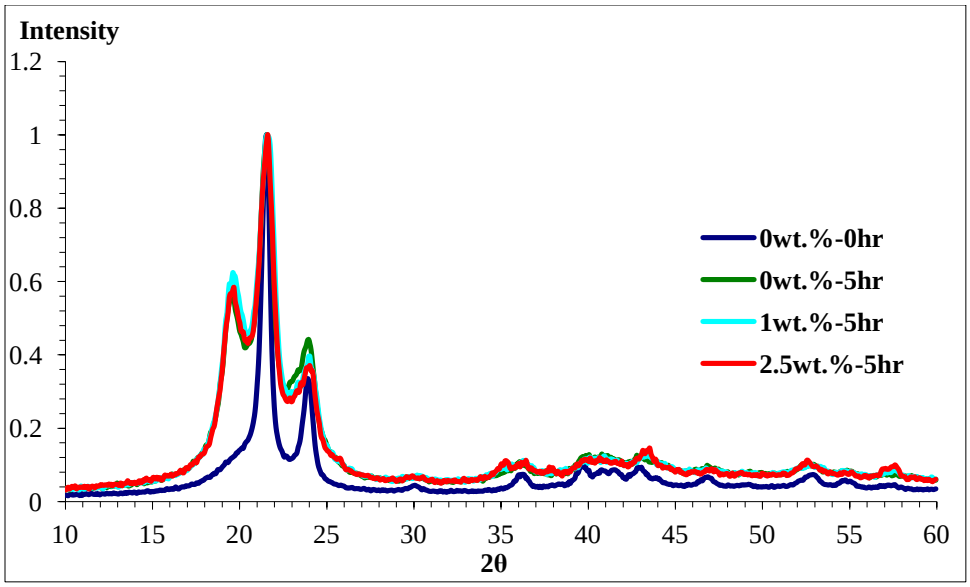

Figure 44: X-ray diffraction patterns for UHMWPE/Al_2O_3 and alloyed for 5 hours.

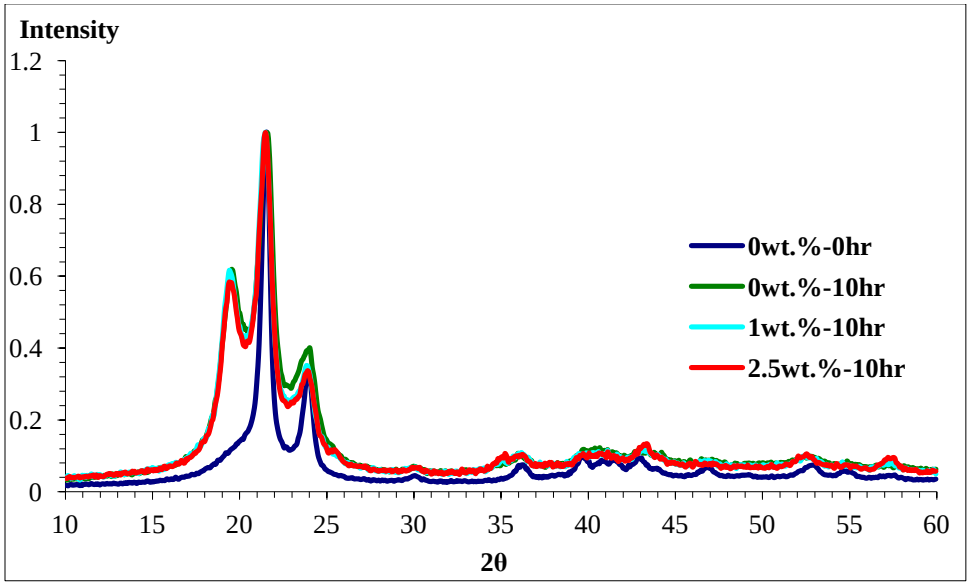

Figure 45: X-ray diffraction patterns for UHMWPE/Al_2O_3 and alloyed for 10 hours.

4.1.2 Determination of Crystallinity

UHMWPE is semi-crystalline, and as discussed above the mechanical milling process has induced the phase transformation of a monoclinic structure in UHMWPE and its alloys with alumina and this is supported by the x-ray results. To study the structural evolution in these

materials during milling, it is necessary to isolate the various peaks in the convoluted x-ray spectra. This is achieved using MDI Jade software. A fixed background and pseudo-Voigt fitting function is used in deconvolution and the integrated peak intensities are used to calculate the amounts of each phase present in the bulk as exemplified in Figure 46 for the amorphous and major peaks of the orthorhombic and monoclinic phases. The volume fraction of each phase is then obtained from the ratio between the area under its crystalline peaks and the total area under the diffraction curve.

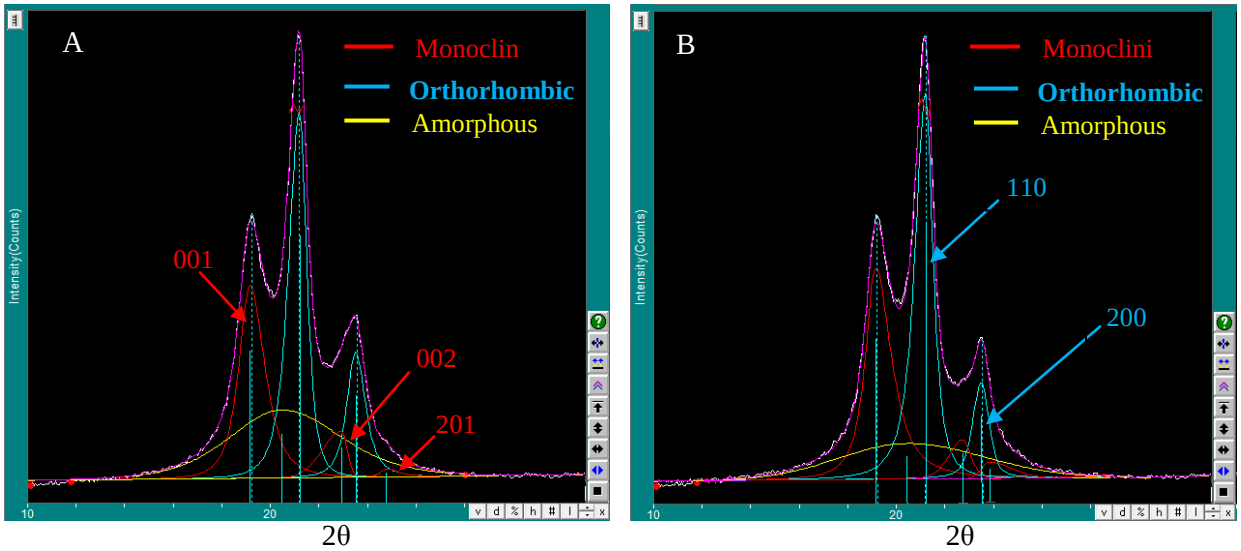

Figure 46: X-ray diffraction patterns analysis by the MDI Jade software (a) UHMWPE powder milled for 10 hours. (b) UHMWPE- 1wt. % Al_2O_3 powder milled for 10 hours.

4.1.2.1 The Effect of Milling Time on Crystallinity

Figures 47, 48, and 49 show the results for the relative change in the crystallinity as a function of milling time. Overall, the total crystallinity of the UHMWPE and UHMWPE/Al_2O_3 samples increases substantially at the end of 10h milling from the original un-milled state, from 54 % for the un-milled to between 65 and 80%. The volume fraction of the orthorhombic phase drops during the first two hours of milling while that of the monoclinic phase increases; in fact the volume fraction of the monoclinic phase surpasses that of the orthorhombic after two hours of milling. However, by the end of 10h milling, the volume fraction of orthorhombic is higher than that of monoclinic. It seems clear from Figures 47, 48, and 49 that both the original amorphous and orthorhombic phases contribute to the new developing monoclinic phase. The amorphous

phase seems to contribute the most. The specific reaction steps by which this process takes place is however not understood.

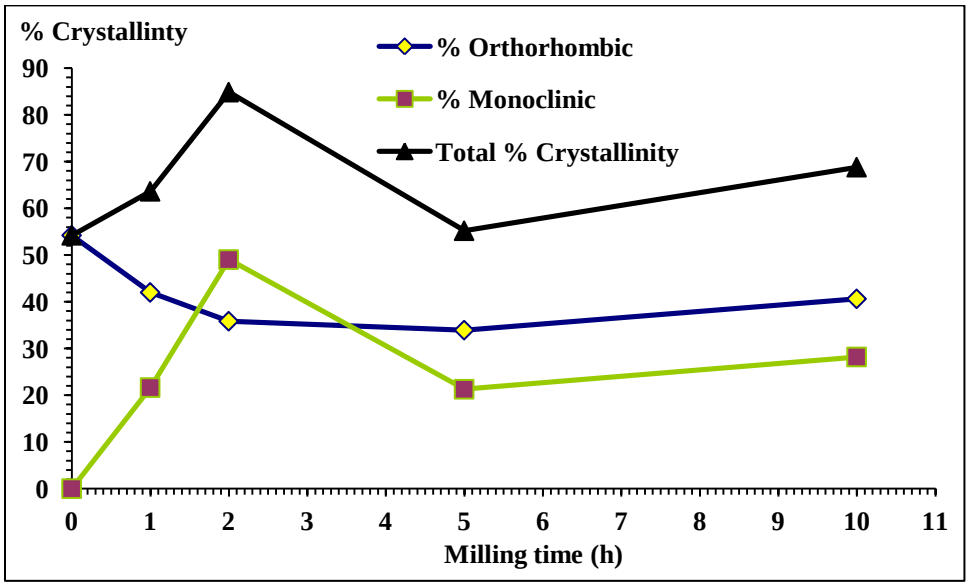

Figure 47: Evolution of the crystalline phase for UHMWPE powder as a function of the milling time as calculated from the integrated X-ray diffraction by the MDI Jade software.

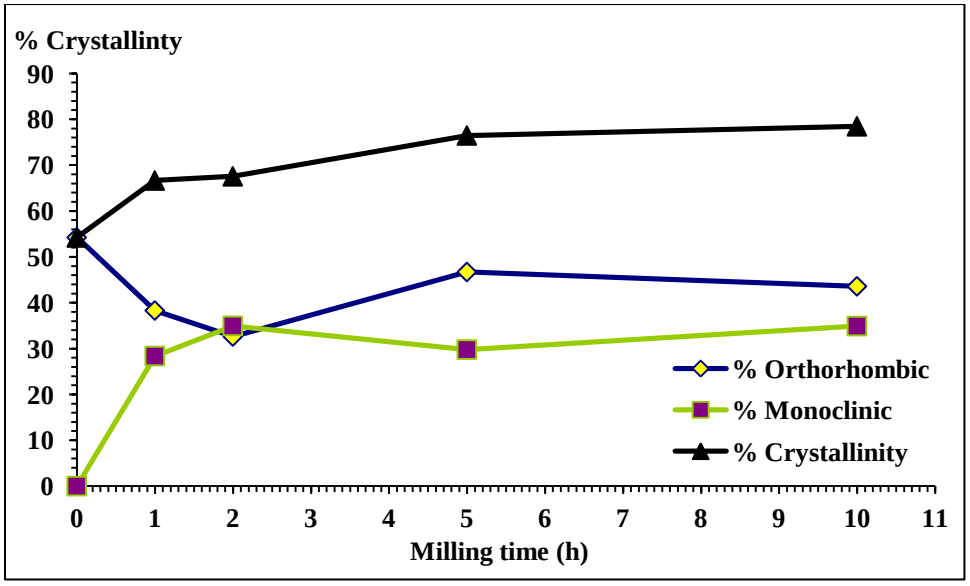

Figure 48: Evolution of the crystalline phase for UHMWPE- 1wt. % Al_2O_3 powder as a function of the milling time as calculated from the integrated X-ray diffraction by the MDI Jade software.

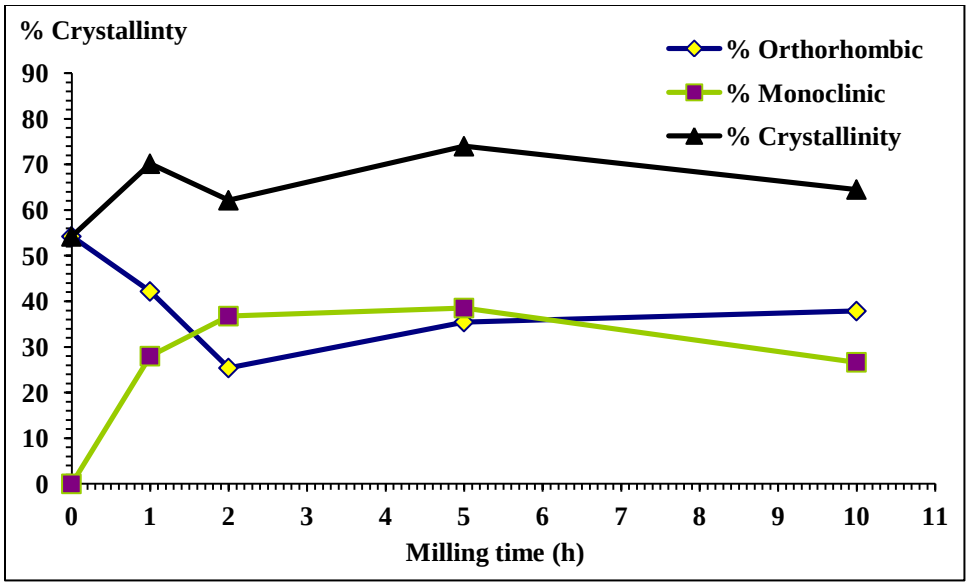

Figure 49: Evolution of the crystalline phase for UHMWPE- 2.5wt. % Al_2O_3 powder as a function of the milling time as calculated from the integrated X-ray diffraction by the MDI Jade software.

4.1.2.2 The Effect of wt. % Al_2O_3 Contents on Crystallinity

Figures 50, 51, and 52 show the results for the corresponding relative changes in crystallinity of the milled specimens as a function of the Al_2O_3 composition. There are not obvious trends in the plots. A key observation is that the highest volume fraction (49 %) of the evolving monoclinic phase is observed after milling pure UHMWPE for 2h as shown in Figure 51. Also, there seem to be a linear relationship between the total crystallinity and the composition of alumina in the 1h milled samples as seen in Figure 52. While the 2-h milled UHMWPE yield the highest crystallinity when it is pure, it also has the lowest crystallinity at 2.5 wt. % alumina (Figure 52).

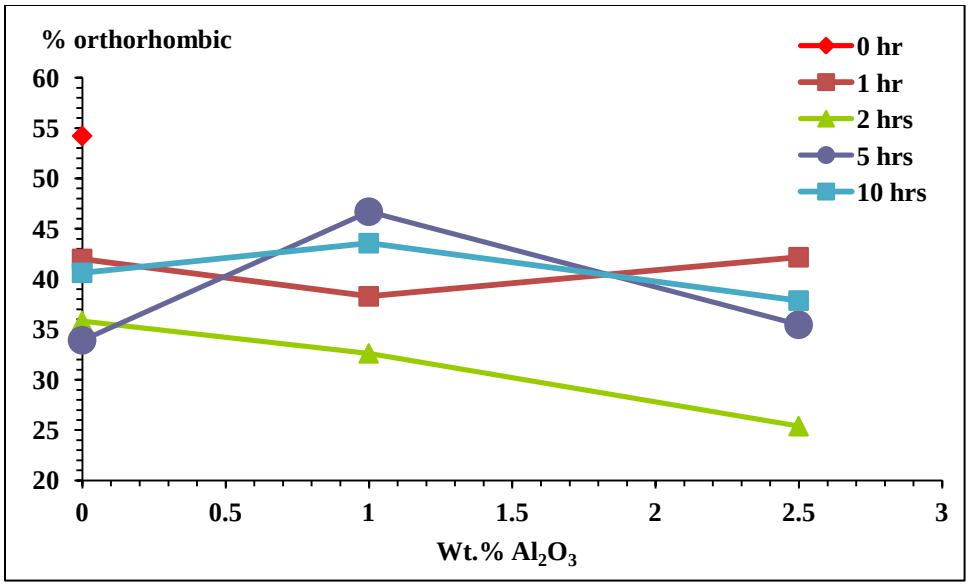

Figure 50: Changes in the % orthorhombic with the wt. % Al_2O_3 for different milling time.

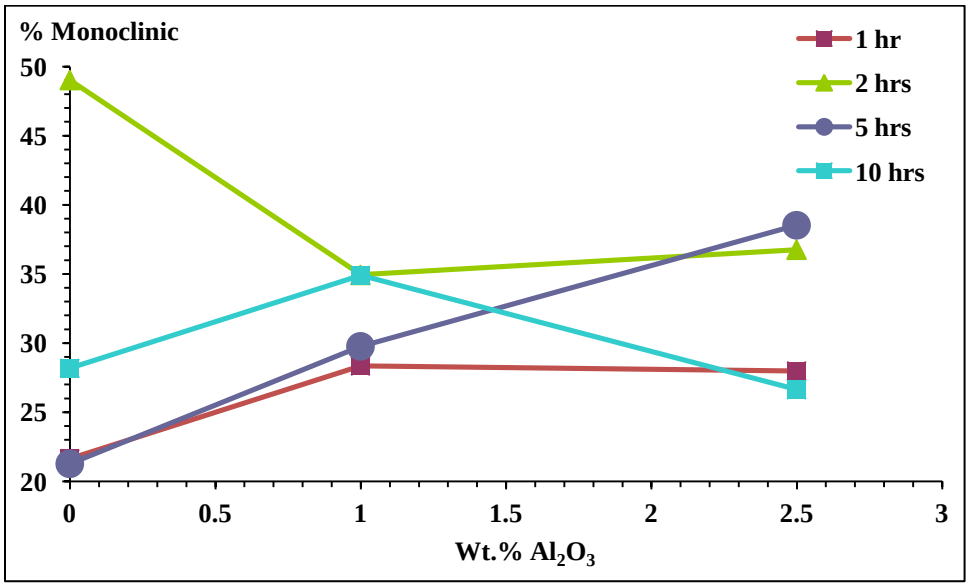

Figure 51: Changes in the % monoclinic with the wt. % Al_2O_3 for different milling time.

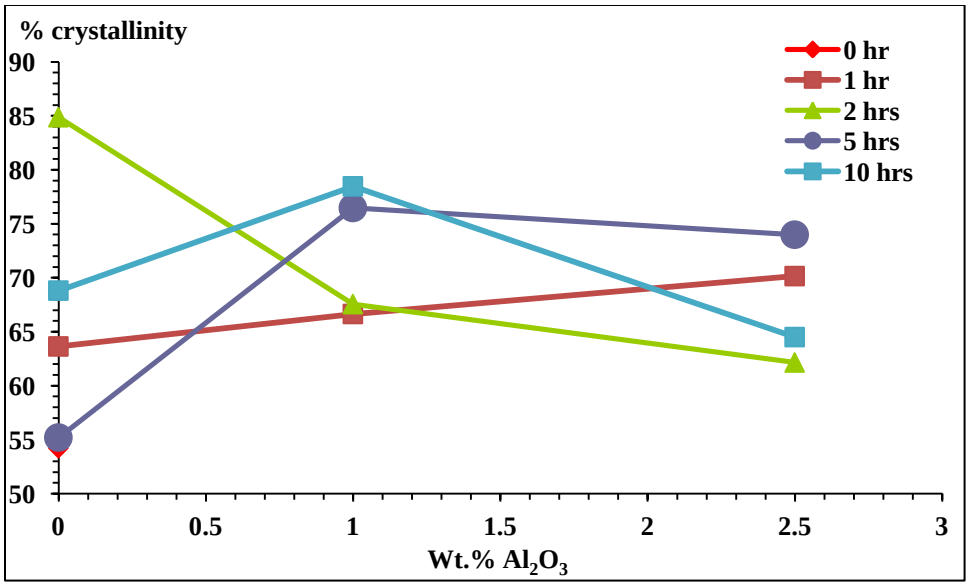

Figure 52: Changes in the total % crystallinity with the wt. % Al_2O_3 for different milling time.

Figure 53 shows amorphous volume fraction versus alumina composition. Overall, the volume fraction drops from a value of 45 % for un-milled pure UHMWPE down to between 26 and 37 % for the various milling times, and as mentioned in the crystalline case, there seem to be a linear relationship between amorphous fraction and alumina composition.

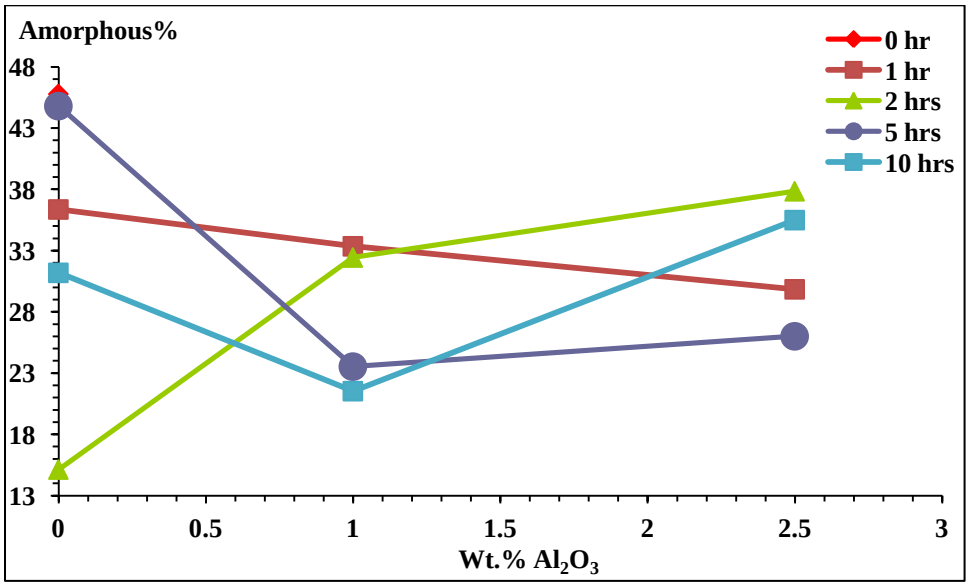

Figure 53: Changes in the % amorphous with the wt. % Al_2O_3 for different milling time.

4.1.3 Differential Scanning Calorimetry Analysis

Typical differential scanning calorimetry (DSC) results are shown in Figures 54 – 56 for a heating rate of 5°C/min. The melting point decreases for both unreinforced and alumina reinforced UHMWPE samples as milling time increased. This is due to the lowering of molecular weight resulting from the breaking of carbon bonds in the chains [82, 133].

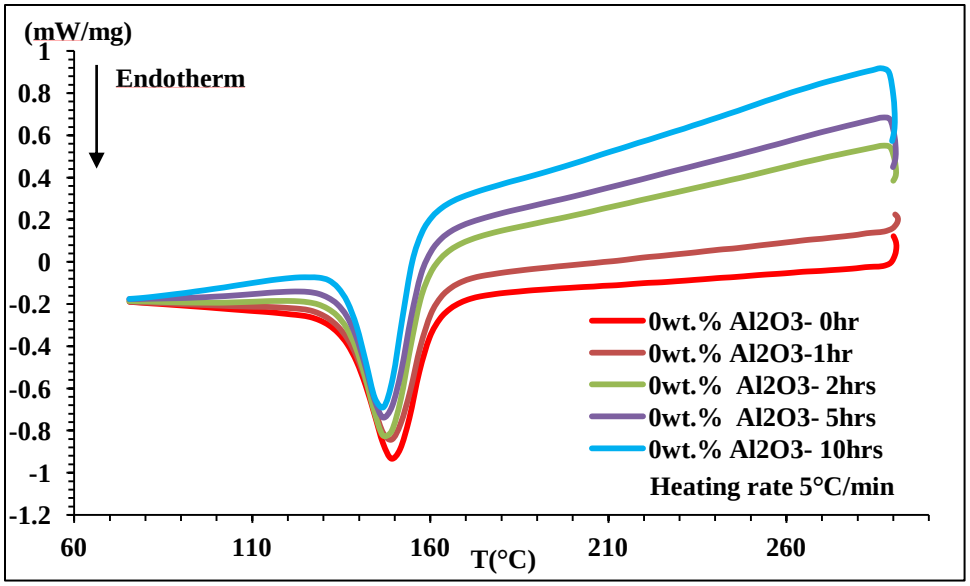

Figure 54: Differential scanning calorimetry curves for pure UHMWPE milled for different times at heating rate of 5°C/min.

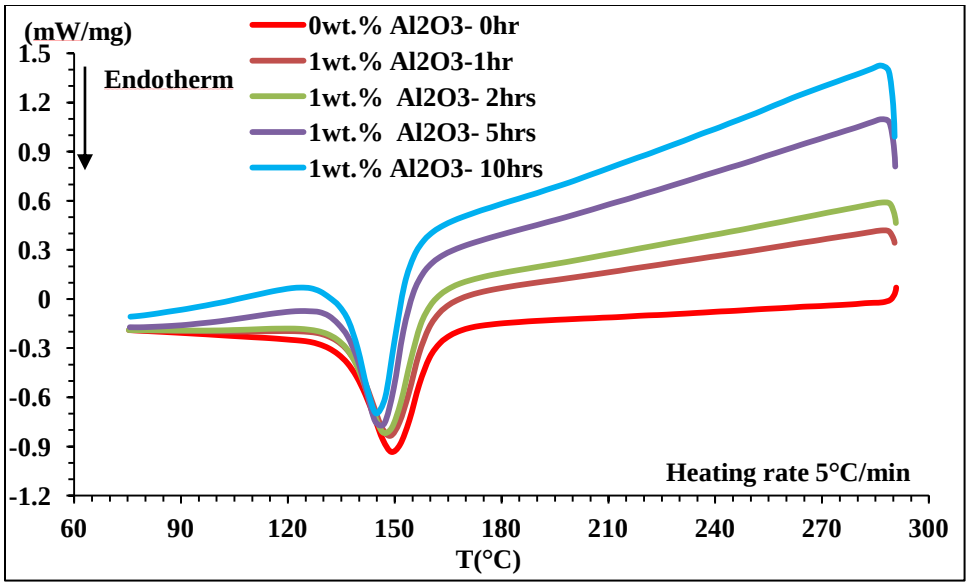

Figure 55: Differential scanning calorimetry curves of the UHMWPE- 1wt. % Al_2O_3 milled for different times at a heating rate of 5°C/min.

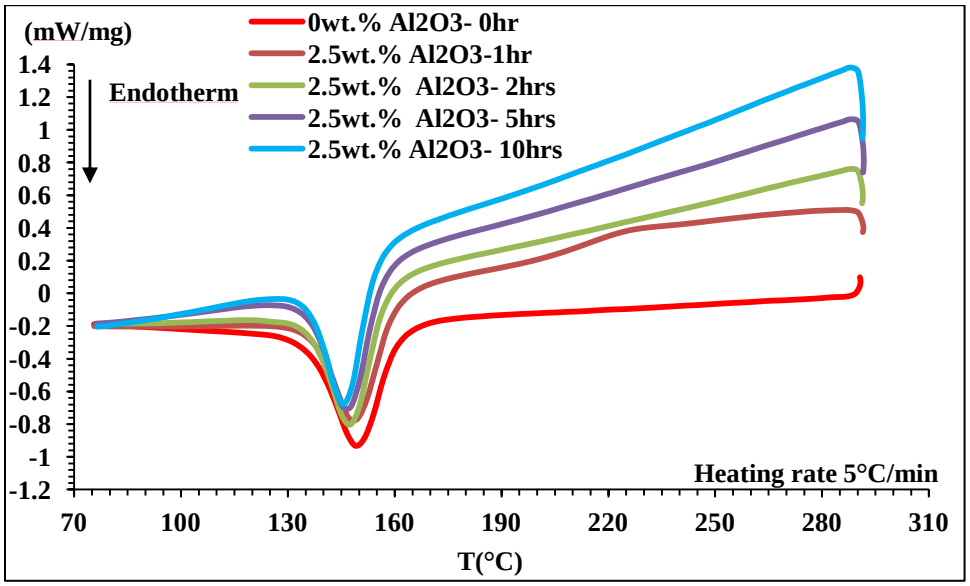

Figure 56: Differential scanning calorimetry curves of the UHMWPE- 2.5 wt. % Al_2O_3 milled for different times at a heating rate of 5°C/min.

Analyses of the effect of milling time and alumina composition on the melting temperature, activation energy, and enthalpy of melting from the DSC results are discussed in greater detail in the next section.

4.1.3.1 The Effect of Milling Time and Reinforcement on Melting Temperature

The melting point of milled powders is plotted as a function of milling time for up to 10 hours, and the results are shown in Figures 57 – 59. As noted in the previous section, the melting point for both pure UHMWPE and UHMWPE/alumina composites decreases with milling time. The temperature decrease is steeper in the composites, getting bigger as the mass of alumina is increased. In Figure 58 the drop is nearly 10 °C for the UHMWPE-2.5 wt% Al_2O_3 as compared with the pure as-received UHMWPE. The temperature drop is also presented in Figures 60 – 62 for three heating rates 5, 20 and 40°C/min. The relationship between melting point and alumina composition is linear for a given heating rate, with the negative slope getting bigger with increased heating rate.

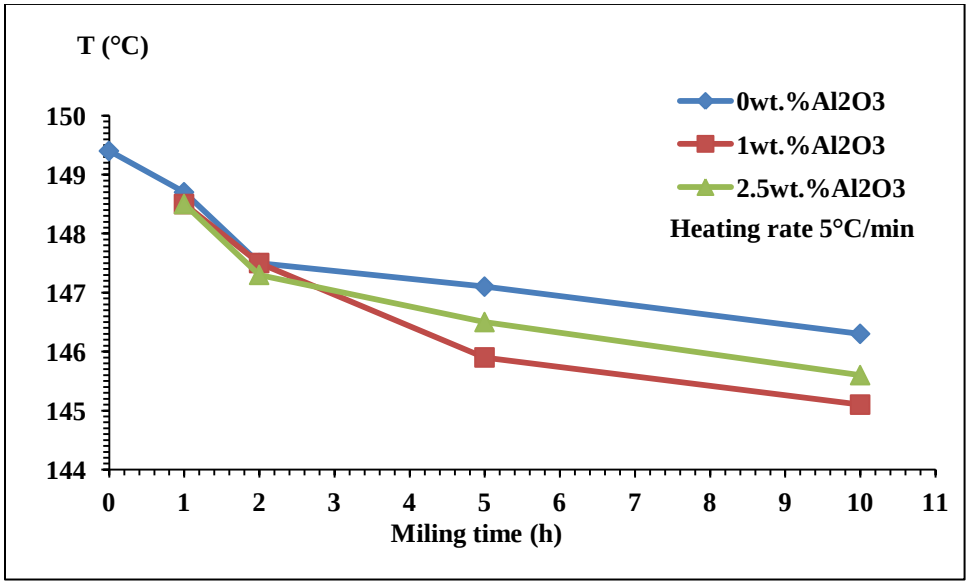

Figure 57: The effect of milling time on the melting temperature for UHMWPE/Al_2O_3 with different milling time at heating rate of 5°C/min.

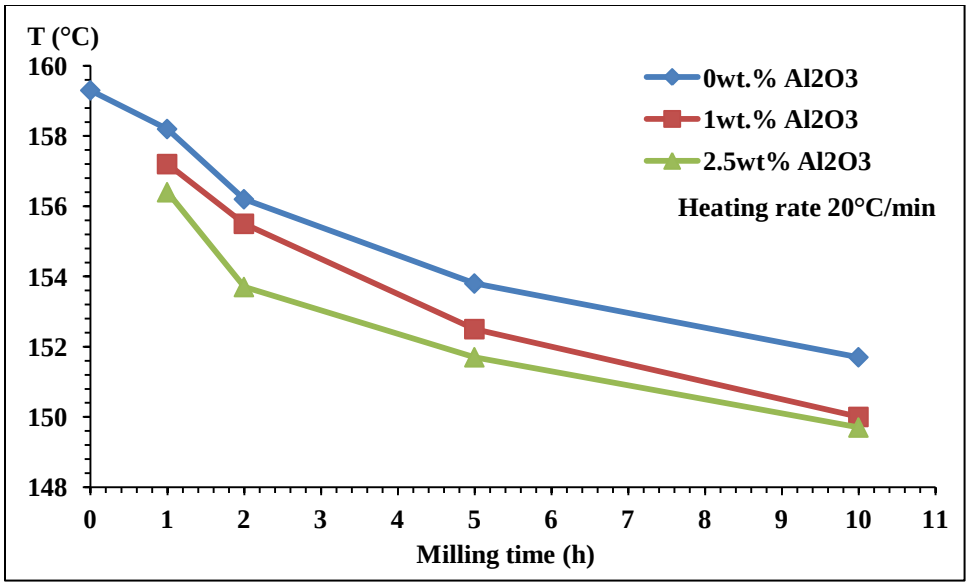

Figure 58: The effect of milling time on the melting temperature for UHMWPE/Al_2O_3 with different milling time at heating rate of 20°C/min.

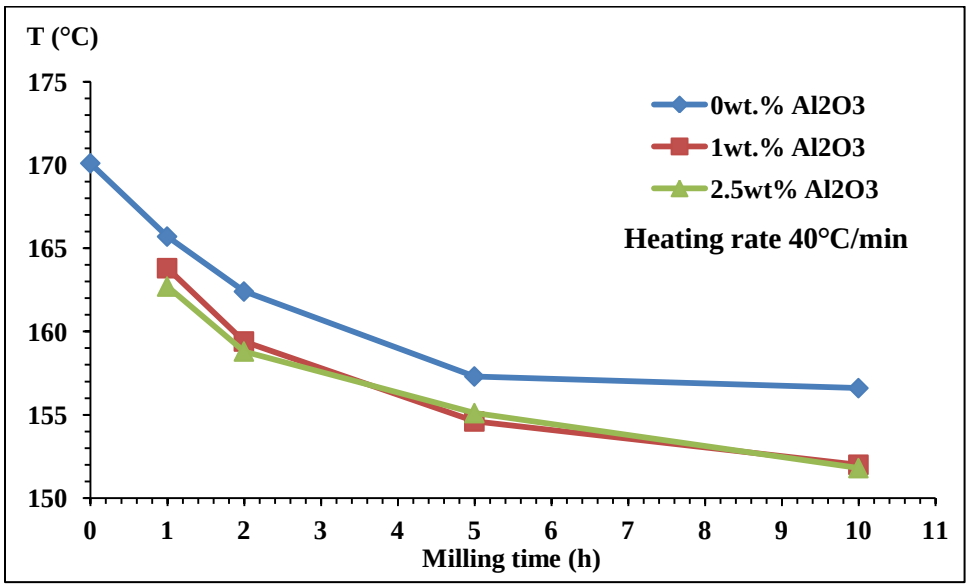

Figure 59: The effect of milling time on the melting temperature for UHMWPE/Al_2O_3 with different milling time at heating rate of 40°C/min.

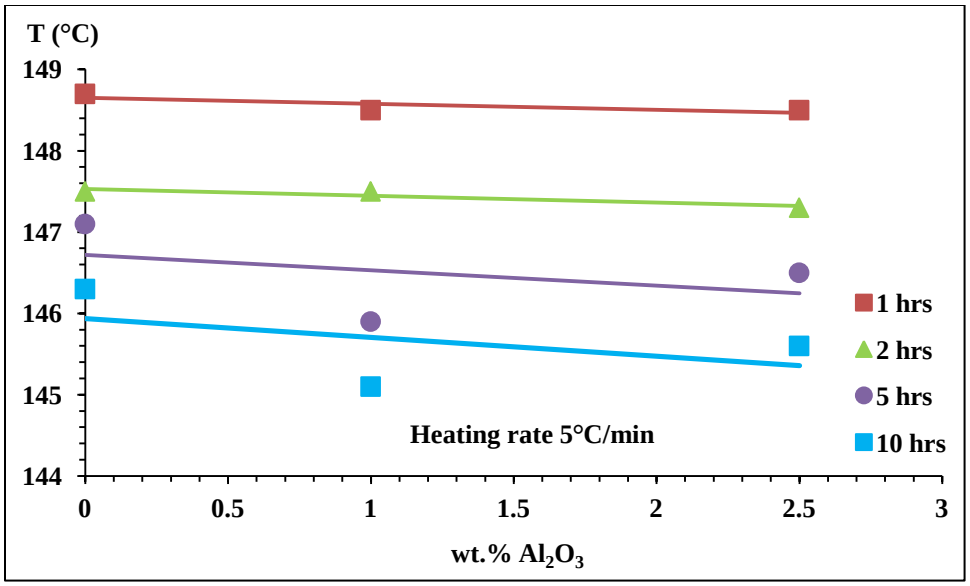

Figure 60: The effect of wt. % Al_2O_3 contents on the melting temperature for UHMWPE/Al_2O_3 with different milling time at heating rate of 5°C/min.

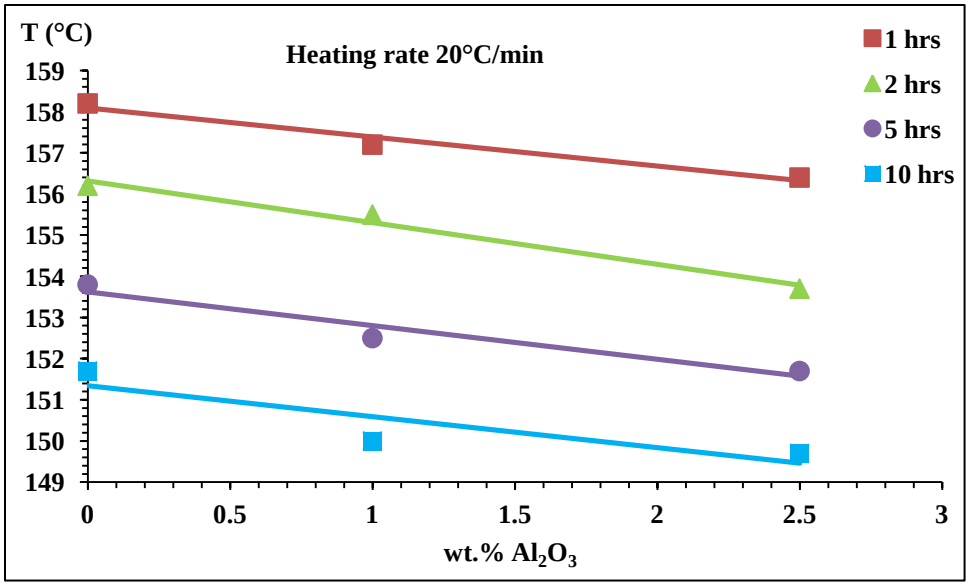

Figure 61: The effect of wt. % Al_2O_3 contents on the melting temperature for UHMWPE/Al_2O_3 with different milling time at heating rate of 20°C/min.

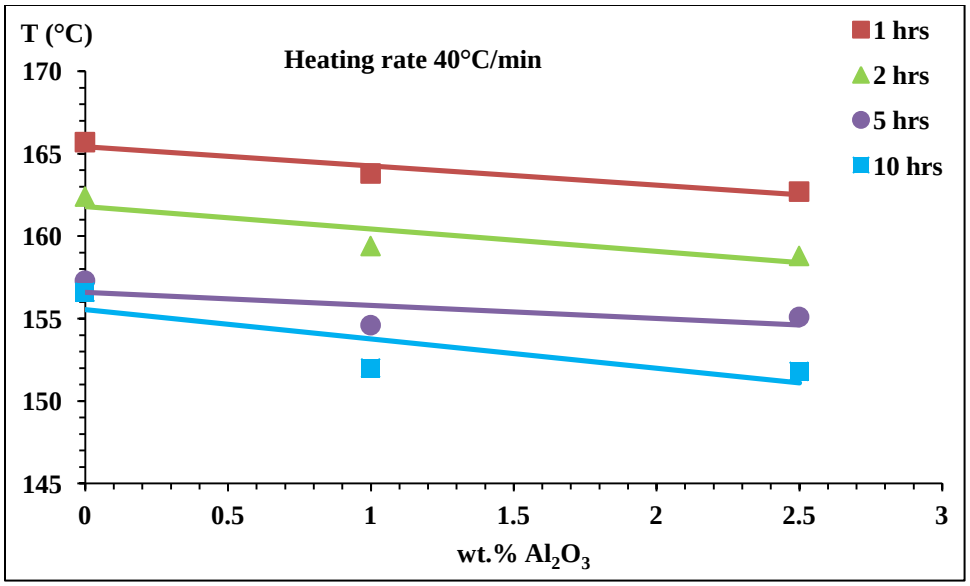

Figure 62: The effect of wt. % Al_2O_3 contents on the melting temperature for UHMWPE/Al_2O_3 with different milling time at heating rate of 40°C/min.

4.1.4 Activation Energy for Melting

The evaluation of activation energy for phase transformations or chemical reactions from the heating rate dependence of the transformation is widely used in the literature. Kissinger's relation method has been used for this purpose [147]. The Kissinger method is based upon a series of experiments in which small milligram quantities of the reacting material are heated at several heating rates (β) while the reaction peak is recorded. The peak temperature (T_m), taken to be a point of constant conversion, is measured at each heating rate. The activation energy for the reaction (E_a) can be calculated using the Kissinger's relation in following form:

$$\ln\left[\frac{\beta}{T_m^2}\right] = C - \frac{E_a}{R}\left(\frac{1}{T_m}\right) \qquad \text{Eq. 1 [136]}$$

Where C is a constant and R is the universal gas constant. The plot of $\ln[\beta/T_m^2]$ versus $1/T_m$ yields a straight line. The activation energy can then be determined from the slope, $-E_a/R$:

$$E_a = -(\text{slope} * R) \qquad \text{Eq. 2}$$

In this work the Kissinger's relation was used to analyze the melting point of the UHMWPE and UHMWPE/Al_2O_3 powders as a function of milling time and also as a function of wt. % Al_2O_3. Samples were heated at 5, 20, and 40 K/min. The plots are shown in Figures 63, 64, and 65 for pure UHMWPE, UHMWPE- 1wt. % Al_2O_3 and UHMWPE- 2.5wt. % Al_2O_3. In each of the three figures, the curves for the Kissinger plots for the milling times seem to converge at approximately 140^{o}C; this could represent the DSC peak performed at a very slow rate. The calculated activation energy values for the UHMWPE and UHMWPE/Al_2O_3 systems milled for up to 10 hours are provided in Table 2 and also plotted in Figures 66 and 67 as a function of milling time and alumina composition, respectively.

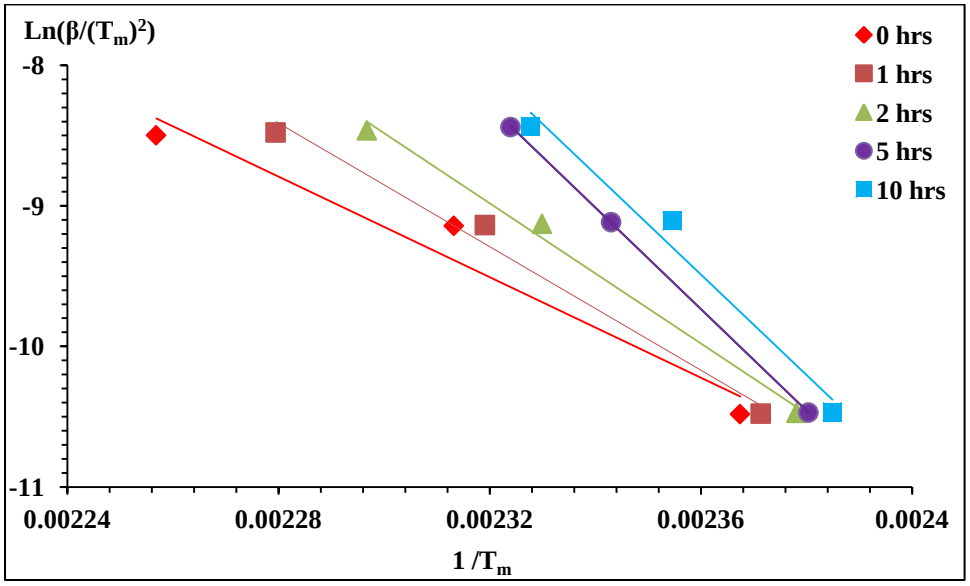

Figure 63: Plots of ln[β/T_m^2] versus $1/T_m$ for UHMWPE- 0wt. % Al_2O_3 for different milling time.

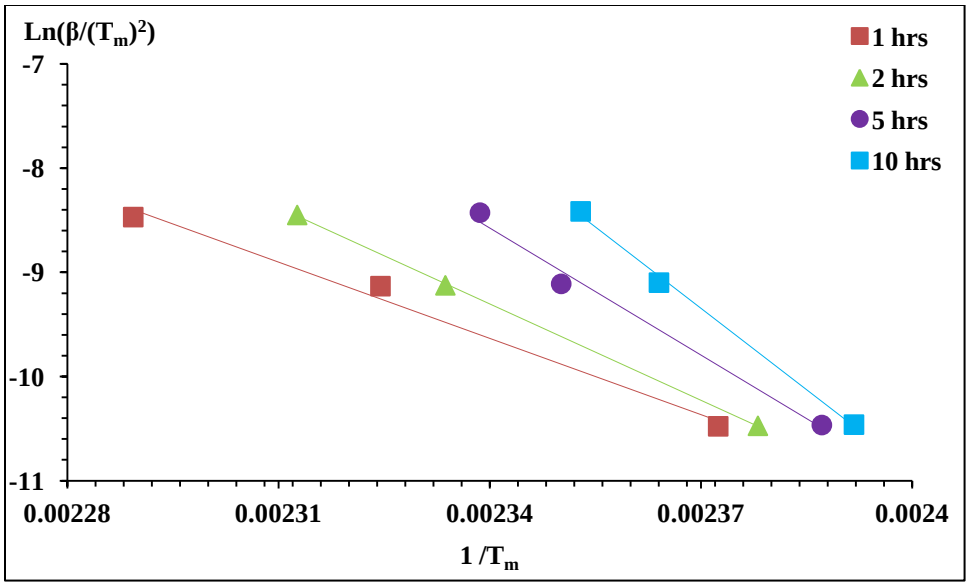

Figure 64: Plots of $\ln[\beta/T_m^2]$ versus $1/T_m$ for UHMWPE- 1wt. % Al_2O_3 for different milling times.

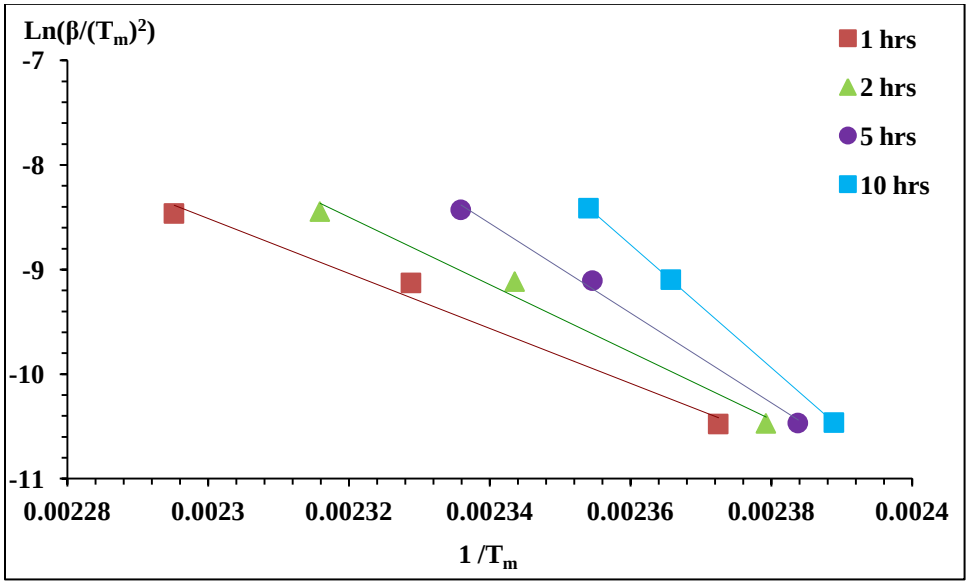

Figure 65: Plots of $\ln[\beta/T_m^2]$ versus $1/T_m$ for UHMWPE- 2.5wt. % Al_2O_3 for different milling times.

Table 2: Activation energy of melting E_a for UHMWPE and UHMWPE/Al_2O_3 systems.

Milling time (hrs)	**Activation energy of melting (kJ/mol)**		
	UHMWPE- 0wt.% Al_2O_3	**UHMWPE- 1wt.% Al_2O_3**	**UHMWPE- 2.5wt.% Al_2O_3**
0	148.7		
1	182.6	202.8	218.4
2	207.2	256.3	268.1
5	299.6	338	356.9
10	296.9	432.6	489

It is clear from Figures 66 and 67 and Table 2 that activation energy for melting increases both as a function of milling time and alumina composition. In Figure 66, there is a linear relationship between activation energy and milling time with the slope increasing with alumina composition. As milling proceeds the amorphous phase and the crystalline phases heavily deform and blend intimately and, also, become refined. The increase in activation energy with milling may be due to topological constraints brought about by the intimate and small scale blending of the phases caused by mechanical alloying [148]. This situation is aggravated when alumina particles are present for they get in the way, as seen in Figure 67 where activation energy increases linearly with alumina composition for a given milling time. Here also, the slope becomes steeper with milling time.

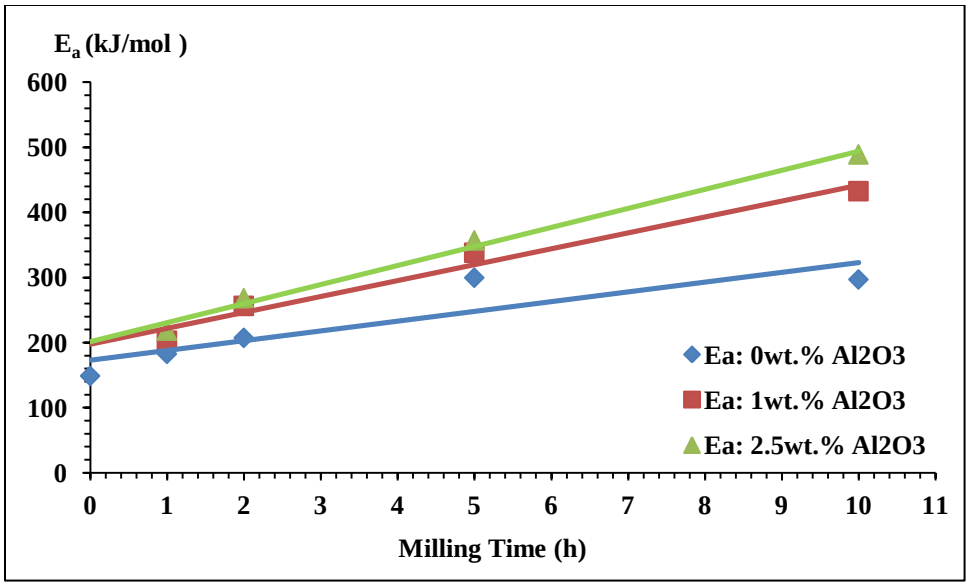

Figure 66: Activation energy of melting E_a for UHMWPE and WHMWPE/wt. % Al_2O_3 as a function of milling time.

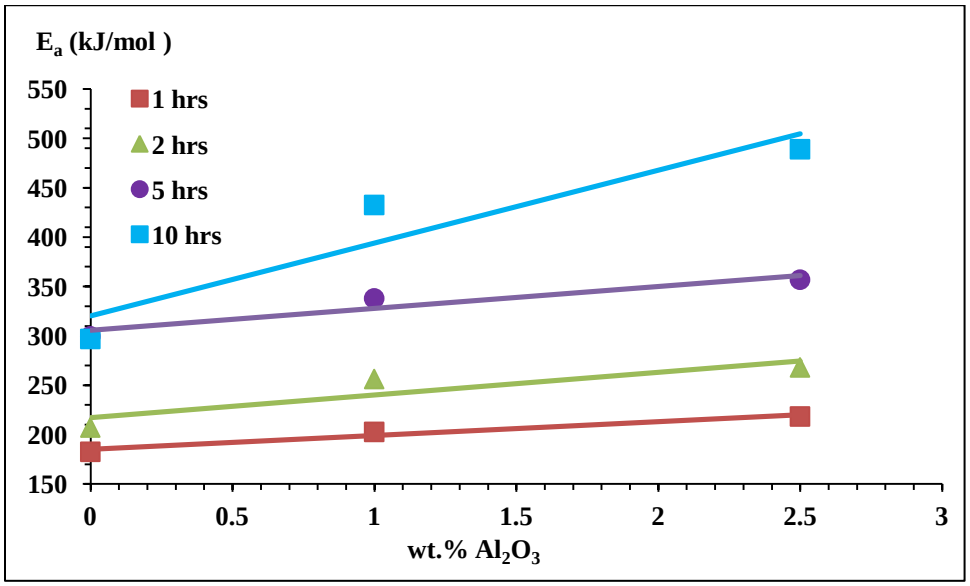

Figure 67: Activation energy of melting E_a for UHMWPE and WHMWPE/wt. % Al_2O_3 with different milling time as a function of wt. % Al_2O_3 contents.

4.1.5 Enthalpy of melting

The enthalpy of melting for milled UHMWPE and UHMWPE/Al_2O_3 powders were calculated from the DSC scans using the Proteus software. The results are plotted in Figures 68 and 69 for constant alumina compositions and constant milling times, respectively. For the samples tested at 5°C/min and 40°C/min, there do not seem to be any empirical relationship. However, at 20°C/min, there is a linear relationship between enthalpy and milling time, as well as enthalpy and alumina composition. The enthalpy values decrease as a function of both milling time and alumina composition. Even though it is difficult to initiate melting, because of the reduced molecular weight caused by the milling the melting enthalpy decreases with milling time. The presence of hard alumina particles contribute to the incision of polymer molecules, so their presence does reduce melting enthalpy as well.

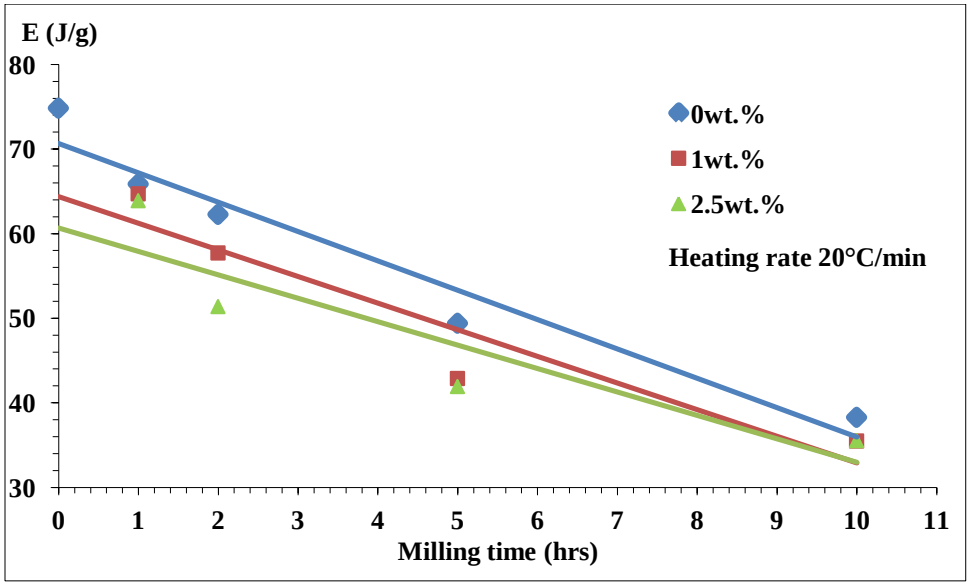

Figure 68: Enthalpy of melting for UHMWPE and WHMWPE/wt. % Al_2O_3 as a function of milling time.

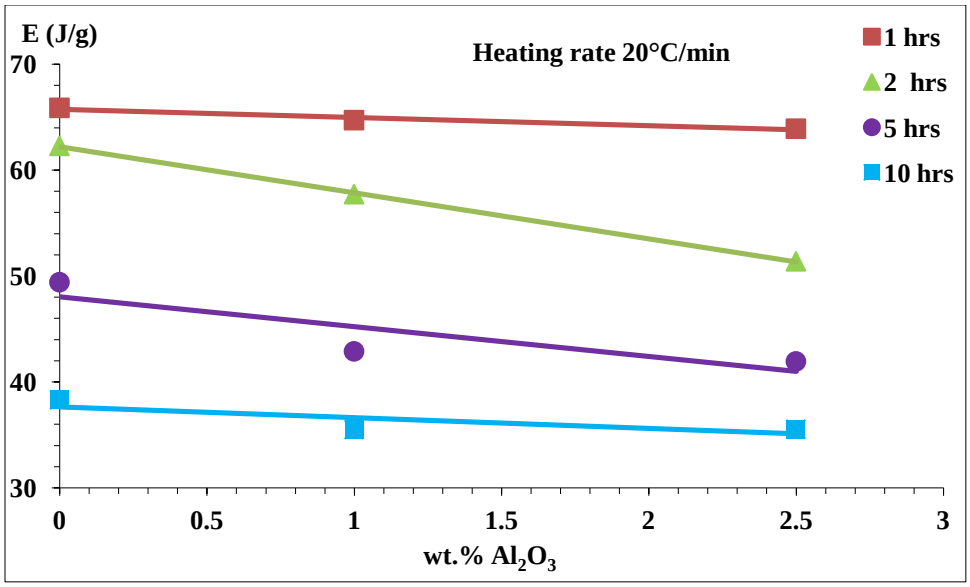

Figure 69: Enthalpy of melting for UHMWPE and WHMWPE/wt. % Al_2O_3 with different milling time as a function of wt. % Al_2O_3 contents.

4.2 Compression Molded Sheets Characterization

Characterization of the of the sheets compression molded from milled UHMWPE and UHMWPE/Al_2O_3 powders were performed using x-ray diffraction, differential scanning calorimetry, and tensile testing.

4.2.1 X-ray Diffraction

Typical x-ray diffraction patterns for the melt-processed sheets in Figures 70 and 71. Figure 70 shows scans of 1 wt. % alumina samples at different milling times, and Figure 71 shows scans of samples with different alumina compositions milled for 1h. Clearly, the metastable monoclinic phase that was induced in the milled powders is not present in the compression molding sheets. There is no significant difference in the x-ray diffraction patterns for the sheets prepared from as received or milled powders. An alumina reflection peak is observed at 25.44° in 2.5 wt. % alumina. Figures 72 and 73 are typical of the comparison of x-ray data between powders (milled and un-milled) and their corresponding compression molding sheets.

Monoclinic phase has disappeared after melting, and amorphous volume fraction has decreased after melting.

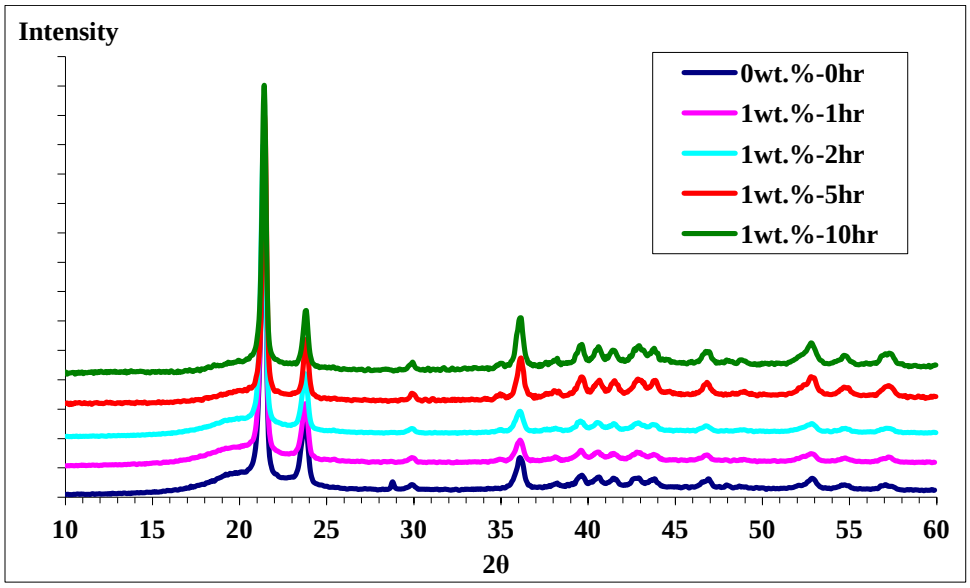

Figure 70: X-ray diffraction patterns for UHMWPE-1wt. % Al_2O_3 sheets milled up to 10 hours compared with sheets prepared from as received UHMWPE.

.

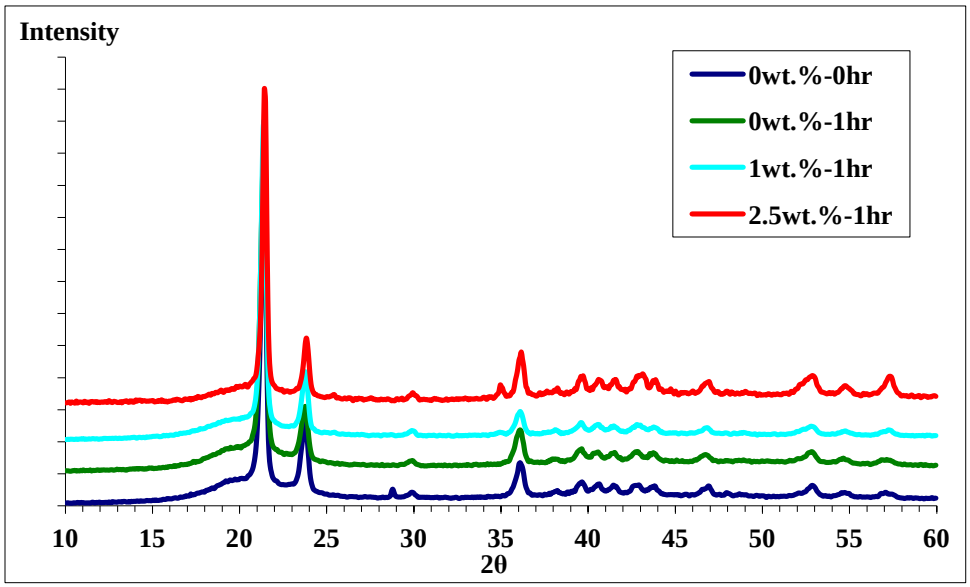

Figure 71: X-ray diffraction patterns for UHMWPE/Al_2O_3 sheets milled for 1 hour compared with sheets prepared from as received UHMWPE.

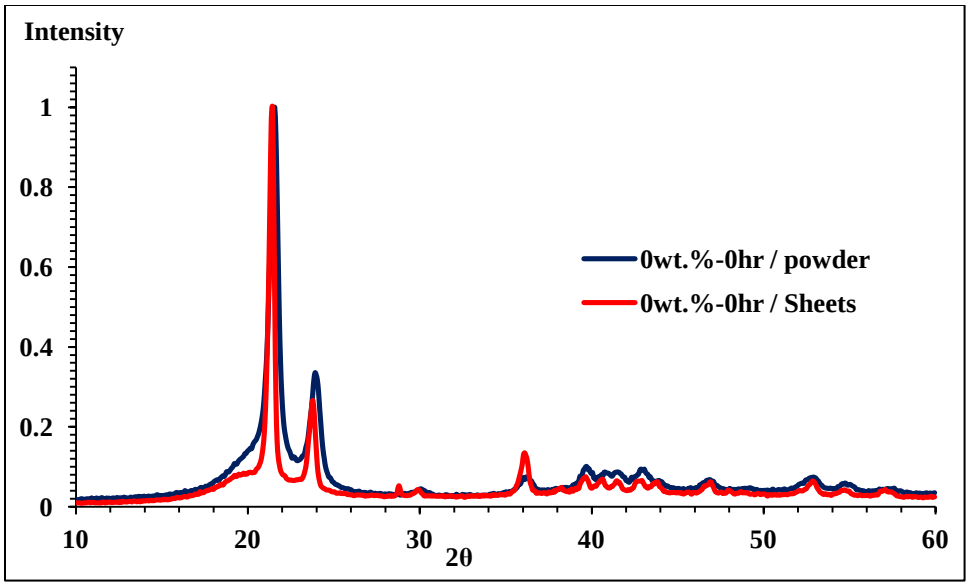

Figure 72: X-ray diffraction patterns of UHMWPE as received powder and sheet.

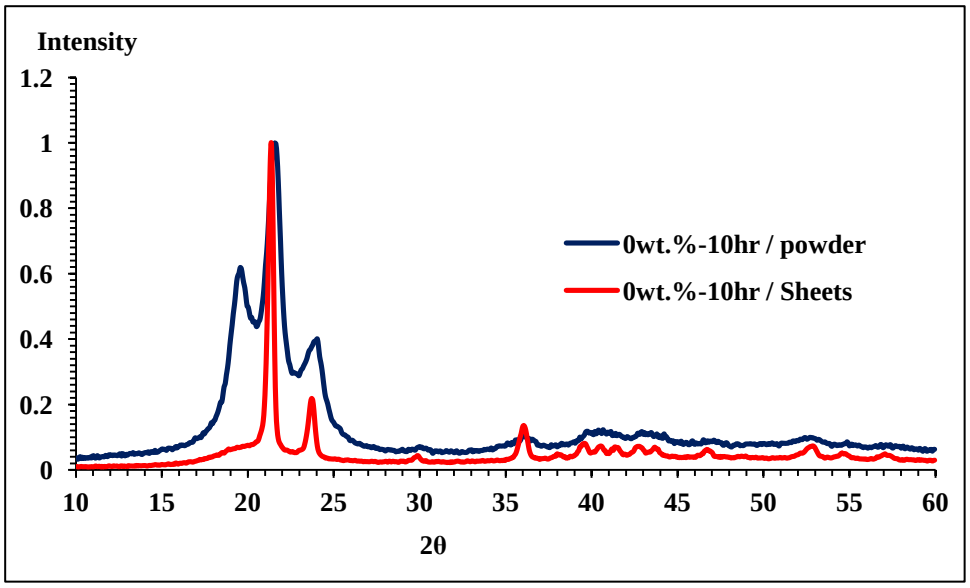

Figure 73: X-ray diffraction patterns of UHMWPE milled 10 hours as powder and sheet.

4.2.2 Determination of Crystallinity

Crystallinity of melt-processed polymer sheets was determined using MDI Jade software as used for the milled powders in Section 4.1.2 to isolate the amorphous and major crystalline peaks as shown in Figure 74; this makes it possible to determine the crystallinity, and the result is plotted as a function of milling time, as well as alumina content.

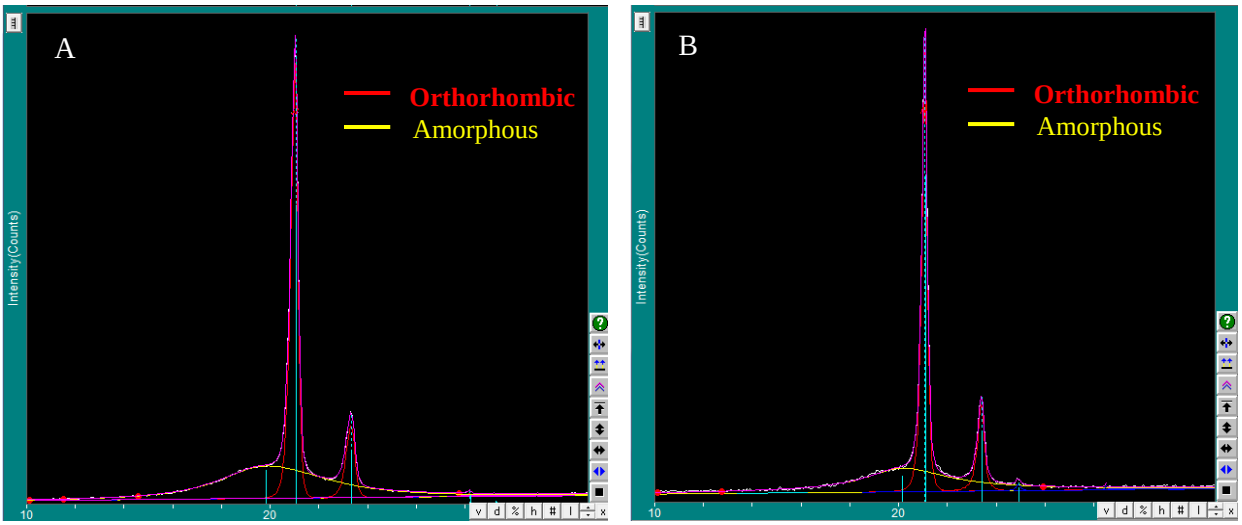

Figure 74: X-ray diffraction patterns analysis by the MDI Jade software (a) UHMWPE sheet of powder milled for 5 hours. (b) UHMWPE- 2.5wt. % Al_2O_3 sheet of powder alloyed for 5 hours.

4.2.2.1 The Effect of Milling Time on Crystallinity

Figure 75 shows the results for the relative change in the crystallinity of the three compositions of UHMWPE/Al_2O_3 sheets as a function of the milling time. There is not any specific trend. The highest crystallinity is found in the 10h milled 2.5 wt. % alumina at about 70 %, followed by the 10h 1.0 wt. % alumina. This is understandable since long milling results in a homogeneous dispersion of very fine alumina particles which can become nucleation sites for crystallization during the compression molding process. After 5h of milling, the crystallinity of the 1.0 wt. % alumina is about twice that of the 2.5 wt. % alumina. This is probably due to the fact that it would take a shorter time for the alumina to refine and homogeneously disperse in the 1.0 wt. % alumina sample than the 2.5 wt. % sample, leading to a more homogeneous crystalline structure.

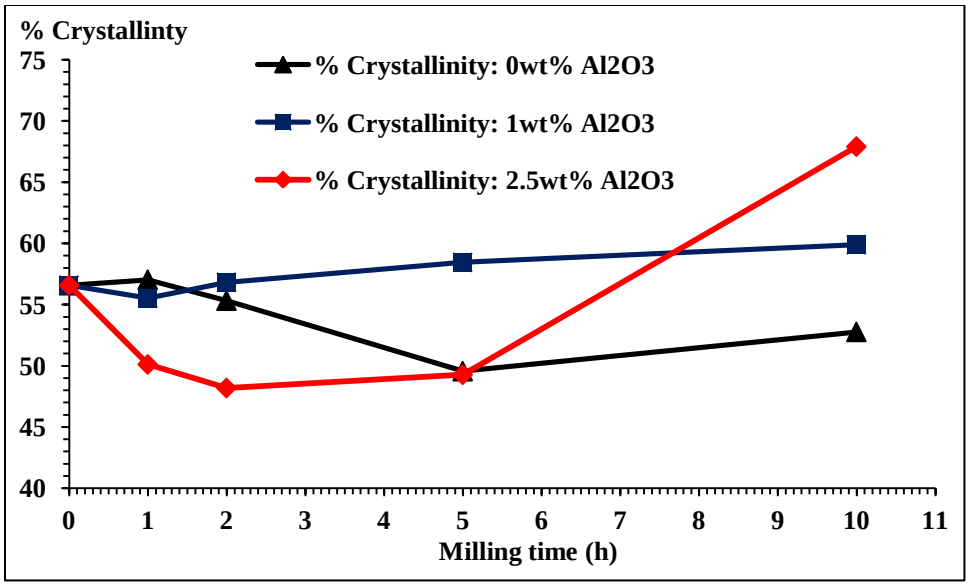

Figure 75: Evolution of the crystalline phase for UHMWPE/wt. % Al_2O_3 sheets as a function of the milling time as calculated from the integrated X-ray diffraction by the MDI Jade software.

In Figures 76, 77, and 78, crystallinity of milled powders is compared with that of their corresponding compression molding sheets as a function of milling time. Overall the total crystallinity (monoclinic plus orthorhombic) of the powders is substantially greater than that of the compression molding sheets. The main reason is the metastable monoclinic structure disappears with melting. However, when only orthorhombic phases are considered, crystallinity of the sheets tends to be greater than their corresponding milled pre- compression molding powders. This can be explained by the fact that nucleation of crystallization is helped by the defects introduced by the milling process and the presence of fine alumina particles.

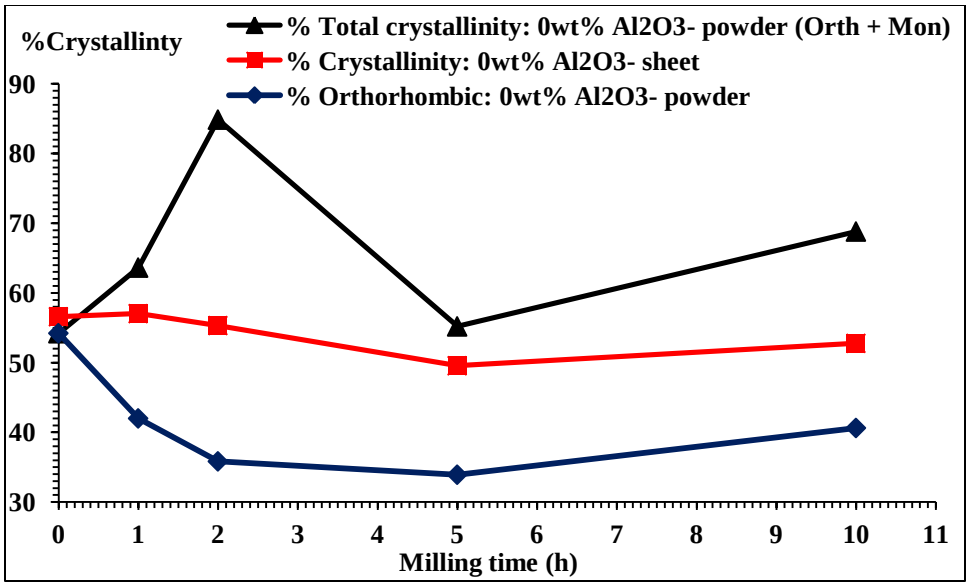

Figure 76: Evolution of the crystalline phase for the UHMWPE powder including orthorhombic and monoclinic phase, sheet and orthorhombic as a function of the milling time as calculated from the integrated X-ray diffraction by the MDI Jade software.

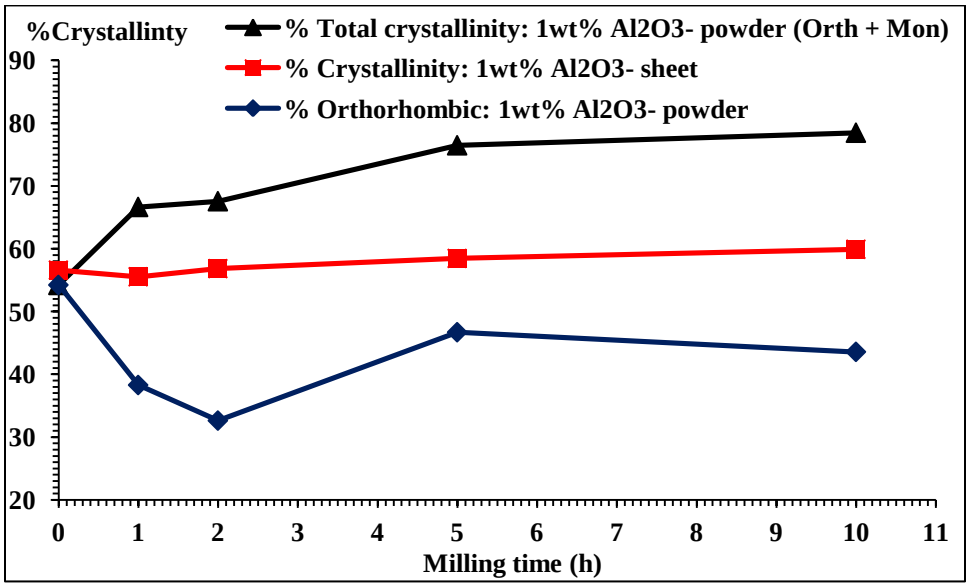

Figure 77: Evolution of the crystalline phase for the UHMWPE- 1wt. % Al_2O_3 powder including orthorhombic and monoclinic phase, sheet and orthorhombic as a function of the milling time as calculated from the integrated X-ray diffraction by the MDI Jade software.

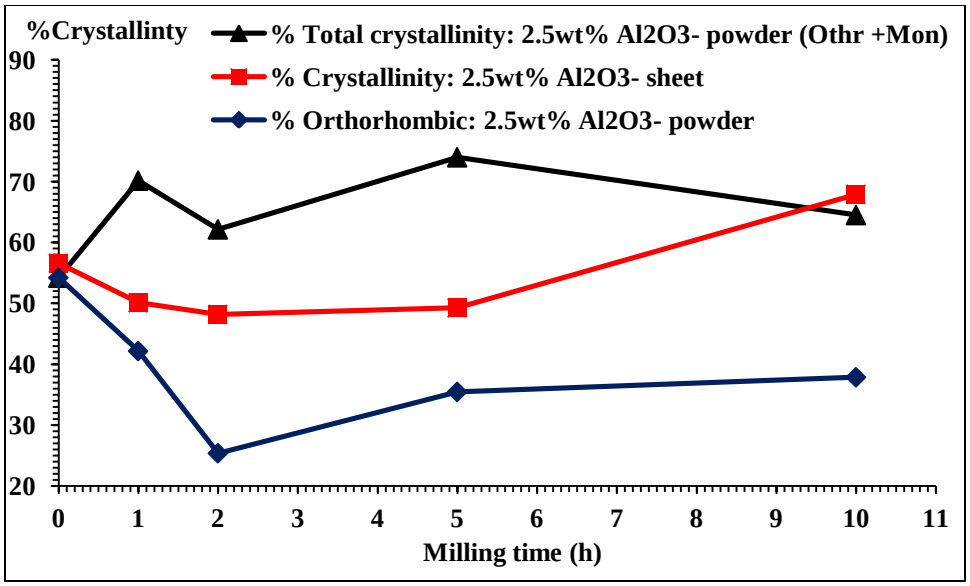

Figure 78: Evolution of the crystalline phase for the UHMWPE- 2.5wt. % Al_2O_3 powder including orthorhombic and monoclinic phase, sheet and orthorhombic as a function of the milling time as calculated from the integrated X-ray diffraction by the MDI Jade software.

4.2.2.2 The Effect of Al_2O_3 Composition on Crystallinity

For a given milling time, crystallinty in UHMWPE/ Al_2O_3 sheets tends to peak at 1 wt. % alumina, with the exception of the one with 10h milling history; this is shown in Figure 79. Again, this can be explained by the speed with which particles in the 1.0 wt. % alumina refines and disperse homogeneously as compared with the 2.5 wt. % alumina sample. Just like the effect of milling time, the total crystallinity of the milled powders is substantially larger than their corresponding compression molding samples, and the volume fraction of orthorhombic phase is larger in the sheets than in the milled powders as shown in Figures 80 - 83.

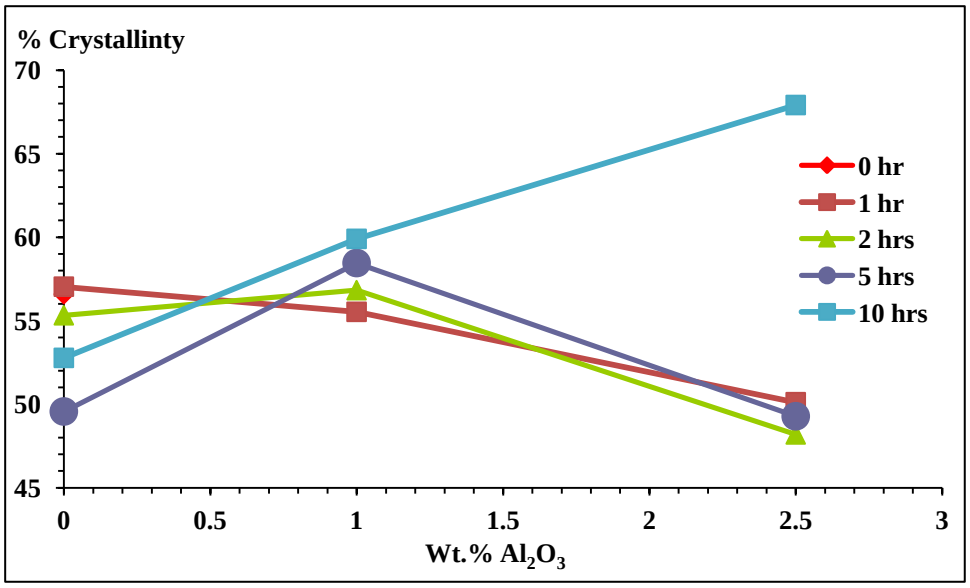

Figure 79: Evolution of the crystalline phase for UHMWPE/Al_2O_3 sheet with different milling time as a function of the wt. % Al_2O_3 as calculated from the integrated X-ray diffraction by the MDI Jade software.

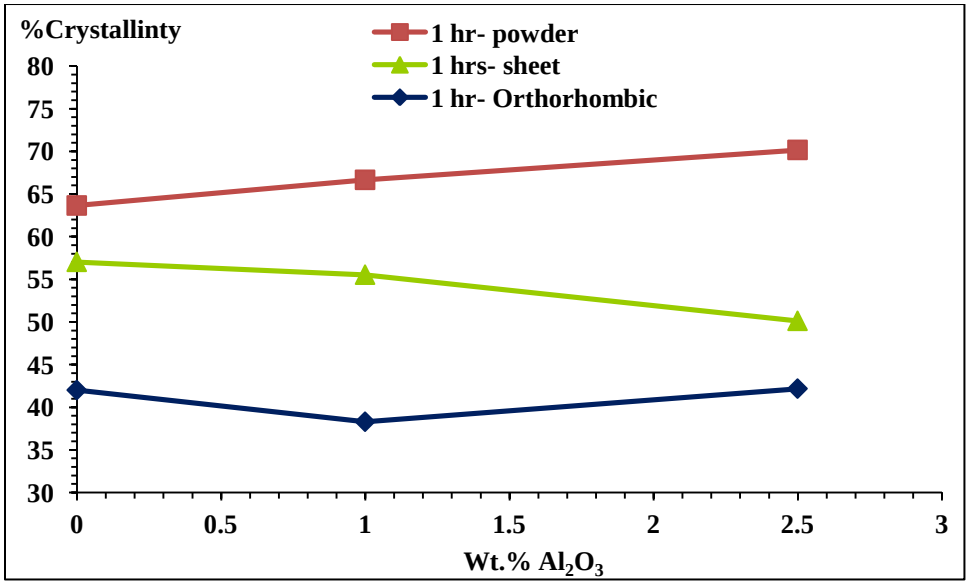

Figure 80: Evolution of the crystalline phase for UHMWPE/Al_2O_3 powder, sheet and orthorhombic at one hour as a function of the wt. % Al_2O_3 as calculated from the integrated X-ray diffraction by the MDI Jade software.

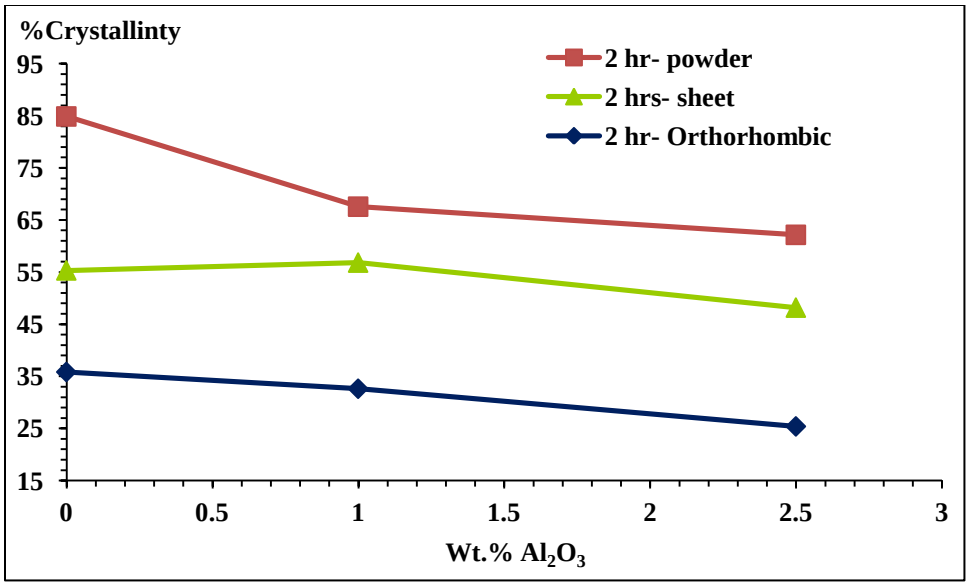

Figure 81: Evolution of the crystalline phase for UHMWPE/Al_2O_3 powder, sheet and orthorhombic at 2 hours as a function of the wt. % Al_2O_3 as calculated from the integrated X-ray diffraction by the MDI Jade software.

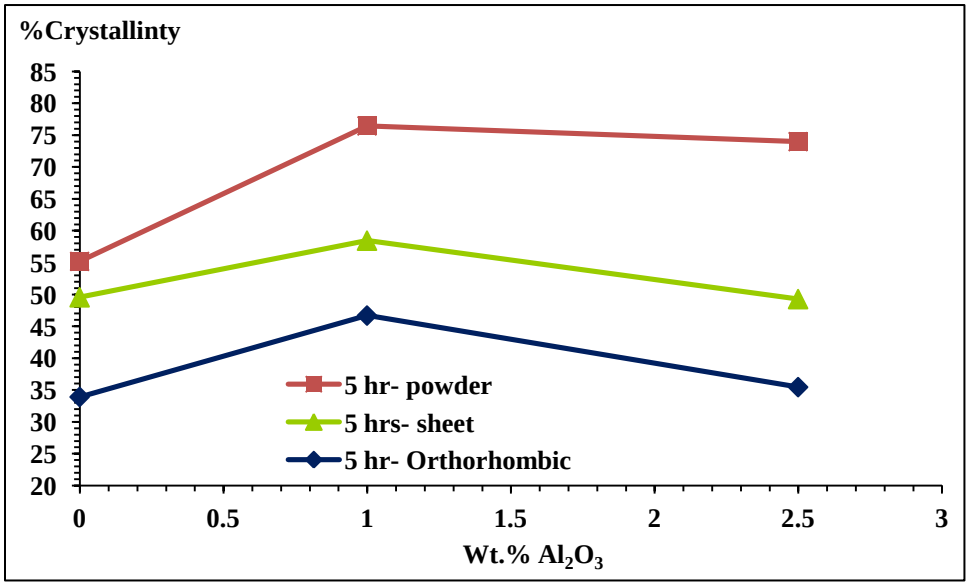

Figure 82: Evolution of the crystalline phase for UHMWPE/Al_2O_3 powder, sheet and orthorhombic at 5 hours as a function of the wt. % Al_2O_3 as calculated from the integrated X-ray diffraction by the MDI Jade software.

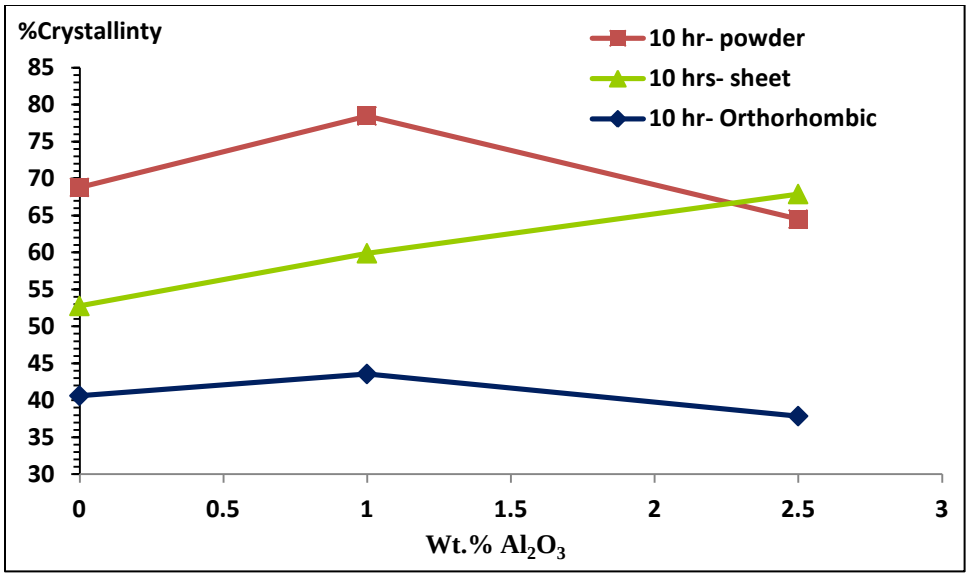

Figure 83: Evolution of the crystalline phase for UHMWPE/Al_2O_3 powder, sheet and orthorhombic at 10 hours as a function of the wt. % Al_2O_3 as calculated from the integrated X-ray diffraction by the MDI Jade software.

4.2.3 Differential Scanning Calorimetry Analysis

Figures 84, 85, and 86 an examples show the typical DSC traces obtained for UHMWPE sheets of different wt. % Al_2O_3 contents and milling time at a heating rate of 5, 20, and 40°C/min. DSC results were used to determine the effect of milling time and wt. % Al_2O_3 contents on the melting temperature, activation energy, and enthalpy of melting to the UHMWPE sheets.

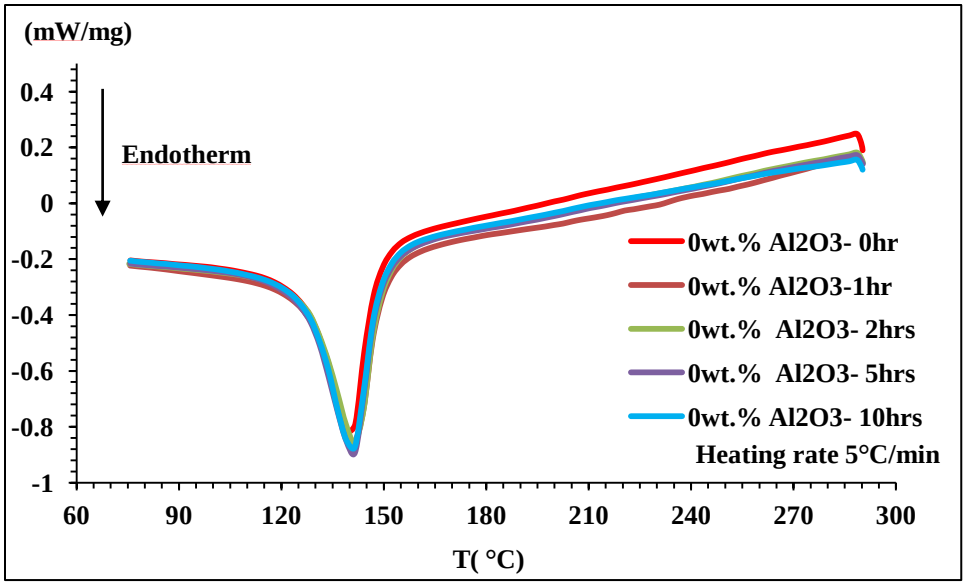

Figure 84: Differential scanning calorimetry curves of the UHMWPE- 0wt. % Al_2O_3 sheets for different milling time with heating rate of 5°C/min.

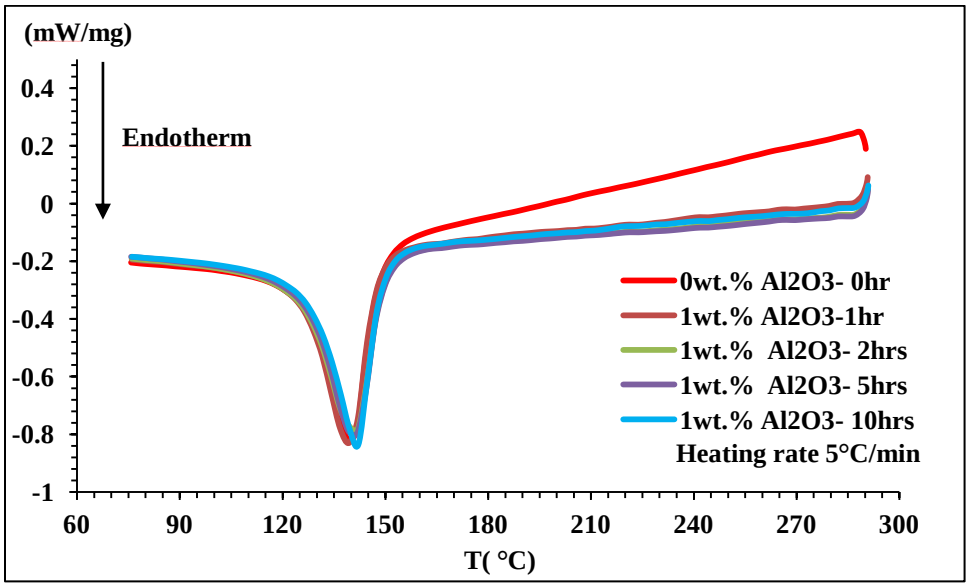

Figure 85: Differential scanning calorimetry curves of the UHMWPE- 1wt. % Al_2O_3 sheets for different milling time with heating rate of 5°C/min.

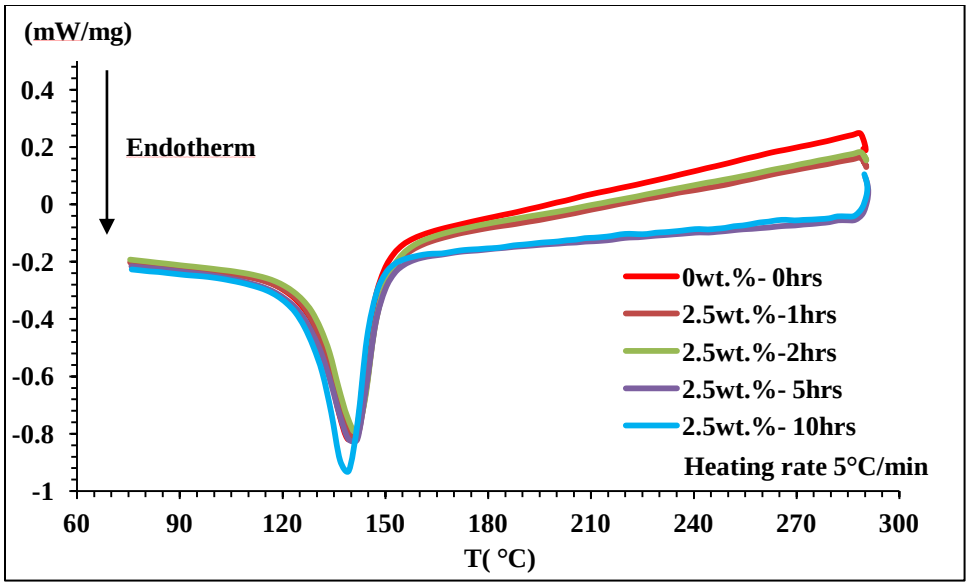

Figure 86: Differential scanning calorimetry curves of the UHMWPE- 2.5wt. % Al_2O_3 sheets for different milling time with heating rate of 5°C/min.

4.2.3.1 The Effect of Milling Time on the Melting Temperature

The effect of milling on melting temperature of UHMWPE/Al_2O_3 sheets for different wt. % Al_2O_3 contents and at different heat rates 5, 20, and 40°C/min are shown in Figures 87, 88, and 89.

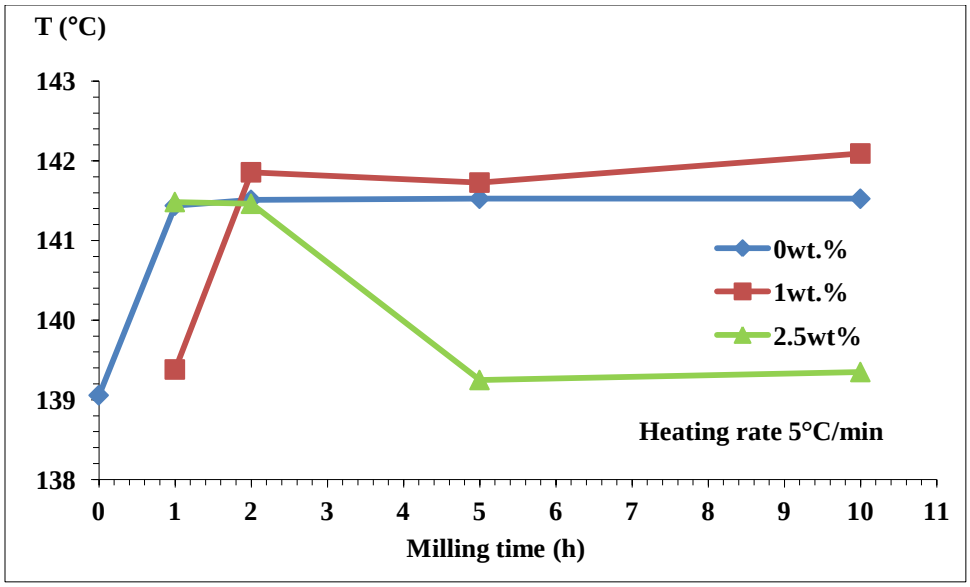

Figure 87: The effect of milling time on the melting temperature for UHMWPE/Al_2O_3 sheets with different milling time at heating rate of 5°C/min.

It is evident that the melting temperature of UHMWPE/ Al_2O_3 alloyed sheets, represented by 0, 1, and 2.5wt. % in Figures 87, 88, and 89, reached highest points in 1wt. % Al_2O_3 sheets at various milling times (between 2 and 10h) at every heating rate. It is unclear why this composition behaves this way.

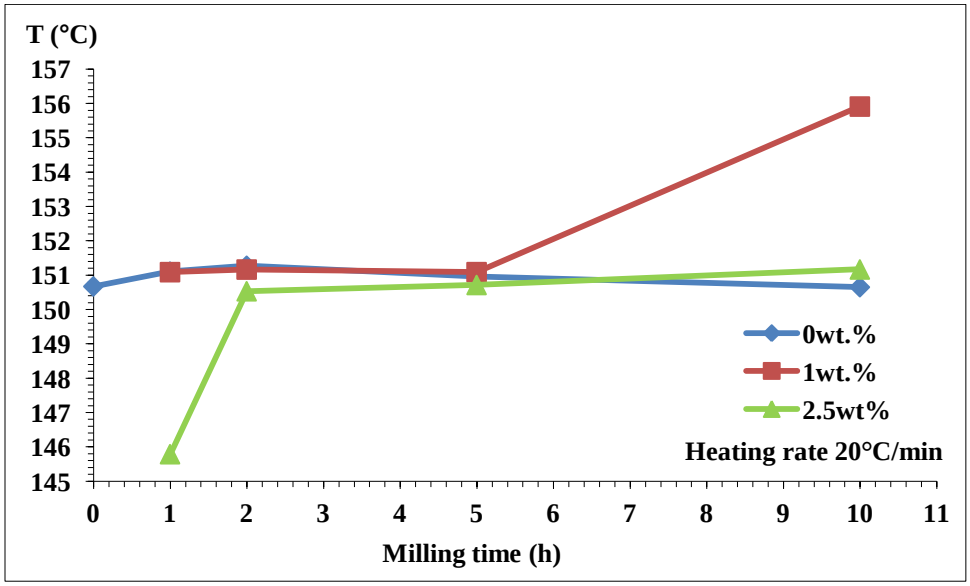

Figure 88: The effect of milling time on the melting temperature for UHMWPE/Al_2O_3 sheets with different milling time at heating rate of 20°C/min.

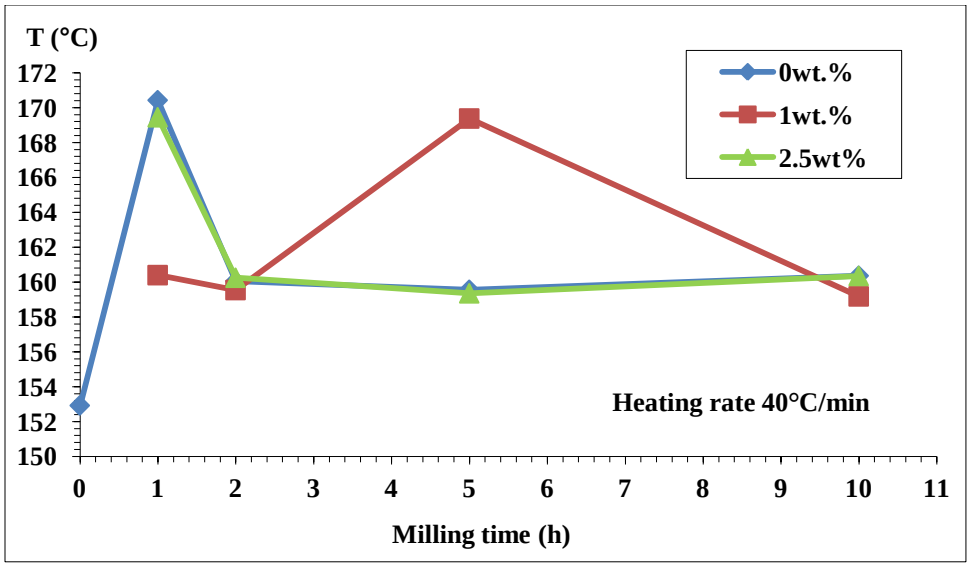

Figure 89: The effect of milling time on the melting temperature for UHMWPE/Al_2O_3 sheets with different milling time at heating rate of 40°C/min.

4.2.3.2 The Effect of wt. % Al_2O_3 contents on the Melting temperature

As mentioned in the effect of milling time on the melting temperature section that the melting temperature of UHMWPE/Al_2O_3 alloyed sheets is highest for the 1.0 wt. % Al_2O_3 content within the milling time range. Figures 90, 91, and 92 illustrate this effect. With the exception of the 1h milled samples where the melting point crests, the melting point peaks at 1 wt. % alumina for all milling times.

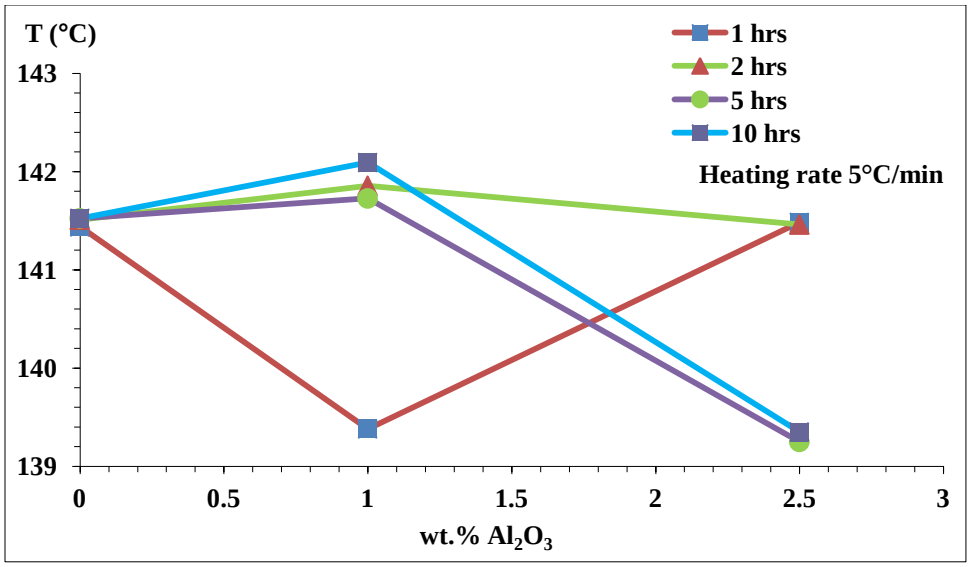

Figure 90: The effect of wt. % Al_2O_3 contents on the melting temperature for UHMWPE/Al_2O_3 sheets with different milling time at heating rate of 5°C/min.

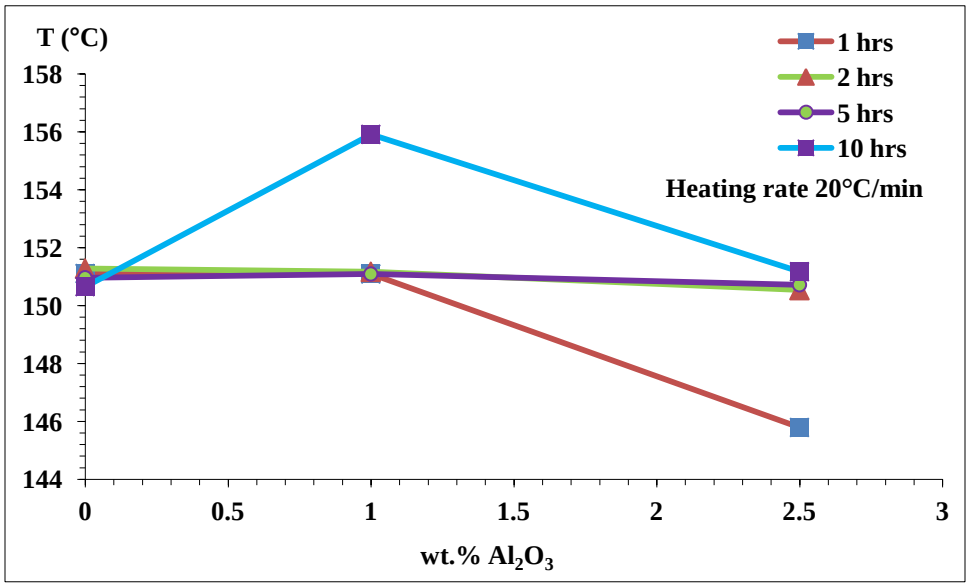

Figure 91: The effect of wt. % Al_2O_3 contents on the melting temperature for UHMWPE/Al_2O_3 sheets with different milling time at heating rate of 20°C/min.

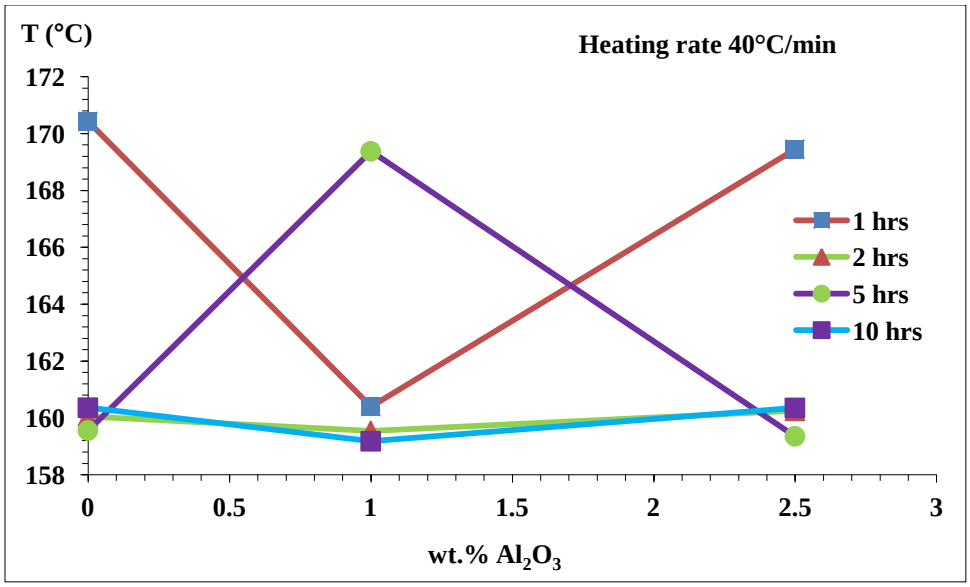

Figure 92: The effect of wt. % Al_2O_3 contents on the melting temperature for UHMWPE/Al_2O_3 sheets with different milling time at heating rate of 40°C/min.

Tables 3, 4, and 5 present the results of melting temperature of UHMWPE/Al_2O_3 powder and sheets that obtained at various heating rate 5, 20, and 40°C/min to see the effect the milling time on the melting temperature. As seen in Tables 3, 4, and 5, the melting temperature of UHMWPE/Al_2O_3 sheets samples are generally lower than the powder samples.

Table 3: Melting temperature of UHMWPE- 0wt. % Al_2O_3 as powder and sheets with different heating rate.

Melting temperature of UHMWPE- 0wt. % Al_2O_3 (°C)								
	Heating rate 5°C/min			**Heating rate 20°C/min**			**Heating rate 40°C/min**	
Milling time (hr)	**Powder**	**Sheet**		**Powder**	**Sheet**		**Powder**	**Sheet**
0	**149.4**	**139.057**		**159.3**	**150.675**		**170.1**	**152.921**
1	**148.7**	**141.437**		**158.2**	**151.107**		**165.7**	**170.426**
2	**147.5**	**141.51**		**156.2**	**151.277**		**162.4**	**160.052**
5	**147.1**	**141.524**		**153.8**	**150.962**		**157.3**	**159.556**
10	**146.3**	**141.524**		**151.7**	**150.654**		**156.6**	**160.36**

Table 4: Melting temperature of UHMWPE- 1wt. % Al_2O_3 as powder and sheets with different heating rate.

Melting temperature of UHMWPE- 1wt. % Al_2O_3 (°C)								
	Heating rate 5°C/min			Heating rate 20°C/min			Heating rate 40°C/min	
Milling time (hr)	Powder	Sheet		Powder	Sheet		Powder	Sheet
1	148.5	139.381		157.2	151.091		163.8	160.398
2	147.5	141.856		155.5	151.167		159.4	159.543
5	145.9	141.727		152.5	151.091		154.6	169.378
10	145.1	142.092		150	155.913		152	159.179

Table 5: Melting temperature of UHMWPE- 2.5wt. % Al_2O_3 as powder and sheets with different heating rate.

Melting temperature of UHMWPE- 2.5wt. % Al_2O_3 (°C)								
	Heating rate 5°C/min			Heating rate 20°C/min			Heating rate 40°C/min	
Milling time (hr)	Powder	Sheet		Powder	Sheet		Powder	Sheet
1	148.5	141.483		156.4	145.791		162.7	169.449
2	147.3	141.461		153.7	150.535		158.8	160.247
5	146.5	139.249		151.7	150.718		155.1	159.354
10	145.6	139.349		149.7	151.17		151.8	160.352

4.2.4 Activation Energy of Melting for Sheets

Using Kissinger's relation (Eq. (1)) and (Eq. (2)) in section 4.1.4, the plots of $\ln[\beta/T_m^2]$ against $(1/T_m)$ are shown in Figures 93, 94, and 95 for UHMWPE and UHMWPE/Al_2O_3 sample sheets corresponding the various milling times. Activation energy of melting was determined from slopes of the plots, and they are displayed in Table 6.

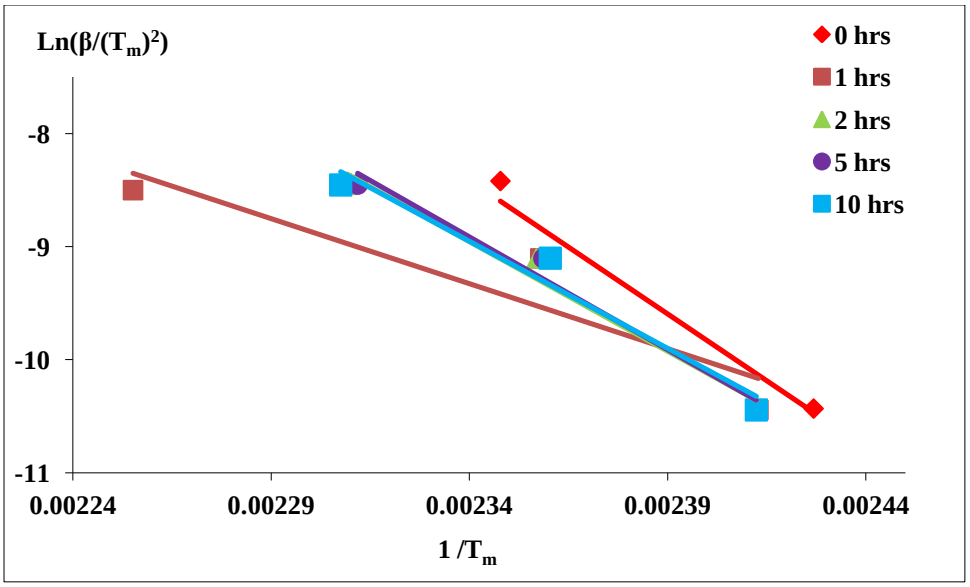

Figure 93: Plots of ln[β/T_m^2] versus $1/T_m$ for UHMWPE- 0wt. % Al_2O_3 sheets with different milling time.

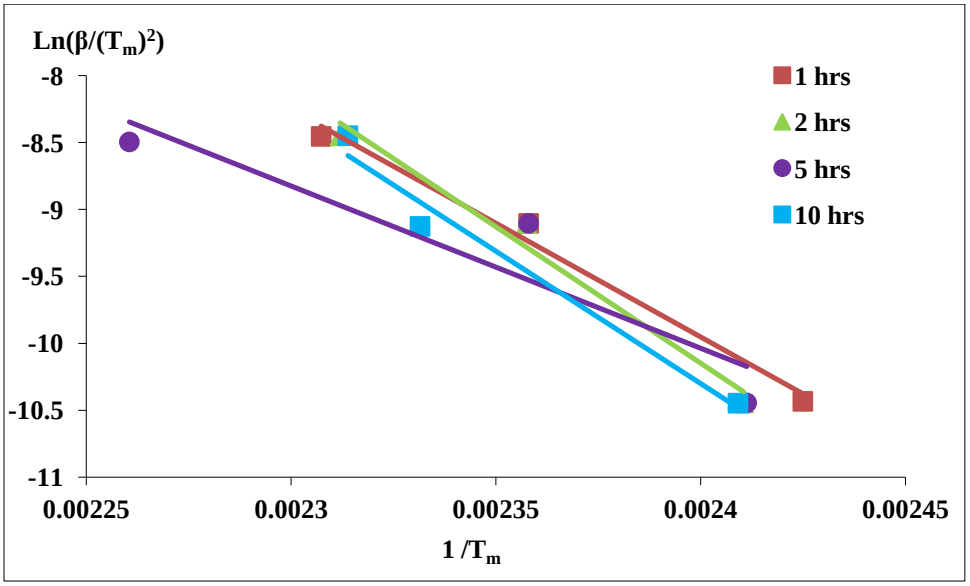

Figure 94: Plots of ln[β/T_m^2] versus $1/T_m$ for UHMWPE- 1wt. % Al_2O_3 sheets with different milling time.

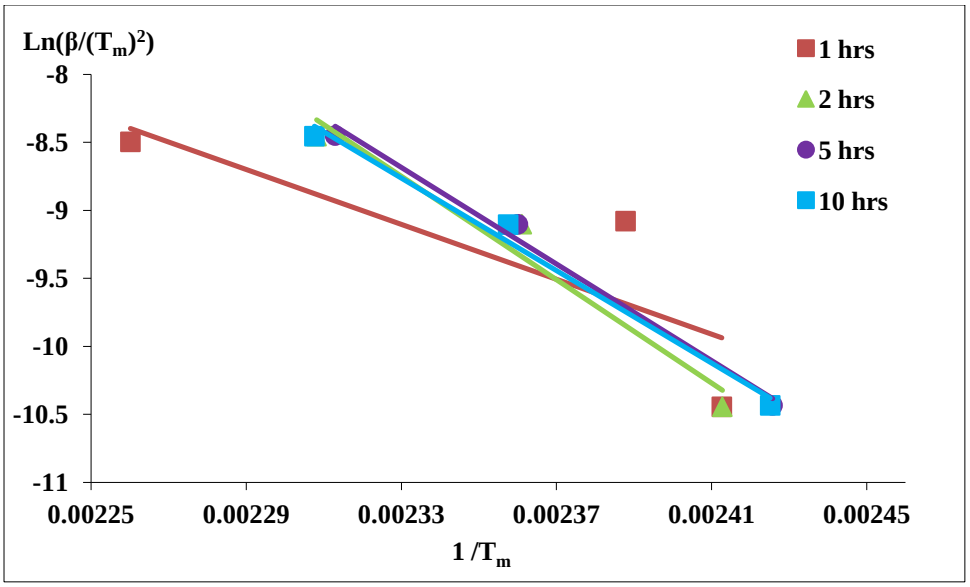

Figure 95: Plots of ln[β/T_m^2] versus $1/T_m$ for UHMWPE- 2.5wt. % Al_2O_3 sheets with different milling time

The results shown in Table 6 and Figures 96 and 97 show no clear trend in terms on milling time or composition in the activation energy of melting E_a of UHMWPE/Al_2O_3 sheet samples.

Table 6: Activation energy of melting E_a for UHMWPE and UHMWPE/Al_2O_3 sheets systems.

Milling time (hrs)	**Activation energy of melting (kJ/mol)**		
	UHMWPE- 0wt.% Al_2O_3	**UHMWPE- 1wt.% Al_2O_3**	**UHMWPE- 2.5wt.% Al_2O_3**
0	196.7163		
1	95.64771	141.3098	83.93286
2	161.4138	169.4787	157.9883
5	165.9119	100.7444	147.662
10	157.6807	164.4901	141.4096

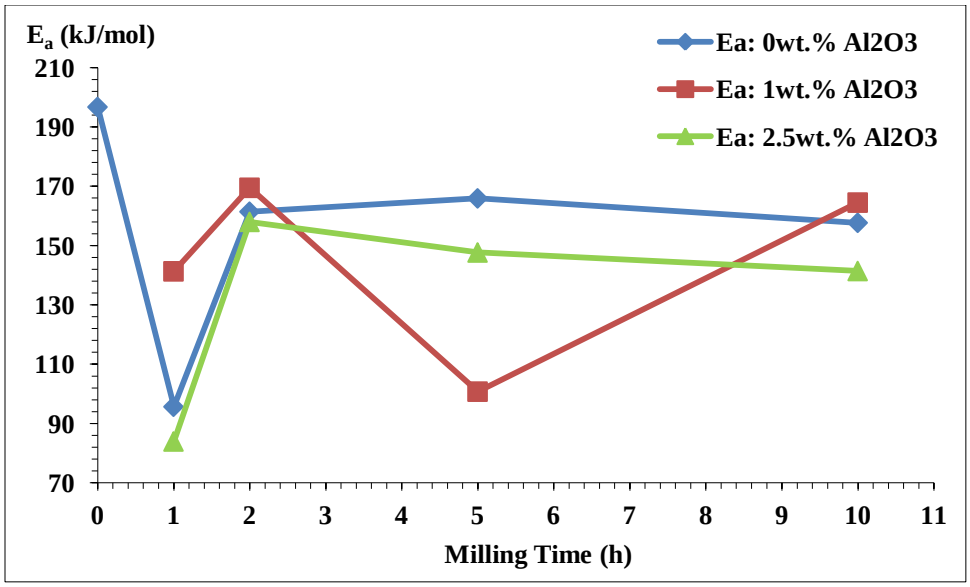

Figure 96: Activation energy of melting E_a for UHMWPE and WHMWPE/wt. % Al_2O_3 sheets samples as a function of milling time.

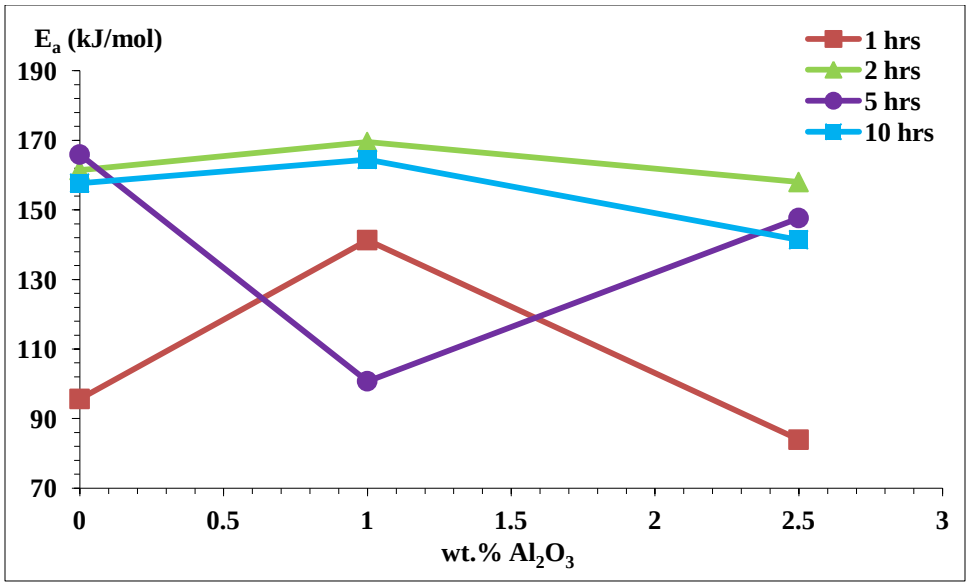

Figure 97: Activation energy of melting E_a for UHMWPE and WHMWPE/wt. % Al_2O_3 sheets samples with different milling time as a function of wt. % Al_2O_3 contents.

4.2.5 Enthalpy of melting

The enthalpies of melting for the samples were calculated from the DSC graphs by Proteus software. Typical plots of the enthalpy of melting for UHMWPE and UHMWPE/Al_2O_3 sample

sheets as a function of milling time, and alumina composition are shown in Figures 98 and 99 for the 5°C/min rate. Overall it is highest for pure UHMWPE and lowest for the 1wt. % alumina in the milling time range. When plotted as a function of alumina composition, the enthalpy crests at 1wt. % alumina.

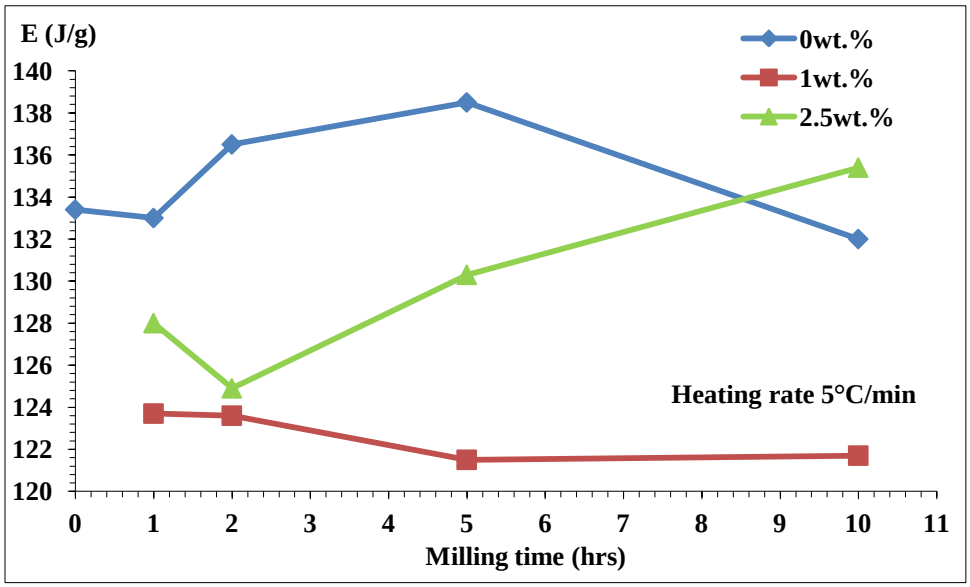

Figure 98: Enthalpy of melting for UHMWPE and WHMWPE/wt. % Al_2O_3 sample sheets as a function of milling time.

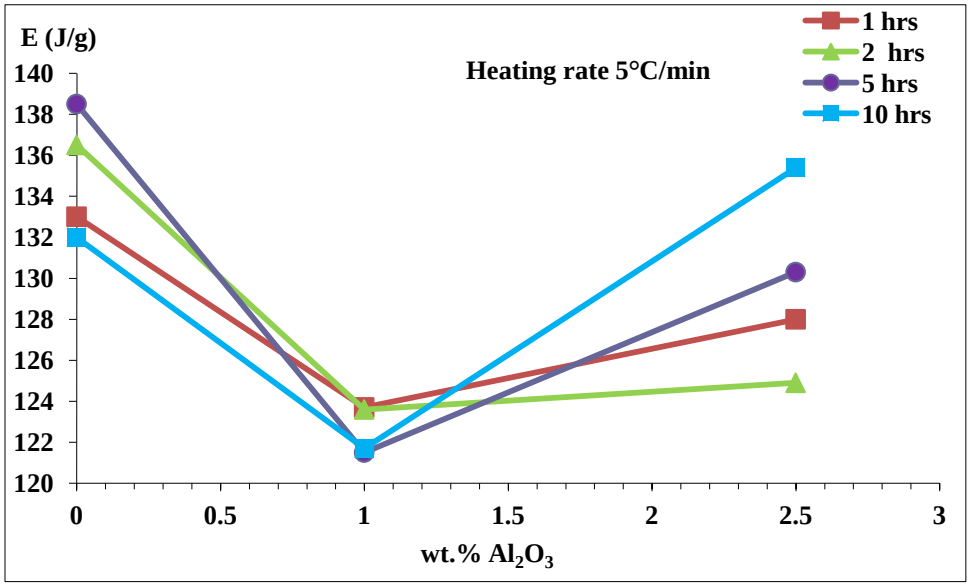

Figure 99: Enthalpy of melting for UHMWPE and WHMWPE/wt. % Al_2O_3 with different milling time as a function of wt. % Al_2O_3 contents.

4.2.6 Microscopy

Representative optical micrographs of compaction molded samples which were microtomed are presented in Figures 100 and 101. Figure 100 shows equiaxed grains in the compression molded sheet of the UHMWPE-1wt% alumina powders that were milled for 1 hour. However the 10h milled sample in Figure 101 shows a different microstructure; it is fibrous in nature.

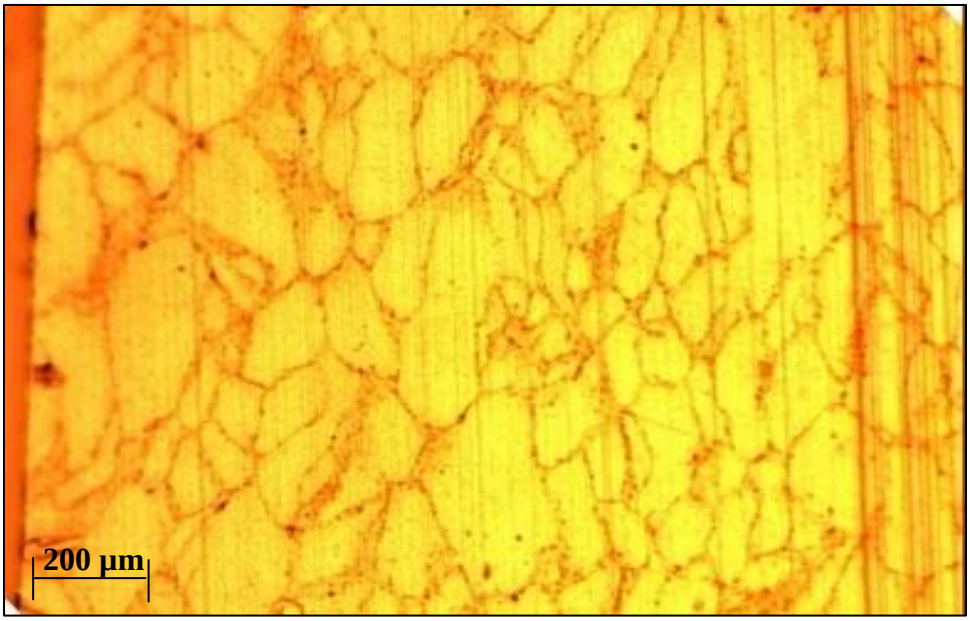

Figure 100: Photomicrograph of a compression molded sheet of the composite of the 1wt.% Al_2O_3 that was milled for 1 hour.

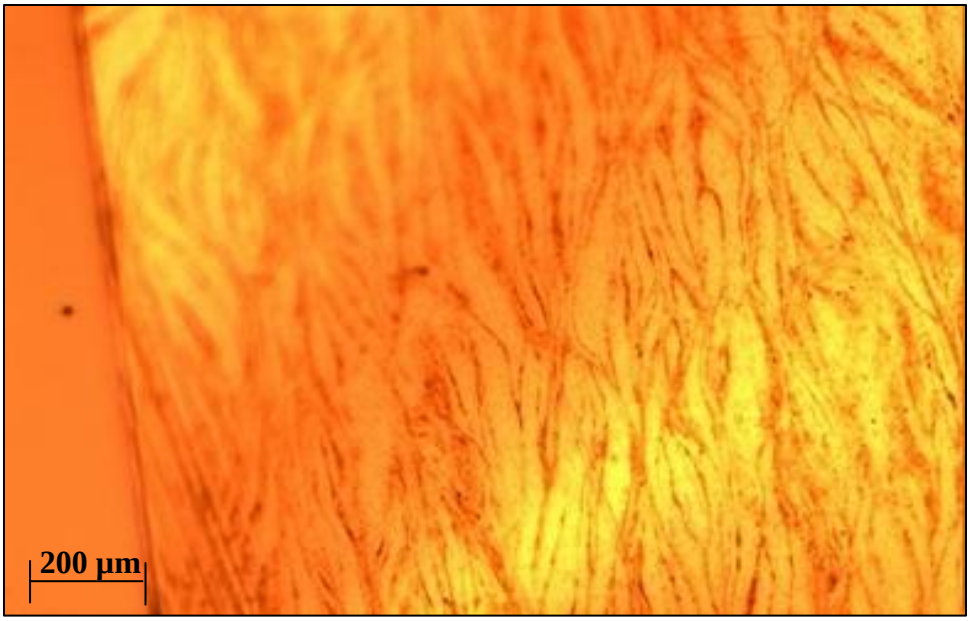

Figure 101: Photomicrograph of a compression molded sheet of the composite of the 1wt.% Al_2O_3 that was milled for 10 hours.

4.2.7 Tensile test

Representative engineering stress-strain curves for the UHMWPE and UHMWPE/Al_2O_3 samples are shown in Figures 102, 103, and 104. Average yield strength, tensile strength, Young's modulus, and elongation to failure values were determined from the tensile tests and are recorded in Tables 7- 18.

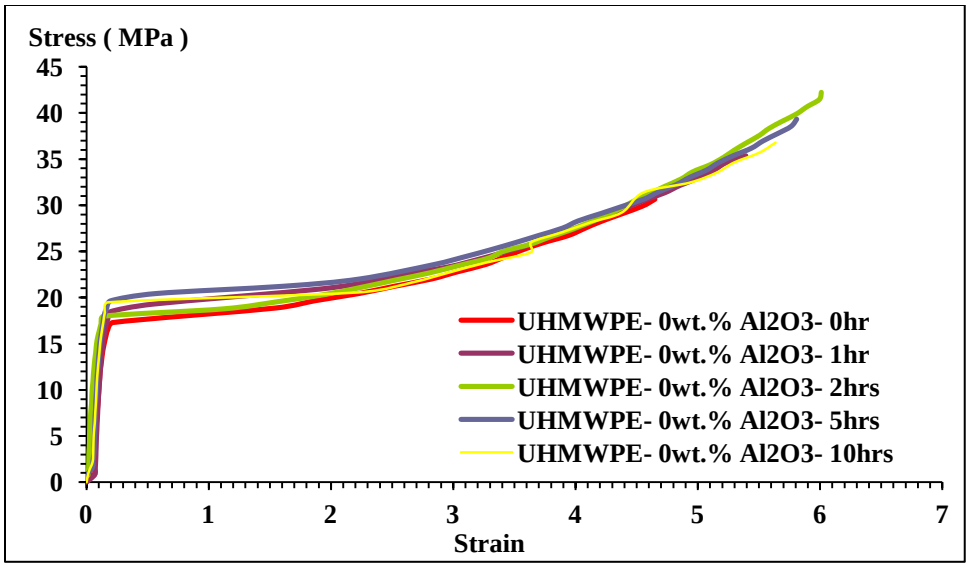

Figure 102: Representative engineering stress-strain curves for tensile tests performed on UHMWPE samples milled for different hours.

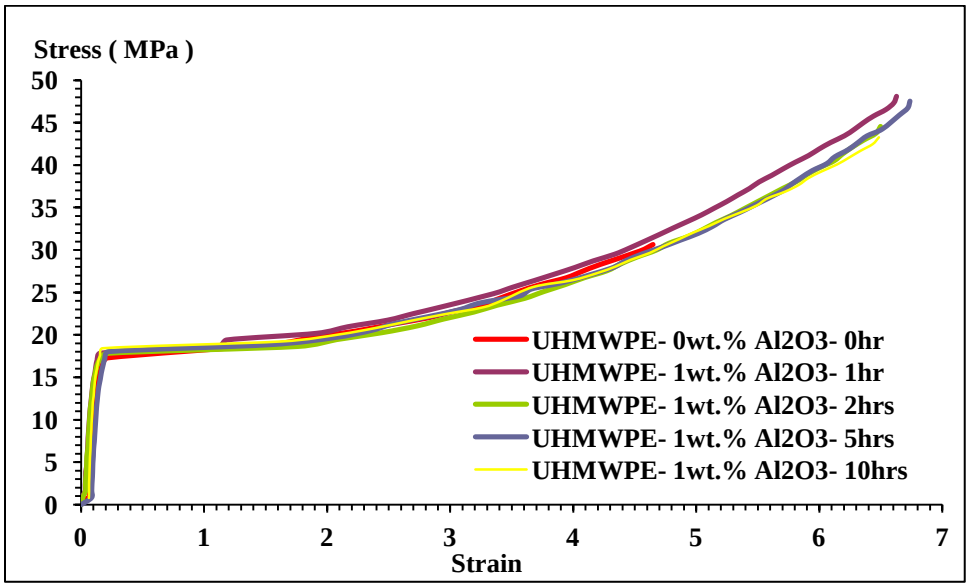

Figure 103: Representative engineering stress-strain curves for tensile tests performed on WHMWPE- 1wt. % Al_2O_3 samples milled for different hours.

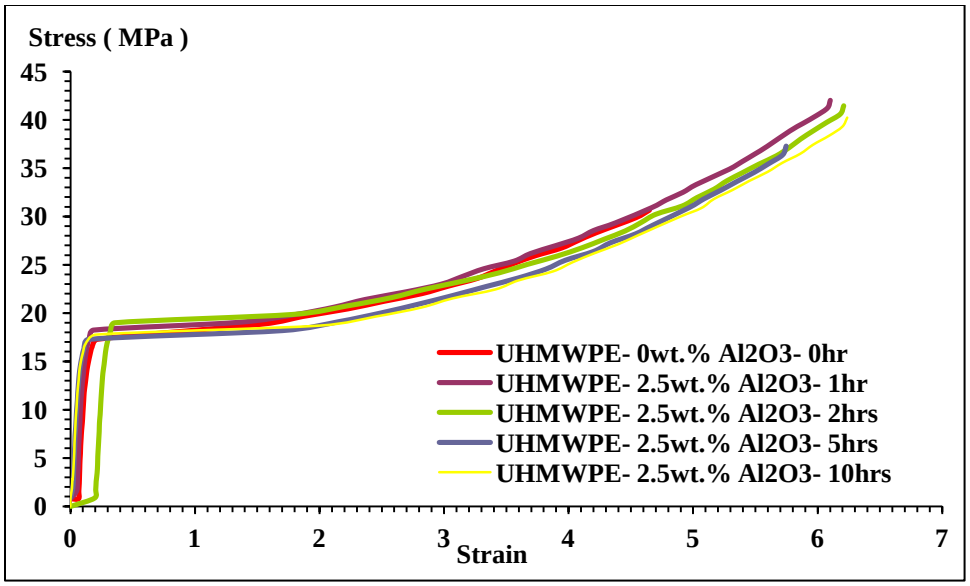

Figure 104: Representative engineering stress-strain curves for tensile tests performed on WHMWPE- 2.5wt. % Al_2O_3 samples milled for different hours.

Table 7: Averages of yield strength measurements on compression molded sheets of pure UHMWPE milled up 10 hours.

Milling time (h)	0	1	2	5	10
Mean of yield strength (MPa)	18.2	18.2	17.7	19.1	19.7
standard deviation	0.15	2.1	0.65	1.6	1.0

Table 8: Averages of tensile strength measurements on compression molded sheets of pure UHMWPE milled up 10 hours.

Milling time (h)	0	1	2	5	10
Mean of tensile strength (MPa)	36.3	40.9	44.1	38.4	40.7
standard deviation	5.0	3.4	1.7	1.3	1.5

Table 9: Averages of modulus measurements on compression molded sheets of pure UHMWPE milled up 10 hours.

Milling time (h)	0	1	2	5	10
Mean of modulus (MPa)	227.3	221.2	216.3	223.9	240.1
standard deviation	17.5	15.5	6.2	13.2	7.1

Table 10: Averages of % elongation measurements on compression molded sheets of pure UHMWPE milled up 10 hours.

Milling time (h)	0	1	2	5	10
Mean of % elongation	553.4	621.1	635.0	557.7	618.5
standard deviation	56.9	21.6	27.7	36.2	23.6

Table 11: Averages of yield strength measurements on compression molded sheets of composite UHMWPE- 1wt.% Al_2O_3 milled up 10 hours.

Milling time (h)	1	2	5	10
Mean of yield strength (MPa)	18.9	18.5	19.1	19.1
standard deviation	1.3	0.92	0.64	0.319

Table 12: Averages of tensile strength measurements on compression molded sheets of composite UHMWPE- 1wt.% Al_2O_3 milled up 10 hours.

Milling time (h)	1	2	5	10
Mean of tensile strength (MPa)	43.0	41.3	47.3	40.2
standard deviation	3.9	2.2	1.5	2.3

Table 13: Averages of modulus measurements on compression molded sheets of composite UHMWPE- 1wt.% Al_2O_3 milled up 10 hours.

Milling time (h)	1	2	5	10
Mean of modulus (MPa)	231.2	229.0	220.8	242.36
standard deviation	8.3	11.3	11.7	19.2

Table 14: Averages of % elongation measurements on compression molded sheets of composite UHMWPE- 1wt.% Al_2O_3 milled up 10 hours.

Milling time (h)	1	2	5	10
Mean of % Elongation	646.3	562.3	596.2	620.5
standard deviation	11.3	30.4	70.6	21.8

Table 15: Averages of yield strength measurements on compression molded sheets of composite UHMWPE- 2.5wt.% Al_2O_3 milled up 10 hours.

Milling time (h)	1	2	5	10
Mean of yield strength (MPa)	19.3	19.1	18.2	18.3
standard deviation	0.73	1.2	1.5	1.21

Table 16: Averages of tensile strength measurements on compression molded sheets of composite UHMWPE- 2.5wt.% Al_2O_3 milled up 10 hours.

Milling time (h)	1	2	5	10
Mean of tensile strength (MPa)	41.3	41.2	38.3	40.1
standard deviation	1.8	0.50	1.6	

Table 17: Averages of modulus measurements on compression molded sheets of composite UHMWPE- 2.5wt.% Al_2O_3 milled up 10 hours.

Milling time (h)	1	2	5	10
Mean of Modulus (MPa)	245.9	234.3	229.1	232.4
standard deviation	13.4	7.9	6.5	6.6

Table 18: Averages of % elongation measurements on compression molded sheets of composite UHMWPE- 2.5wt.% Al_2O_3 milled up 10 hours.

Milling time (h)	1	2	5	10
Mean of % Elongation	567.2	589.7	594.8	625.4
standard deviation	29.0	22.1	14.1	43.0

The UHMWPE and UHMWPE/Al_2O_3 samples exhibited reasonable and comparable tensile strength and elongation values of about 36- 47 MPa and 553- 646 % respectively, when compared to those reported in the literature for UHMWPE which is 38- 48 MPa and 350- 525 % [28]. The results presented in this study suggest that deformation of UHMWPE and reinforcing it with Al_2O_3 particulates result in improvement in the tensile strength and elongation of UHMWPE as evident in Figures 105 and 106. In general most of the improvement is found in the 1.0 wt. % alumina samples, and/or the longest milled samples. This has already been explained as caused by homogeneous dispersion of defects. The mechanical properties of the longest (10h) milled samples are the most consistent/stable.

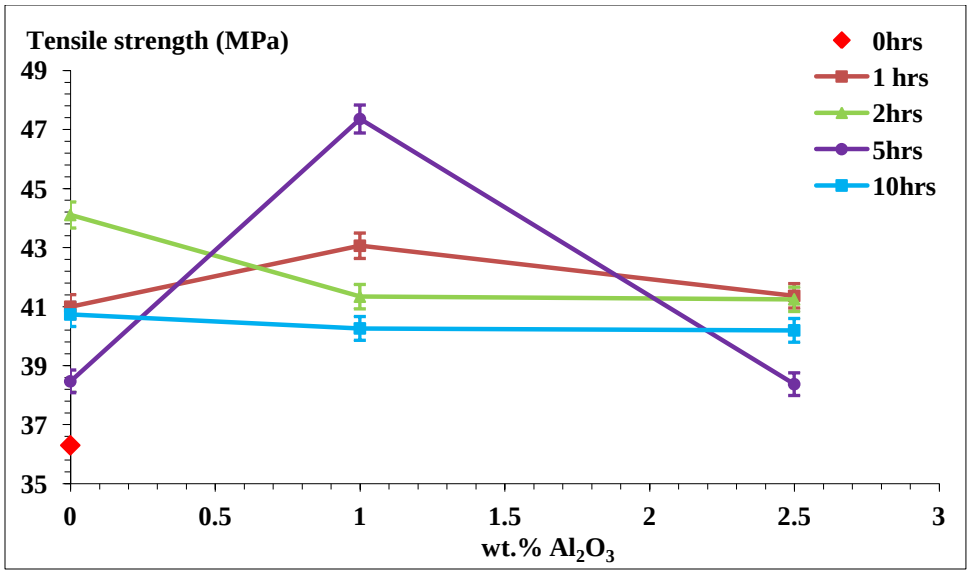

Figure 105: Averages of tensile strength of compression molded sheets WHMWPE/wt. % Al_2O_3 with different milling time as a function of wt. % Al_2O_3 contents.

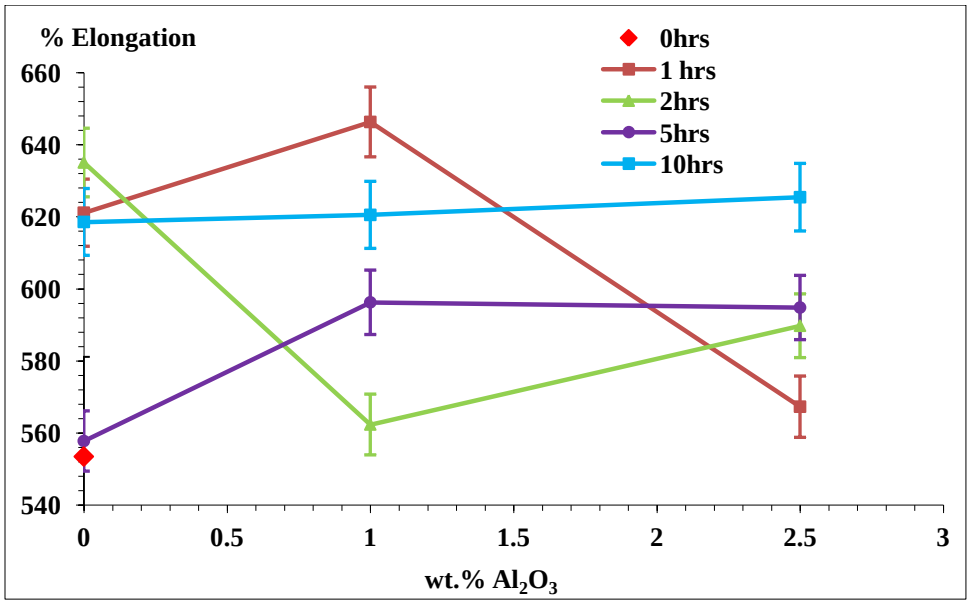

Figure 106: Averages of elongation of compression molded sheets WHMWPE/wt. % Al_2O_3 with different milling time as a function of wt. % Al_2O_3 contents.

It is evident from Figures 107 and 108 that the tensile strength and elongation have very complex trends as the milling time increases. The introduction of defects via milling and alumina particles do influence the crystallization process, for they provide nucleation sites for the process and should contribute to strengthening. At the same time milling is accompanied by molecular

weight reduction, which should lower the mechanical properties. The nature of the dispersion of the reinforcement in the UHMWPE adds to this complexity. It is however clear that all the milled and reinforced sheets have better properties than the compression molding as received UHMWPE and also what has been reported for UHMWPE in the literature [28].

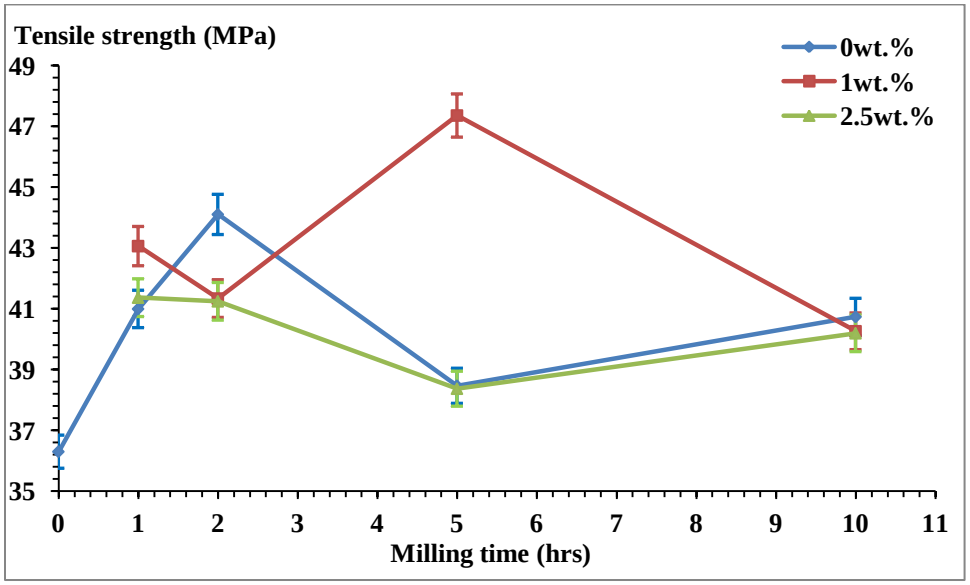

Figure 107: Averages of tensile strength of compression molded sheets for different composition WHMWPE/wt. % Al_2O_3 as a function of milling time.

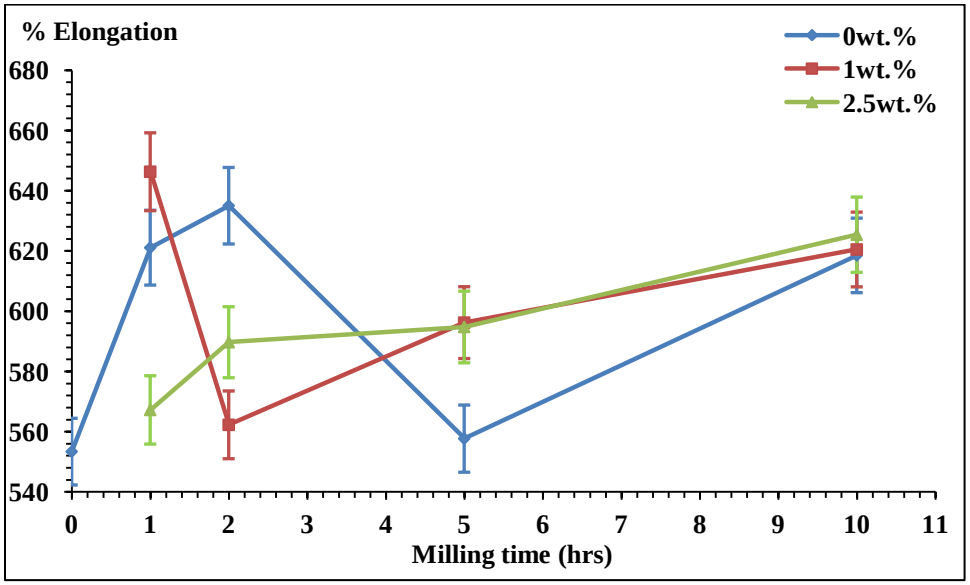

Figure 108: Averages of elongation of compression molded sheets for different composition WHMWPE/wt. % Al_2O_3 as a function of milling time.

Chapter 6

6. Summary

Mechanical alloying (MA), a high-energy ball milling technique, was used to produce composite powders of ultra-high molecular weight polyethylene (UHMWPE) and alumina in the solid state. Three alumina compositions were studied (0.0, 1.0 and 2.5wt. % alumina), and milling was done for up to 10 hours. The resulting MA powder composites were compression-molded to create 1-mm sheets. Both powders and molded sheets were characterized using x-ray diffraction and differential calorimetry. Tensile tests were performed on the sheets.

X-ray results provided information on the phases present in the polymer. UHMWPE is a semicrystalline polymer with orthorhombic structure. MA led to a partial phase transformation from the amorphous and orthorhombic structure to a metastable monoclinic structure, mostly at the expense of the amorphous structure in all milled powders. The volume fraction of the monoclinic phase and also the total crystallinity (monoclinic plus orthorhombic) increased with milling time – up to 85% in one instance as compared to 55% in the as-received UHMWPE. The orthorhombic structure disappears after compression molding. However the volume fraction of monoclinic phase in compression molded sheets remained higher (up 67%) than found in milled UHMWPE powders, and most of the time higher than the volume fraction of the as received powders. Alumina composition did not have a clear trend on crystallinity.

The results of the DSC analysis showed a decrease in the melting temperature as function of milling time, while the activation energy of melting increased as milling time and alumina composition increased. The microstructure of compression molded sheets changes from equiaxed structure for shorter milled powders to fibrous structure for longer milled powders. Generally, the crystallinity of the molded sheets increased with milling time, and this caused the yield strength and elastic modulus to increase with milling time for a given alumina composition. However, the tensile strength and ductility remained about the same.

Chapter 7

7. Future work

For a better understanding of the changes in the powder blends caused by mechanical alloying and the relationship between microstructure and mechanical properties, more studies need to be conducted as listed below:

- Measure the molecular weight of milled powders and compression molded sheets.
- Investigate the effects of higher Al_2O_3 content on the composite microstructure, and its physical and mechanical properties.
- Use AFM and SEM to study distribution and/or dispersion of the three phases and alumina particles present in milled powders as well as the compression molded sheets and relate them to their physical and mechanical properties, and review and determine the contamination that arise from the grinding media (vial and balls) during the MA process.
- Finally, perform wear resistance test on the compression molded composite sheets to see if they would be found beneficial in applications such as artificial joints.

References

1. Capiati, N.J. and R.S. Porter, The concept of one polymer composites modelled with high density polyethylene. Journal of Materials Science, 1975. **10** (10): P. 1671-1677
2. Barkoula, N.M., T. Peijs, T. Schimanski and J. Loos, Processing of single polymer composites using the concept of constrained fibers. Polymer Composites, 2005. **26** (1): P. 114-120.
3. Chawla, K.K., Composite materials: science and engineering. 1987, New York: Springer-Verlag.
4. Schwartz, M.M., Composite Materials, Volume I: Properties, Non-Destructive Testing, and Repair. 1997, New Jersey: Prentice Hall PTR.
5. Jang, B.Z., Advanced Polymer Composites: Principles and Applications. 1994, xx: ASM International.
6. Roulin-Moloney, A.C., Fractography and Failure Mechanisms of Polymers and Composites. 1989, London: Elsevier Applied Science.
7. Shalin, R.E., Polymer Matrix Composites. 1995, London: Chapman and Hall.
8. Móczó, J. and B. Pukánszky, Polymer Micro and Nanocomposites: Structure, Interactions, Properties. Journal of Industrial and Engineering Chemistry, 2008. **14** (5): P. 535 – 563.
9. Murphy, T.P., Reinforced and Filled Thermoplastics- Reinforced. Industrial & Engineering Chemistry, 1966. **58** (5): P. 41 – 49.
10. Sanli, S., A. Durmus, and N. Ercan, Effect of Nucleating Agent on the Nonisothermal Crystallization Kinetics of Glass Fiber- and Mineral-Filled Polyamide-6 Composites. Journal of Applied Polymer Science, 2012. **125** (S1): P. E268 - E281.
11. Ye, L., T. Scheuring, and K. Friedrich, Matrix Morphology and Fibre Pull-Out Strength of T700/PPS and T700/PET Thermoplastic Composites, Journal of Materials Science, 1995. **30** (19): P. 4761 - 4769.
12. Pukánszky, B. and G. Vörös, Stress Distribution around Inclusions, Interaction, and Mechanical Properties of Particulate-Filled Composites. Polymer Composites, 1996. **17** (3): P. 384 – 392.

13. Etcheverry, M. and S.E. Barbosa, Glass Fiber Reinforced Polypropylene Mechanical Properties Enhancement by Adhesion Improvement. Journal of Thermoplastic Composite Materials, 2012. **5** (6): P. 1084 – 1113.
14. Byerlin, Al.Al and L.K. Pakhomova, Polymeric Matrices for High-Strength Reinforced Composites. Review. Polymer Science U.S.S.R, 1990. **32** (7): P. 1275 – 1311.
15. Saira, T., M.Ali Munawar and S. Khan, Natural Fiber-Reinforced Polymer Composites. Proc. Pakistan Acad. Sci., 2007. **44** (2): P. 129 – 144.
16. Saha, D., P.K. Bose, A.K. Banthia and S. Dhabal, Analysis and Characterization of Alumina Particles Reinforced Ultra High Molecular Weight Polyethylene Composite for Acetabular Cup. The International Journal of Artificial Organs, 2007. **30** (30): P. 144-152.
17. Hashimoto, M., H. Takadama, M. Mizuno, Y. Yasutomi and T. Kokubo, Titanium Dioxide/Ultra High Molecular Weight Polyethylene Composite for Bone-Repairing Applications: Preparation and Biocompatibility. Key Engineering Materials, 2003. 240-242: P. 415-418.
18. Farrell, M.P., R.G. Kander, and A.O. Aning, Polymer blends formed by solid-state mechanical alloying. Journal of Materials Synthesis and Processing, 1996. **4**(3): p.151-161.
19. Evora, V. and A. SHUKLA, Fabrication, Characterization, and Dynamic Behavior of Polyester/TiO_2 Nanocomposites. Materials Science and Engineering A, 2003. **361** (1-2): P. 355 – 366.
20. Altan, M. and H. Yildirim, Mechanical and Morphological Properties of Polypropylene and High Density Polyethylene Matrix Composites Reinforced with Surface Modified Nano Sized TiO_2 Particles. World Academy of Science, Engineering & Technology, 2010. 70: P. 289 – 294.
21. Escobar, W.G., A. Ballerini and J. Zhang, Polymer Nanocomposites: Synthetic and Natural Fillers a Review. Maderas. Ciencia y tecnología, 2005. **7** (3): P. 159 – 178.
22. Zhang, G., A.K. Schlarb, S. Tria and O. Elkedim, Tensile and Tribological Behaviors of PEEK/nano-SiO_2 Composites Compounded Using a Ball Milling Ttechnique. Composites Science and Technology, 2008. **68** (15-16): P. 3073 – 3080.
23. Cavalieri, F., F. Cavalieri, F. Padella and S. Bourbonneux, High-nergy Mechanical Alloying of Thermoplastic Polymers in Carbon Dioxide. Polymer, 2002. **43** (4): P. 1155 – 1161.

24. Sheldon, R.P., Composite Polymeric materials. 1982, New York: Applied Science Publishers LTD.
25. Clauser, H.R., Advanced composite materials. Scientific American, 1973. **229** (1): P. 36-44.
26. Ingalls, A.G. and A. F. Caprio, Plastics' Parade. Scientific American, 1943. **169** (4): P. 163-165.
27. Seymour, R.B. and R. D. Deanin, History of polymeric Composites. 1987, Utrecht: VNU Science Press BV.
28. Callister, W.D., Materials Science and Engineering an Introduction- 7th ed. 2007, New York: John Wiley and Sons.
29. Charrier, J-M., Polymeric Materials and Processing. 1990, New York: Oxford University Press.
30. Astrom, B.T., Manufacturing of Polymer Composites. 1997, London: Chapman and Hall.
31. SABIC Innovative Plastics, Properties of Key Products for Aircraft Interiors. Architecture for the Sky.
32. TICONA Engineering Polymers, Fortron PPS for Thermoplastics Composites. www.ticona.com
33. Interiors, National Research Council (U.S.). Committee on Fire- and Smoke-Resistant Materials for Commercial Aircraft Improved Fire- and Smoke-Resistant Materials for Commercial Aircraft Interiors: A Proceedings. 1995, Washington DC: National Academies Press.
34. Kohan, M.I., Nylon Plastics Handbook. 1995, Cincinnati: Hanser.
35. Biron, M., Thermoplastics and Thermoplastic Composites: Technical Information for Plastics Users. 2007, Burlington: Butterworth-Heinemann.
36. Ramakrishna, S., J. Mayer, E. Wintermantel and K.W. Leong, Biomedical Applications of Polymer-Composite Materials: A review. Composites Science and Technology, 2001. **61** (9): P. 1189-1224.
37. Scholz, M.-S., J.P. Blanchfield, L.D. Bloom, B.H. Coburn, M. Elkington, J.D. Fuller, M.E. Gilbert, S.A. Muflahi, M.F. Pernice, S.I. Rae, J.A. Trevarthen, S.C. White, P.M. Weaver and I.P. Bond, The Use of Composite Materials in Modern Orthopaedic Medicine and

Prosthetic Devices: A review. Composites Science and Technology, 2011. **71** (16): P. 1791-1803.

38. Bougherara, H., R. Zdero, A. Dubov, S. Shah, S. Khurshid and E.H. Schemitsch, A preliminary Biomechanical Study of A novel Carbon Fiber Hip Implant Versus Standard Metallic Hip Implants. Medical Engineering and Physics, 2011. **33**(1): P. 121–128.
39. Bougherara, H., M. Bureau, M. Campbell, A. Vadean and L. Yahia, Design of A biomimetic Polymer-Composite Hip Prosthesis. Journal of Biomedical Materials Research Part A, 2007. **82A** (1): P. 27–40.
40. Bougherara, H., M.N. Bureau and L.H. Yahia, Bone Remodeling in A new Biomimetic Polymer-Composite Hip Stem. Journal of Biomedical Materials Research Part A, 2010. **92A** (1): P. 164–174.
41. Dimitrievska, S., J. Whitfield, S.A. Hacking and M.N. Bureau, Novel Carbon Fiber Composite for Hip Replacement with Improved in Vitro and in Vivo Osseointegration. Journal of Biomedical Materials Research Part A, 2009. **91A** (1): P. 37–5.
42. Huang, H. and T. Ramesh, Numerical Simulation of Matrix Micro-cracking in Short Fiber Reinforced Polymer Composites: Initiation and Propagation. Composites Science and Technology, 2006. **66** (15): P. 2743 – 2757.
43. Kumar, P., R. Chandra and S.P. Singh, Interphase Effect on Fiber-Reinforced Polymer Composites. Composite Interfaces, 2010. 17 (1): P. 15 – 35.
44. Bessell, T. and J. B. Shortall, the Crystallization and Interfacial Bond Strength of Nylon 6 at Carbon and Glass Fibre Surfaces. Journal of Materials Science, 1975. **10** (12): P. 2035 – 2043.
45. Fu, S., X. Feng, B. Lauke and Y. Mai, Effects of Particle Size, Particle/Matrix Interface Adhesion and Particle Loading on Mechanical Properties of Particulate–Polymer Composites. Composites Part B, 2008. **39** (6): P. 933 – 961.
46. Wacker, G., A.K. Bledzki and A. Chate, Effect of Interphase on the Transverse Young's Modulus of Glass/Epoxy Composites. Composites Part A, 1998. **29** (5): P. 619 – 626.
47. Munz M., H. Sturm, E.Schulz and G. Hinrichsen, The Scanning Force Microscope as a Tool for the Detection of Local Mechanical Properties within the Interphase of Fiber Reinforced Polymers. Composites Part A, 1998. **29** (9–10): P. 1251 – 1259.

48. Palmese G.R. and R.L. McCullough, Kinetic and Thermodynamic Considerations Regarding Interphase Formation in Thermosetting Composite Systems. Journal of Adhesion, 1994. 44 (1–2): P. 29 – 49.
49. Garton A. and W.T.K. Stevenson, Crosslinking of Epoxy Resins at Interfaces. IV. Anhydride-Cured Resins at Carbon and Graphite Surfaces. Journal of Polymer Science Part A: Polymer Chemistry, 1988. **26** (2): P. 541 – 557.
50. Drzal L.T., The Interphase in Epoxy Composites. Advances in polymer science, 1986. 75: P. 3 – 30.
51. Fink, B.K. and R.L McCullough, Interphase Research Issues. Composites Part A, 1990. **30** (1): P. 1 – 2.
52. J. Pan, W. J. D. Shaw, Microstructural Sci. 21, 95 (1994).
53. Benjamin, J.S., Mechanical Alloying. Scientific American, 1976. **234**(40).
54. Benjamin, J.S., Dispersion strengthened superalloys by mechanical alloying. Metallurgical Transactions, 1970. **1**(10): p. 2943-2951.
55. Benjamin, J.S. and T.E. Volin, Mechanism of mechanical alloying. Metallurgical Transactions, 1974. **5**(8): p. 1929-1934.
56. Benjamin, J.S., Mechanical alloying. Scientific American, 1976. **234**(5): p. 108-16.
57. Suryanarayana, C., Mechanical alloying and milling. Progress in Materials Science, 2001. **46**(1-2): p. 1-184.
58. Suryanarayana, C., Recent Developments in Mechanical Alloying. Reviews on Advanced Materials Science, 2008. **18**(3): p. 203-211.
59. Aikin, B.J.M. and T.H. Courtney, The kinetics of composite particle formation during mechanical alloying. Metallurgical Transactions A (Physical Metallurgy and Materials Science), 1993. **24A**(3): p. 647-57.
60. Koch, C.C., Synthesis of Nanostructured Materials by Mechanical Milling: Problems and Opportunities. Nanostructured Materials, 1997. **9**(1): p. 13–22.
61. Shen, T.D. and C. C. Koch, Formation, solid solution hardening and softening of nanocrystalline solid solutions prepared by mechanical attrition. Acta Materialia, 1996. **44**(2): p. 753–761.
62. Murty, B.S., J. Joardar and S.K. Pabi, Influence of Fe and Cr on the disordering behavior of mechanically alloyed NiAl. Nanostructured Materials, 1996. **7**(6): p. 691–697.

63. Wang G.M., S. J. Campbell, A. Calka, and W.A. Kaczmarek, Synthesis and structural evolution of tungsten carbide prepared by ball milling. Journal of Materials Science, 1997. **32**(6): p. 1461–1467.
64. Koch, C.C., Amorphization by mechanical alloying. Journal of Non-Crystalline Solids, 1990. **117-118**(Part 2): p. 670-678.
65. Murty, B.S., M. Mohan Rao, and S. Ranganathan, Milling maps and amorphization during mechanical alloying. Acta Metallurgica et Materialia, 1995. **43**(6): p. 2443-2450.
66. Eckert, J., M. Seidel, and L. Schultz, Formation of amorphous alloys with significant supercooled liquid region by mechanical alloying. Journal of Non-Crystalline Solids, 1996. **205-207**(Part 2): p. 500-503.
67. Sá Lisboa, R.D., M.N.R.V. Perdigão, C.S. Kiminami and W.J Botta, Phase Evolution and Microstructural Characterisation of High-Energy Ball Milled Al-Si-Fe-Ni Alloys. Materials Science Forum, 2002. **386-388**: p. 59-64.
68. Suryanarayana, C., Non-equilibrium Processing of Materials. 1999, Oxford: Pergamon.
69. Sadrnezhaad, S.K. and A.R Selahi, Effect of Mechanical Alloying and Sintering on Ni–Ti Powders. Materials and Manufacturing Processes, 2004. **19**(3): p. 475-486.
70. Soni, P.R., Mechanical Alloying: Fundamentals and Applications.1999, Oxford: Cambridge International Science Publishing.
71. Zhou, F., D. Witkin, S.R. Nutt, and E.J. Lavernia, Formation of nanostructure in Al produced by a low-energy ball milling at cryogenic temperature. Materials Science and Engineering A, 2004. **375-377**: p. 917–921.
72. Yadav T.P., R.M. Yadav and D.P. Singh, Mechanical Milling: a Top Down Approach for the Synthesis of Nanomaterials and Nanocomposites. Nanoscience and Nanotechnology, 2012. **2**(3): p.22-48.
73. Koch, C.C., The synthesis and structure of nanocrystalline materials produced by mechanical attrition: a review. Nanostructured Materials, 1993. **2**(2): p.109–129.
74. Stawovy, M.T. and A.O. Aning, Processing of amorphous Fe-W reinforced Fe matrix composites. Materials Science and Engineering A, 1998. **256**(1-2): p. 138-143.
75. Wensley, C.A., Processing and Properties of Amorphous NiW Reinforced Crystalline Ni Matrix Composites, in Materials Science & Engineering. 2005, Virginia Polytechnic Institute & State University: Blacksburg, VA. p.50.

76. McDermott, B.T., C.C. Koch, Preparation of beta brass by mechanical alloying of elemental copper and zinc. Scripta Metallurgica, 1986. **20**(5): p.669–672.
77. Pan, J. and W.J.D. Shaw, Microstructure of Mechanically Processed Polymeric Materials. Microstructural science, 1993. **19**: p.659-669.
78. Pan, J. and W.J.D. Shaw, Properties of a Mechanically Processed Polymeric Material. Journal of Applied Polymer Science, 1994. **52**(4): p.507–514.
79. Pan, J. and W.J.D. Shaw, Characterization of a Mechanical Alloyed PA/ABS Polymeric Material. Microstructural science, 1994. **21**(4): p.95.
80. Pan, J. and W.J.D. Shaw, Materials Characterization of Polyamide/Polyethylene Mechanically Alloyed Polymers. Microstructural science, 1993. **20**: p. 351–365.
81. Ishida, T., Mechanical alloying of polytetrafluoroethylene with polyethylene. Journal of Materials Science Letters, 1994. **13**(9): p.623-628.
82. Castricum, H.L., H. Yang, H. Bakker and J.H. Van Deursen, A study of milling of pure polymers and a structural transformation of polyethylene. Materials Science Forum, 1997. **235-238**: p. 211-216.
83. Font, J., J. Muntasell, and E. Cesari, Amorphization of organic compounds by ball milling. Materials Research Bulletin, 1997. **32**(12): p. 1691-1696.
84. Font, J., J. Muntasell, E. Cesari, and J. Pons, Solid-state mechanical alloying of plastic crystals. Journal of Materials Research, 1997. **12**(12): p. 3254-3259.
85. Smith, A.P., C. Bai, H. Ade, R.J. Spontak, C.M. Balik and C.C. Koch, X-ray microscopy of novel thermoplastic/liquid crystalline polymer blends by mechanical alloying. Macromolecular Rapid Communications, 1998. **19**(11), 557-561.
86. Smith, A.p., R.J. Spontak, H. Ade, S.D. Smith and C.C. Koch, High-energy cryogenic blending and compatibilizing of immiscible polymers. Advanced Materials, 1999. **11**(15): p. 1277-1281.
87. Smith, A.P., J.S. Shay, R.J. Spontak, C.M. Balik, H. Ade, S.D. Smith and C.C. Koch, High-energy mechanical milling of poly(methyl methacrylate), polyisoprene and poly(ethylene-alt-propylene). Polymer, 2000. **41**(16): p. 6271-6283.
88. Smith, A.p., R.J. Spontak, C.C. Koch, S.D. Smith and H. Ade, Temperature-induced morphological evolution in polymer blends produced by cryogenic mechanical alloying. Macromolecular Materials and Engineering, 2000. **274**(1): p. 1-12.

89. Smith, A.p., H. Ade, C.C. Koch, S.D. Smith and R.J. Spontak, Addition of a Block Copolymer to Polymer Blends Produced by Cryogenic Mechanical Alloying. Macromolecules, 2000. **33**(4): p. 1163-1172.
90. Smith, A.p., H. Ade, C.M. Balik, C.C. Koch, S.D. Smith and R.J. Spontak, Cryogenic Mechanical Alloying of Poly(methyl methacrylate) with Polyisoprene and Poly(ethylene-alt-propylene). Macromolecules, 2000. **33**(7): p. 2595-2604.
91. Balik, C.M., C. Bai, C.C. Koch, R.J. Spontak and C.K. Saw, Mechanical Alloying of PET and PET/Vectra Blends. MRS Online Proceedings Library, 1996. **461**: p. 39-44.
92. Font, J., J. Muntasell, E. Cesari, Binary mixtures of semicrystalline/noncrystalline polymers formed by ball milling. Materials Research Bulletin, 1999. **34**(14): p.2221–2230.
93. Font, J., J. Muntasell and E. Cesari, Poly(butylene terephthalate) poly(ethylene terephthalate) mixtures formed by ball milling. Materials Research Bulletin. 1999. **34**(1): p.157–165.
94. Lu, D. and S. Pan, Effects of ball milling dispersion of nano-SiOx particles on impact strength and crystallization behavior of nano-SiOx–poly(phenylene sulfide) nano-composites. Polymer Engineering and Science, 2006. **46**(6): p.820–825.
95. Xiong, M., L. Wu, S. Zhou and B. You, Preparation and characterization of acrylic latex/nano-SiO2 composites. Polymer International, 2002. **51**(8): p.693–698.
96. Shaw, W.J.D., Current understanding of mechanically alloyed polymers. Materials Science Forum, 1998. **269-272**: p.19–29.
97. Shaw, W.J.D., J. Pan and M.A. Gowler, Proceedings of the Second International Conference on Structural Applications of Mechanical Alloying, 1993. p. 431-437.
98. Shaw, W.J.D., U.S.A. Patent # 5, 367, 048, 1994.
99. Pan, J. and W.J.D. Shaw, In: Reinhart TS, Rosenow M, Cull RA, Struckholt E, editors. Properties of a mechanically processed polymeric material. Proceedings of the 24th International SAMPE Conference, 1992. **24**: p. T762–T775.
100. Pan, J. and W.J.D. Shaw, Effects of Processing Parameters on Material Properties of Mechanically Processed Polyamide. Journal of Applied Polymer Science, 1995. **56**(5): p. 557-566.

101. Smith, A.p., H. Ade, C.C. Koch and R.J. Spontak, Solid-State Blending of Polymers by Cryogenic Mechanical Alloying. Materials Research Society Proceedings, 2000. **629**: p. FF6.9.1-FF6.9.6.
102. Smith, A.p., H. Ade, S.D. Smith, C.C. Koch and R.J. Spontak, Anomalous Phase Inversion in Polymer Blends Prepared by Cryogenic Mechanical Alloying. Macromolecules, 2001. **34**(6): p. 1536-1538.
103. Smith, A.p., H. Ade, C.C. Koch and R.J. Spontak, Cryogenic mechanical alloying as an alternative strategy for the recycling of tires. Polymer, 2001. **42**(9): p. 4453-4457.
104. Smith, A.p., R.J. Spontak and H. Ade, On the similarity of macromolecular responses to high-energy processes: mechanical milling vs. irradiation. Polymer Degradation and Stability, 2001. **72**(3): p. 519-524.
105. Bai, C., R.J. Spontak, C.C. Koch, C.K. Saw and C.M. Balik, Structural changes in poly(ethylene terephthalate) induced by mechanical milling. Polymer, 2000. **41**(19): p. 7147-7157.
106. Namboodri, S.L., H. Zhou, A. Aning and R.G. Kander, Formation of polymer/ceramic composite grain boundary capacitors by mechanical alloying. Polymer, 1994. **35**(19): p. 4088-4091.
107. Cavalieri, F., F. Padella and S. Bourbonneux, High-energy mechanical alloying of thermoplastic polymers in carbon dioxide. Polymer, 2001. **43**(4): p. 1155-1161.
108. Martin, J.P. and R.G. Kander, Mechanical properties of a cryogenically mechanically alloyed polycarbonate–poly(aryl ether ether ketone) system. Journal of Applied Polymer Science, 2002. **88**(5): p. 1196-1202.
109. Srinivas, J. and J. Lyons, Processing and properties of cryogenically milled post-consumer mixed plastic waste. Polymer Testing, 2005. **24**(4): p. 428-434.
110. Gabriel, M.C., L.B. Mendes, B.D.M. Carvalho, L.A. Pinheiro, J.D.T. Capocchi, E.T. Kubaski and O.M. Cintho, High-Energy Mechanical Milling of Ultra-High Molecular Weight Polyethylene (UHMWPE). Materials Science Forum, 2010. **660-661**: p. 325-328.
111. Azhdar, B., B. Stenberg and L. Kari, Polymer-nanofiller prepared by high-energy ball milling and high velocity cold compaction. Polymer Composites, 2008. **29**(3): p. 252-261.

112. Zhang G., A.K. Schlarb, S. Tria and O. Elkedim, Tensile and tribological behaviors of PEEK/nano-SiO_2 composites compounded using a ball milling technique. Composites Science and Technology, 2008. **68**(15-16): p. 3073-3080.
113. Jose´, D.M., C.R.R. Almeida, C.A. Paskocimas, R.M. Mendonca and A.M. Medeiros, High Energy Mill Processing of Polymer Based Nanocomposites. Journal of Composite Materials, 2008. **42**(22): p. 2363-2375.
114. Vertuccio, L., G. Gorrasi, A. Sorrentino, and V. Vittoria, Nano clay reinforced PCL/starch blends obtained by high energy ball milling. Carbohydrate Polymers. 2009. **75**(1): p. 172-179.
115. Font, J., J. Muntasell, and E. Cesari, Cold-crystallization of Poly(ether-ether-ketone) amorphized by ball milling. Materials Research Bulletin, 2001. **36**(9): p. 1665-1673.
116. Koch, C.C., A.P. Smith, C. Bai, R.J. Spontak, C.M. Balik, Nonequilibrium Processing of Polymeric Materials by Mechanical Attrition. Journal of Metastable and Nanocrystalline Materials, 2000. **8**: p. 49-56.
117. Zerda, A.S. and A.J. Lesser, Intercalated Clay Nanocomposites: Morphology, Mechanics, and Fracture Behavior. Journal of Polymer Science: Part B, 2001. **39**(11): p. 1137–1146.
118. Zhang, H., Z. Zhang, K. Friedrich, and C. Eger, Property Improvements of In Situ Epoxy Nanocomposites with Reduced Interparticle Distance at High Nanosilica Content. Acta Materialia, 2006. **54**(7): p. 1833–1842.
119. Wu, C.L., M.Q. Zhang, M.Z. Rong and K. Friedrich, Tensile Performance Improvement of Low Nanoparticles Filled-polypropylene Composites. Composites Science and Technology, 2002. **62**(10): p. 1327–1340.
120. Liu, X. and Q. Wu, PP/clay Nanocomposites Prepared by Grafting-melt Intercalation. Polymer, 2001. **42**(25): p. 10013–10019.
121. Gu, A. and F. Chang, A Novel Preparation of Polyimide/Clay Hybrid Films with Low Coefficient Thermal Expansion. Journal of Applied Polymer Science, 2001. **79**(2): p. 289–294.
122. Yoon, P.J., T.D. Fornes and D.R. Paul, Thermal Expansion Behavior of Nylon 6 Nanocomposites. Polymer, 2002. **43**(25): p. 6727–6741.
123. Agag, T., T. Koga and T. Takeichi, Studies on Thermal and Mechanical Properties of Polyimide-clay Nanocomposites. Polymer, 2001 **42**(8): p. 3399–3408.

124. Yasmin, A., J.J. Luo, J.L. Abot and I.M. Daniel, Mechanical and Thermal Behavior of Clay/Epoxy Nanocomposites. Composites Science and Technology, 2006. **66**(14): p. 2415–2422.
125. Zheng, Y., Y. Zheng and R. Ning, Effects of Nanoparticles SiO_2 on the Performance of Nanocomposites. Materials Letters, 2003. **57**(19): p. 2940–2944.
126. Peng, Z., L.X. Kong and S.D. Li, Dynamic Mechanical Analysis of Polyvinylalcohol/Silica Nanocomposites. Synthetic Metals, 2005. **152**(1): p. 25–28.
127. Ou, Y.C., F. Yang and Z.Z. Yu, New Conception on the Toughness of Nylon 6/Silica Nanocomposite Prepared Via in Situ Polymerization. Journal of Polymer Science Part B – Polymer Physics, 1998. **36**(5): p. 789–795.
128. Shaw, W.J.D. and M.A. Gowler, High Elastic Modulus Engineered Polymeric/Ceramic Mechanical Alloy. First International Conference on Processing Materials for Properties, The Minerals, Metals and Materials Society, 1993. P. 687-690.
129. Hedayati, M., M. Salehi, R. Bagheri, M. Panjepour and A. Maghzian, Ball milling preparation and characterization of poly (ether ether ketone)/surface modified silica nanocomposite. Powder Technology, 2011. **207**(1): p. 296-303.
130. Castrillo, P.D., D. Olmos, D.R. Amador and J. González-Benito, Real dispersion of isolated fumed silica nanoparticles in highly filled PMMA prepared by high energy ball milling. Journal of Colloid and Interface Science, 2007. **308**(2): p. 318-324.
131. Kaloshkin, S.D., L.-J. Vandi, V.V. Tcherdyntsev, E.V. Shelekhov and V.D. Danilov, Multi-scaled polymer-based composite materials synthesized by mechanical alloying. Journal of Alloys and Compounds, 2009. **483**(1): p. 195-199.
132. Lingaraju, D., K. Ramji, M.P. Devi and U. R. Lakshmi, Mechanical and tribological studies of polymer hybrid nanocomposites with nano reinforcements. Bulletin of Materials Science, 2011. **34**(4): p. 705-712.
133. Tadayyon, G., S.M. Zebarjad and S.A. Sajjadi, Effect of Mechanical Milling on the Thermal Behavior of Polyethylene Reinforced with Nano-sized Alumina. International Polymer Processing, 2011. **26**(4): p. 354-360.
134. Pierce, R.H.Jr., J.P. Tordella, and W.M.D. Bryant, A Second Crystalline Modification of Polyethylene. Journal of the American Chemical Society, 1952. **74**(1): p. 282.

135. Teare, P.W., and D.R. Holmes, Extra Reflections in the X-ray Diffraction Pattern of Polyethylenes and Polymethylenes. Journal of Polymer Science, 1957. **24**(107): p. 496-499.
136. Russell, K.E., B.K. Hunter and R.D. Heyding, Monoclinic polyethylene revisited. Polymer, 1997. **38**(6): p. 1409-1414.
137. Seto, T., T. Hara, and K. Tanaka, Phase transformation and deformation processes in oriented polyethylene. Japanese Journal of Applied Physics, 1968. **7**(1): p. 31- 42.
138. Takahashi, Y., T. Ishida, M. Furusaka, Monoclinic-to-Orthorhombic Transformation in Polyethylene. Journal of Polymer Science Part B: Polymer Physics, 1988. **26**(11): p. 2267-2277.
139. Gerrits, N.S.J.A., and R.J. Young, Deformation Mechanisms in Biaxially Drawn Polyethylene. Journal of Polymer Science Part B: Polymer Physics, 1991. **29**(7): p. 825-835.
140. Painter, P. C., J. Runt, M.M. Coleman, I.R. Harrison, Effect of Polymorphism on the C-H Stretching Region of the Infrared Spectrum of Polyethylene. Journal of Polymer Science: Polymer Physics Edition, 1978. **16**(7): p. 1253- 1260.
141. Allan, P., E.B. Crellin, and M. Bevis, Stress-Induced Twinning and Phase Transformations in Polyethylene Single Crystals. Philosophical Magazine, 1973. **27**(1): p. 127- 145.
142. Turner-Jo, The Triclinic Crystal Form of Polymethylenes and Polyethylenes. Journal of Polymer Science, 1962. **62**(174): p. S53- S56.
143. Peacock, A.J., Handbook of polyethylene: structures, properties, and applications. Plastics Engineering, 2000. **57:** p. vii, 534.
144. Hendra, P.J., M.A. Taylor, and H.A. Willis, Plastic deformation in linear polyethylene. Polymer, 1985. **26**(10): p. 1501-1506.
145. Kiho H., A. Peterlin, and P.H. Geil, Polymer Deformation. VI. Twinning and Phase Transformation of Polyethylene Single Crystals as a Function of Stretching Direction. Journal of Applied Physics, 1964. **34**(5): p. 1599- 1605.
146. Gieniewski, C., and R.S. Moore, Deformation and Structure of Cylindrical "Spherulites" in Transcrystalline Polyethylene. Detection and Characterization of the Pseudomonoclinic Crystalline Component. Macromolecules, 1969. **2**(4): p. 385- 394.

147. Chen, D., X. Gao and D. Dollimore, A generalized form of the Kissinger equation. Thermochimica Acta, 1993. **215**: p. 109-117.
148. Lippits, D.R., S. Rastogi, and G.W.H. Höhne, Melting kinetics in polymers. Physical review letters, 2006. **96**(21): p. 218303.